NTNU – Trondheim
Norwegian University of
Science and Technology

Optimization of Bow Shape for Large, Slow Ships

Daniel Edward Nordås

Marine Technology
Submission date: June 2012
Supervisor: Sverre Steen, IMT

Norwegian University of Science and Technology
Department of Marine Technology

PROBLEM DEFINITION

MASTER THESIS IN MARINE TECHNOLOGY

SPRING 2012

FOR

Daniel Nordås

Optimization of bow shape of large slow ship

With respect to green shipping, the main challenge for the hydrodynamics community is to help reducing the consumption of fossil fuels. Traditionally, ships have been optimized for minimum fuel consumption in calm water. For large slow ships like VLCCs, this has led to very blunt bow shapes. Such bow shapes have high added resistance due to waves. Thus, one might think that the optimum bow shape, when realistic wave conditions are taken into account, should be more slender than the current shapes. Furthermore, the operational area of the ship (the route it sails) could influence what is the optimum bow shape. The objective of the thesis is therefore to explore optimum bow shapes for large slow ships (like large tankers and bulkers), taking typical wave conditions into account.

To reach the objective, the candidate is recommended to do the following:

- Review previous scientific work on design of hull shape of large slow ships like tankers and bulkers.
- Establish a method to predict the resistance of such hull forms in calm water and in waves (or added resistance due to waves). Verify that the method gives reliable results by comparing with benchmark data.
- Identify a number of different routes, typical for large tankers and bulkers, representing different operational conditions with respect to waves. Use completely calm water as a reference route.
- Optimize the bow shape for minimum resistance (or power consumption) on the different routes. Discuss how the optimum bow shape is influence by the choice of route.
- Several innovative bow shapes to reduce added resistance in waves, which mainly involves re-designing the above-water area, have been proposed, like “ax-bow”, “beak-bow” and “X-bow”. Give a review of these bow shapes, and discuss their working principles and which of them that look promising for your ships.
- If time allows, evaluate the efficiency of one such bow design.

In the thesis the candidate shall present his personal contribution to the resolution of problem within the scope of the thesis work.

Theories and conclusions should be based on mathematical derivations and/or logic reasoning identifying the various steps in the deduction.

The candidate should utilize the existing possibilities for obtaining relevant literature.

The thesis should be organized in a rational manner to give a clear exposition of results, assessments, and conclusions. The text should be brief and to the point, with a clear language. Telegraphic language should be avoided.

The thesis shall contain the following elements: A text defining the scope, preface, list of contents, summary, main body of thesis, conclusions with recommendations for further work, list of symbols and acronyms, reference and (optional) appendices. All figures, tables and equations shall be numerated.

The supervisor may require that the candidate, in an early stage of the work, present a written plan for the completion of the work. The plan should include a budget for the use of computer and laboratory resources that will be charged to the department. Overruns shall be reported to the supervisor.

The original contribution of the candidate and material taken from other sources shall be clearly defined. Work from other sources shall be properly referenced using an acknowledged referencing system.

The thesis shall be submitted in two copies:

- Signed by the candidate
- The text defining the scope included
- In bound volume(s)
- Drawings and/or computer prints that cannot be bound should be organized in a separate folder.
- The bound volume shall be accompanied by a CD or DVD containing the written thesis in Word or PDF format. In case computer programs have been made as part of the thesis work, the source code shall be included. In case of experimental work, the experimental results shall be included in a suitable electronic format.

Supervisor : Professor Sverre Steen
Advisor : Olav Rognebakke (DNV)
Start : 16.01.2012
Deadline : 10.06.2012

Trondheim, 16.01.2012

Sverre Steen
Supervisor

PREFACE

This thesis is submitted to the Norwegian University of Science and Technology (NTNU) as a requirement for the degree of Master of Science. The workload is equivalent to 30 credits, or one semester, at NTNU.

This Master thesis has been performed at the Department of Marine Technology, NTNU, Trondheim, with Professor Sverre Steen as supervisor, and Olav Rognebakke, DNV, as advisor.

During the work with this thesis several software packages like Friendship/Shipflow, Maxsurf Pro, ShipX and Rhinoceros that were more or less new to me have been utilized. Especially the work with Friendship/Shipflow has been very time consuming. Due to lack of experience with Friendship/Shipflow everything from generating geometry offsets to the setup for generating calm water wave resistance has been an iterative process with a lot error-searching. Poor results have resulted in a lot of testing with little success.

The last objective in the problem definition asks for an evaluation of the efficiency of innovative bow designs by computational fluid dynamics. Due to the unforeseen time demanding work with the Shipflow this objective has not been answered and has been stated as further work.

Many different sources of information have been utilized throughout the work of this thesis. I would like to thank Jaeouk Sun at DNV for sharing his knowledge on hull design and his help with Friendship/Shipflow as well as discussions on the results and all the people at Ship Hydrodynamics and Stability that has motivated and willingly helped with issues throughout the work with this thesis. I would also like to thank Olav Rognebakke for sharing his insight to the investigated problem and introducing me to the correct persons to ask. Lastly, I would thank Prof. Sverre Steen for sharing his knowledge and opinions on the subject and being of great assistance in structuring and discussing different topics in this thesis.

Trondheim, 08.06.2012

Daniel E. Nordås

ABSTRACT

Traditionally ships have been optimized for minimizing the fuel consumption in calm water. For slow, large ships like tankers and bulk carriers this has resulted in very blunt bows with high added resistance due to waves. The objective of this thesis has been to investigate if the optimal bow shape, when realistic wave conditions are taken into account, should be more slender than the current blunt bows. The added resistance is also highly dependent on the actual wave conditions the vessel experiences. Thus a question has been if the optimal bow changes with the operational area, or route, of the vessel.

Five designs have been investigated representing a range of waterlines from blunt to sharp. They are based on the MOERI Tanker KVLCC2. KVLCC2A is the original design of the MOERI Tanker with no flare. KVLCC2B has the same water line curve as KVLCC2A, but with straight sides and small bilge radius in the bow. KVLCC2C has a more slender bow by moving volume from the shoulders to above the bulb. KVLCC2D is a blunter design than KVLCC2A and KVLCC2E has been elongated by 8 m compared to KVLCC2C to get a more slender bow.

Four routes have been chosen to represent trades and ocean areas. The routes are; Arabian Gulf (AG) to the Gulf of Mexico (GM), AG to Japan, Brazil to China and Norway to the East Coast of US.

Calm water resistance has been calculated and verified against experimental data. The wave resistance was calculated numerically using Shipflow. These calculations were not satisfying and should be taken a closer look at. Modification of the results had to be done.

The results show that KVLCC2A, KVLCC2C and KVLCC2E have very similar calm water resistance. They have slightly lower values than KVLCC2D. KVLCC2B has the greatest calm water resistance.

The added resistance was calculated by ShipX. The sharper bow designs have significantly lower resistance in the diffraction regime, as intended. KVLCC2E has slightly a slightly lower added resistance coefficient in the short wave regime than KVLCC2C.

The speed-loss calculations were performed by combining wave statistics for the routes, calm water resistance, added resistance and engine and propulsion characteristics in ShipX. The result is an attainable speed at a given power input, 27 000 kW.

The results show that KVLCC2C and KVLCC2E have the lowest speed-loss. The attainable speed is highest for KVLCC2C and it can thus be concluded that a sharper design is more optimal when realistic wave conditions are taken into account.

The relative speed loss on different routes between KVLCC2C and KVLCC2A shows that the speed loss of KVLCC2C is 14.2% lower for the AG to GM, 13.8%, 16.2 % and14.9 % for respectively AG to Chiba, Mongstad to East coast of US and Brazil to China. Thus, a small difference can be seen, but not enough to change the best design in this case.

A review of innovative bow shapes dealing with added resistance was performed and an evaluation based on working principles and applicability to a large, slow vessel was discussed. The designs reviewed were X-bow (Ulstein Design), a new bow from STX OSV and Beak-bow, Ax-bow and LEADGE-bow designed in Japan especially for larger ships.

The two first bows are designed primarily with offshore service vessels in mind and focus more on the long waves. The LEADGE-bow, which is based more or less on the same principles as KVLCC2C, shows that a simple sharpening of the bow is an easy and effective measure. This seems like the most promising bow for large, slow ships of those evaluated.

SAMMENDRAG

Historisk har skip blitt optimalisert for å minimere drivstofforbruket i stille vann. For store, saktegående skip, som tankere og bulkskip, har dette resultert i veldig butte baugformer med høy tilleggsmostand i bølger. Formålet med denne oppgaven har vært å undersøke om slankere baugformer, når realistiske bølgetilstander er tatt i betraktning, kan være mer optimalt enn de tradisjonelle butte baugene. Tilleggsmotstand er også svært avhenging av hvor store de faktiske bølgetilstandene er, og et spørsmål har vært om den optimale baugformen kan være avhengig av operasjonsområdet (ruten) et skip trafikkerer.

Fem design, som representerer variasjon fra butt til slank baug, har blitt undersøkt. De er basert på MOERI tankeren KVLCC2. KVLCC2A er originaldesignet av MOERI tankeren, men med rette sider over vann. KVLCC2B har samme form i vannlinjen som KVLCC2A, men med rette sider under og over vann. KVLCC2C har en slankere baug, formet ved å flytte volum fra fremre skulder til tomrommet over bulben på KVLCC2A. KVLCC2D har en enda buttere baug enn KVLCC2A. KVLCC2E har blitt forlenget med 8 meter i forhold til KVLCC2C for å få en slankere baug.

Fire har blitt valgt ut for å representerer handelsruter og bølgetilstander. Rutene er den Arabiske Gulfen (AG) til Mexico Gulfen (MG), AG til Japan, Brasil til Kina og (Norge) til Østkysten av USA .

Stillevannsmotstanden har blitt beregnet og verifisert mot eksperimentelle data. Bølgemotstanden ble kalkulert numerisk ved hjelp av Shipflow. Disse beregningene ga ikke tilfredsstillende resultater og burde bli sett nøyere på. Modifikasjon av resultatene har blitt gjort.

Resultatene viser at KVLCC2A, KVLCC2C og KVLCC2E har veldig lik stillevannsmotstand og resultatene ligger litt under motstanden til KVLCC2D. KVLCC2B har størst stillevannsmotstand.

Tilleggsmotstanden ble beregnet ved hjelp av ShipX. De slankeste baugformene har signifikant reduksjon av tilleggssmotstanden i korte bølger, som ønsket. KVLCC2E har litt lavere tilleggsmotstand i korte bølger enn KVLCC2C.

Beregning av fartstapet ble beregnet ved å kombinere bølgestatistikk, stillevanns- og tilleggs-motstand og maskineri og propulsjons egenskaper i ShipX. Resultatet er presenter i form av et fartstap og en oppnåelig hastighet for rutene ved en gitt effekt på maskineriet, 27 000 kW.

Resultatene viser at KVLCC2C og KVLCC2D har de laveste fartstapene. Den oppnåelige hastigheten er høyest for KVLCC2C og det kan dermed konkluderes med at et noe slankere design er mer optimalt når realistiske bølgedata er tatt i betraktning.

Det relative fartstapet på forskjellige ruter mellom KVLCC2A og KVLCC2C viser at KVLCC2C har 14.2 % mindre fartstap på ruten fra AG til MG, 13.8 %, 16.2% og 14.9% for rutene fra henholdsvis AG til Japan, Norge til østkysten av USA og Brasil til Kina. En liten forskjell kan altså ses på forskjellige ruter, men dette påvirker ikke resultatet i denne oppgaven.

En betraktning av nye innovative baugformer, med hensikt å redusere totalmotstanden i bølger, har også blitt gjennomført. I tillegg har anvendbarhet på store, saktegående skip blitt diskutert. Designene som har blitt undersøkt er X-bow (Ulstein Design), STX sin nye baugform og Beak-bow, Ax-bow og LEADGE-bow designet i Japan spesielt med tanke på større skip.

De to første baugformene er hovedsakelig designet med tanke på offshore service skip og fokuset ligger mer på tilleggsmotstanden i lange bølger siden disse vanligvis er betraktelig mindre enn store tankere og bulkskip. LEADGE-bow, som er baser på mer eller mindre de samme prinsippene som KVLCC2C, viser at et enkelt tiltak som en slankere baug er effektivt. Dette virker også som den mest lovende baugen for store skip av de som ble evaluert.

CONTENTS

LIST OF FIGURES

LIST OF TABLES

NOMENCLATURE

Symbol	SI unit	Explanation
A_{proj}	[m^2]	Projected area of above water hull and superstructure
α	[deg]	Wave propagation direction with respect to the x-axis
B_{wl}	[m]	Beam in water line
B_Z	[N·s/m]	Heave damping coefficient
B_θ	[N·s/rad]	Pitch damping coefficient
$B_{Z\theta}$	[N·s/rad]	Coupled heave and pitch damping coefficient
C_A	[-]	Correlation allowance
$C_{AA(s,m)}$	[-]	Air resistance coefficient for ship or model
$C_{App(s,m)}$	[-]	Appendix resistance coefficient for ship or model
C_B	[-]	Block coefficient
$C_{DB(s,m)}$	[-]	Wet transom stern resistance coefficient for ship or model
$C_{F(s,m)}$	[-]	Skin friction resistance coefficient for ship or model
C_M	[-]	Midship coefficient
C_P	[-]	Prismatic coefficient
C_R	[-]	Residual resistance coefficient
C_{Stern}	[-]	Coefficient describing the shape of the stern
$C_{T(s,m)}$	[-]	Total friction coefficient for ship or model
C_{VS}	[-]	Viscous resistance coefficient
C_X	[-]	Air resistance coefficient given in ShipX
$\epsilon_z, \epsilon_\theta, \epsilon_S$	[rad]	Heave, pitch and relative motion phase angle
ΔC_F	[-]	Hull roughness allowance
D	[m]	Moulded depth
F_a	[N]	Amplitude of heave force
F_N	[-]	Froude number
$\bar{F}_n$	[N/m]	Force per unit length normal to hull
$\hat{F}_{T_Z}$	[-]	Cumulative distribution function
f^*	[N/m]	Mean added resistance on a strip
g	[m/s^2]	Gravitational acceleration
H	[µm]	Hull roughness
H_S	[m]	Significant wave height
k	[rad/m]	Wave number
k	[-]	Form factor
k_f	[-]	Form factor due to form effect on friction
k_p	[-]	Form factor due to form effect on pressure
L_1	[m]	Non-shadow line segment of water line
L_{pp}	[m]	Length between perpendiculars
L_R	[m]	Distance from bow to parallel mid ship
L_{wl}	[m]	Length in water line
M_a	[Nm]	Amplitude of pitch moment
n	[-]	Total number of observations
n_{T_Z}	[-]	Number of observations lower or equal to T_Z
ω_e	[1/s]	Encounter frequency
∇	[m^3]	Volume displacement
ρ	[kg/m^3]	Density
R_{aw}	[N]	Added resistance
R_N	[-]	Reynolds number

R_T	[N]	Total resistance
S	[m^2]	Wetted surface area
S_B	[m^2]	Transom stern wetted surface area
s	[m]	Relative vertical motion amplitude
T	[m]	Draught
T_Z	[s]	Zero crossing period
θ	[deg]	Angle between tangent of water line and centre line
θ_a	[rad]	Pitch amplitude
V	[m/s]	Speed in m/s or knots
V_{attCW}	[m/s]	Attainable speed in calm water
x_b	[m]	Longitudinal position of strip
Z_a	[m]	Heave amplitude
z_x	[m]	Vertical motion due to pitch
ζ	[m]	Wave elevation
ζ_a	[m]	Wave amplitude

Abbreviation and Acronyms

AP	Aft Perpendicular
CDF	Cumulative Distribution Function
CFD	Computational Fluid Dynamics
DWT	DeadWeight Tonnage
EUT	Enhanced Unified Theory
FP	Fore Perpendicular
ITTC	International Towing Tank Conference
JONSWAP	JOint North Sea WAve Project
LCB	Longitudinal Centre of Buoyancy
LCG	Longitudinal Centre of Gravity
RANS	Reynolds Averaged Navier-Stokes
RPM	Revolutions per minute
VERES	VEssel RESponses (ShipX plug-in)
VLCC	Very Large Crude Carrier, 160 000 – 319 999 DWT
VOF	Volume Of Fluids

1 BACKGROUND AND MOTIVATION

Historically, merchant ship owners have tended to be conservative and new innovative solutions have been hard to introduce. Merchant vessel design has focused on low hull resistance and high propulsion efficiency where the verification process has been model testing in calm water conditions, (Laursen, 2001).

Added resistance, or involuntary speed-loss, due to incident waves and wind has been included by adding a sea margin. This sea margin has a typical value between 15%-30% of calm-water power, based on experience with similar ships (Arribas, 2007). This focus on calm water resistance has led to hull forms with good performance in calm water, which for large, slow ships like Very Large Crude Carriers (VLCC) or bulk carriers, have resulted in very blunt bows.

The major resistance component of large, slow ships is the viscous resistance. Wave making resistance is only a small part of the total resistance component for such ships, due to the low Froude number, even with blunt bows.

Blunt bows have a larger volume to wetted surface ratio than a sharper bow with equal displacement. Thus more cargo can be transported per wetted surface area. Also, due to the low Froude number and hence low ratio of wave resistance, the benefit of decreasing the wave resistance by sharpening the bow may be cancelled by an increase in viscous resistance or a decrease in cargo capacity. These two arguments support a blunt bow.

The sheltered calm water conditions the ships are verified for are rare on the typical trade routes for these types of vessels. Involuntary speed-loss due to wind and waves may slow down the vessel. Two separate issues arise here. Firstly, the design of the vessel with respect to added resistance in wind and waves may be poor resulting in significant speed-loss that needs to be compensated for by increasing the power consumption. Thus, this increases the fuel consumption i.e. the environmental impact as well as the fuel expenses. Secondly, the speed-loss may be impossible to compensate for, as the available installed power reserve is too small, resulting in delays possibly causing economic loss for the ship owner. In addition, if the installed power reserve is too small, it may cause issues with manoeuvring which may be a critical safety issue.

In Faltinsen and Svensen (1990) a 198 meter long container vessel was used to investigate the speed-loss during a round-trip on a North-Atlantic route. They found that on a target speed of 22 knots, the ship had a speed-loss of 1.7 knots westbound and 0.9 knots round-trip voyages due to involuntary speed-loss. Economically, a speed-loss of 0.5 knots when translated directly into lost cargo carried represents a total economic loss of ~$2 million over one year (in 1990).

1.1 HYPOTHESIS

Reflection of waves off the bow and radiation of waves due to ship motions are two of the major effects contributing to involuntary speed-loss due to added resistance in incident waves. Reflection of waves is dominant when the wavelengths are short compared to the ship length, while the radiation effect dominates when the wavelengths are in the range of the ship length (refer to chapter 1.3).

The majority of the sea states that a large ship encounters on a voyage are small, and thus is associated with small wavelengths. Even though the added resistance in magnitude is largest around resonance in heave and pitch, added resistance due to short waves are important in the long term (Faltinsen, 2010).

One relatively simple measure to reduce the reflection of waves is to sharpen the entrance angle of the bow, (Guo and Steen, 2010b). Thus the incident waves will be reflected more to the sides than forward, decreasing the momentum change of the incident waves and thus their impact on the vessel. This is depicted in Figure 1.1 and Figure 1.2.

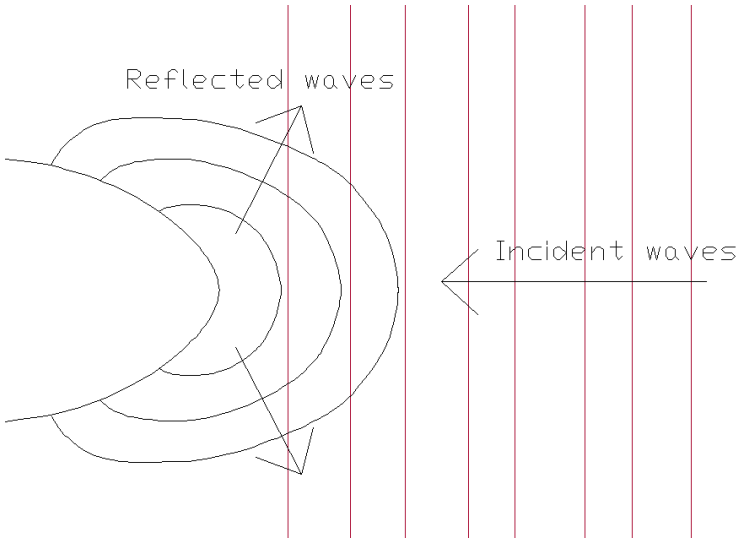

FIGURE 1.1 - WAVE REFLECTION OFF BLUNT BOW

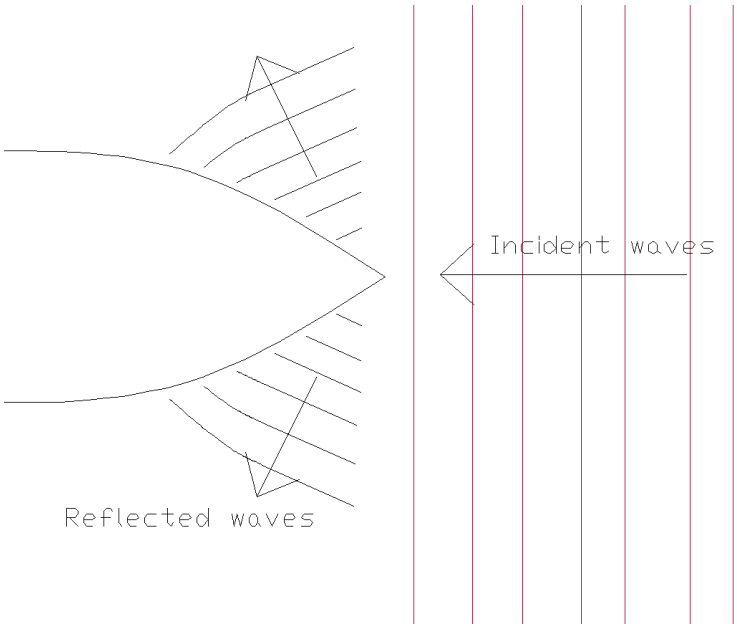

FIGURE 1.2 - WAVE REFLECTION OFF SHARP BOW

Thus the hypothesis of this thesis is that a possible increase in the calm water resistance due to a sharper bow, would be compensated, and maybe surpassed by a decrease in the added resistance due to waves. This may contribute to a vessel with a better total performance; less fuel consumption, lower emissions and better delivery precision.

However, the result is expected to depend on the trade-off between increased calm water resistance and decreased added resistance, the time spent in practically calm water and waves and the degree of severity of the sea states on the routes. A ship trading on a route with

practically no waves will be expected to have less benefit from a sharper bow than a ship trading on routes with severe wave conditions most of the time.

1.2 Scope Of Work

The objective of this thesis is to investigate the performance of bow designs with different slenderness for a large, slow vessel on a typical route with realistic wave conditions. The aim of the calm water resistance analysis is to estimate the calm water resistance of each design, capturing the changes in resistance due to changes in the bow design. The added resistance analysis is performed to investigate the influence of the bow design on the added resistance in both short and long waves. Scatter diagrams is established from wave statistics databases to such that the designs can be evaluated in a realistic wave environment.

The MOERI tanker, KVLCC2, has been chosen as a basis for the designs. This is a VLCC with dimensions shown in Table 1.1. It has become an academic standard for validation of Computational Fluid Dynamics (CFD), and the original 3D model is provided on the website of Simman2008 (2008).

TABLE 1.1 - MAIN DIMENSIONS OF THE ORIGINAL KVLCC2 DESIGN

Main Particulars	KVLCC2 original
L_{pp} (m)	320.0
L_{wl} (m)	325.5
B_{wl} (m)	58.0
D (m)	30.0
T (m)	20.8
Displacement ∇ (m^3)	312622.0
S excl. rudder (m^2)	27194.0
C_B	0.8098
C_M	0.9980
LCB (%). fwd+ from amidship	3.4800
LCB (m) from AP	171.3

The rest of this chapter gives a brief review of the theory of added resistance and a literature review of work done on added resistance in waves. This review focuses on methods to calculate the added resistance and ends with a discussion of the most promising methods for this thesis.

Chapter 2 establishes and explains the methods and software used to calculate the calm water resistance, added resistance and the simulation of the performance on typical routes.

Chapter 3 discusses the process of developing alternative bow designs and issues with changing the bow design. The designs used in this thesis is presented and evaluated. In total 5 designs have been chosen to represent the range from blunt to sharp bows.

Chapter 4 establishes typical routes for VLCCs and bulk carriers. The long term wave statistics will be established with scatter diagrams for each route, representing the probability of occurrence of sea states on the route.

Chapter 5 verifies the methods described in chapter 2 and discusses issues regarding the methods. Calm water resistance, added resistance and finally route simulation results is presented and discussed.

Due to restrictions of methods used in this thesis, the models have straight sides. In chapter 7 innovative bow shapes, some with more complex geometry, already developed is presented. The working principles are discussed and the efficiency is evaluated on the basis of applicability to large, slow ships like VLCCs.

1.3 Added Resistance Due to Waves

The added resistance is commonly referred to as the difference between the resistance of a ship in waves and the calm water resistance. Due to the large variations in resistance when the ship is travelling in waves, the most sensible measure is the average added resistance in a wave condition, or the involuntary speed-loss caused by the added resistance in waves (refer to Figure 1.3).

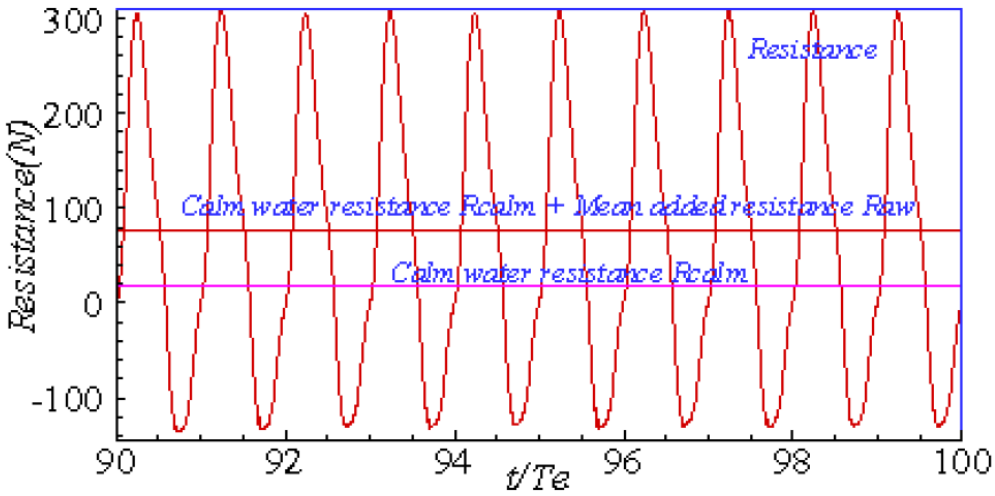

FIGURE 1.3 - ADDED RESISTANCE OF KVLCC2 MODEL IN WAVES, (GUO, 2011).

The energy dissipated from a ship due to incident waves can, according to classical sea keeping theories, be split into two main components, (Wilson, 1985).

- The interference between the incident wave system and the radiated waves resulting from ship motions, where the vertical motions, heave and pitch, are the most important. This is often referred to as drift force.
- The wave system will experience some wave reflection of the incident waves off the ship. This component becomes important when the wavelengths are small compared to the ship length. This component is commonly known as wave diffraction.

When applying analytical consideration, these three components are in principle additive and can be superimposed. However, in reality they interact and a division in the three components cannot be strictly observed. In practice, all these components are proportional to the square of wave amplitude and hence will be non-linear. In general, the drift force component has the greatest magnitude, but this is dependent on hull shape and wave conditions (Arribas, 2007). In Figure 1.4 the relative magnitude of the radiated and diffracted effects are shown conceptually.

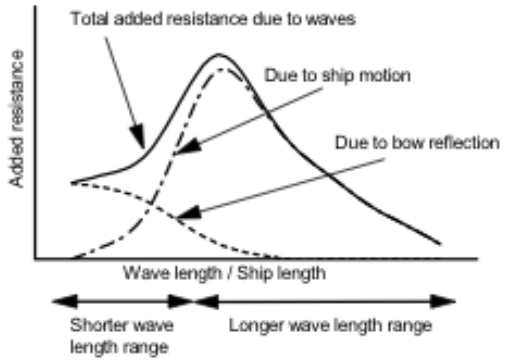

FIGURE 1.4 - COMPONENTS OF ADDED RESISTANCE AND THEIR CONCEPTUAL RELATIVE SIGNIFICANCE AT DIFFERENT WAVELENGTHS (HIROTA ET AL., 2005)

1.4 CALCULATION OF ADDED RESISTANCE IN WAVES

Havelock (1942) was one of the first to estimate the added resistance in waves. By integrating the longitudinal components of the pressure on the wetted surface of an oscillating ship hull, he obtained a simple formula for the mean added resistance due to ship motions in heave and pitch. He assumed that the incident wave system was undisturbed, hence no diffraction of waves, which is called the Froude-Krylov approximation. The formulation requires no integration along the ship length. Havelock's expression for the added resistance, R_{aw}, is,

$$R_{aw} = -\frac{k}{2}[F_a Z_a \sin(\epsilon_z) + M_a \theta_a \sin(\epsilon_\theta)] \qquad \text{Equation 1-1}$$

k – wave number
F_a – amplitude of heave force
Z_a – heave amplitude
M_a – amplitude of pitch moment
θ_a - pitch amplitude
ϵ_z, ϵ_θ – heave and pitch phase angle

The expression is not accurate due to exclusion of diffracted waves, coupled motions and viscous damping. However, it shows that added resistance is partly due to the relative motion between exciting waves and ship motions. It can be seen that the maximum of added resistance will be obtained in resonance of vertical motions, thus poor sea keeping characteristics will induce larger added resistance.

1.4.1 MOMENTUM AND ENERGY METHOD

Maruo (1957) also contributed to analytical calculation of the added resistance with a potential flow solution. He used the equations for conservation of energy and momentum to derive his method. The hull form was represented by a centre line distribution of singularities, and the wave field potential consists of the potential associated with the original wave field and the velocity potential of waves produced by the singularities.

This is a far field method, which is also called drift force method. Maruo (1960) developed the basis of this method. He developed a general far-field theory to calculate the non-linear hydrodynamic forces experience by a ship oscillating in incident waves without forward speed.

The method derives an energy and momentum balance on a control volume around the ship. The velocity potential is divided into three parts, incident wave potential, diffracted wave potential

and radiated wave potential. The added resistance is then found from solving a boundary value problem.

The incident wave potential is known, and solving the problem then becomes finding the harmonic potential that satisfies a linearized free surface condition, a far-field radiation condition and the ship hull boundary condition. (Arribas, 2007)

However, the diffraction effect is not included and it seems to over predict the added resistance at low frequencies.

Joosen (1966) obtained a formula equal to Havelock (1942), except for an additional term for coupled motions, by expanding Maruo's results in an asymptotic series in terms of length to beam ratio. He included forward speed by considering the encounter frequency, ω_e. The expression also includes damping. The expression found can be written as,

$$R_{aw} = -\frac{1}{2}\frac{{\omega_e}^3}{g}[B_Z Z_a^2 + B_\theta \theta_a^2 - 2B_{Z\theta} Z_a \theta_a \cos(\epsilon_z - \epsilon_\theta)] \qquad \text{Equation 1-2}$$

$B_Z, B_\theta, B_{Z\theta}$ – motion damping coefficients
ω_e – encounter frequency

He concluded that the added resistance due to waves is mainly caused by radiated waves. The diffraction effects could be neglected, except for very small waves (Arribas, 2007). It also shows best results for finer ship hulls with low C_b when compared to experimental tests (Arribas, 2007).

Kashiwagi (2009) calculated the added resistance of a ship with the modified version of Maruo's approach, using the Enhanced Unified Theory (EUT). In strip theory, 3D and forward speed effects are ignored, but are incorporated in the EUT. In Kashiwagi et al. (2010) discrepancies between experimental results and estimated values with the method are especially large for a ship with forward speed in short waves.

1.4.2 Integrated Pressure Method

This method is based on the classical hydrodynamic solution as is the one performed by Havelock (1942). However, a more sophisticated method of calculating motions is applied with e.g. a strip theory. This also enables one to calculate a small contribution of vertical motions due to the pitch angles that produces a longitudinal force component.

When using strip theory, the longitudinal force must be estimated as a mean value for each section. This is due to one of the approximations of strip theory dictating that no longitudinal effects can be transferred between the strips. Boese (1970) obtained a mean value for a section (strip), f^*, at x_b which is,

$$f^* = \frac{\rho g \zeta^2}{4}\left(-1 + \frac{z_x^2}{\zeta^2} + \frac{2s \cdot cos(-kx_b \cos(\mu) - \epsilon_S}{\zeta}\right) \qquad \text{Equation 1-3}$$

ζ – wave elevation
$z_x = Z_a - x_b\theta_a$ – vertical motion due to pitch
s – relative vertical motion amplitude
ϵ_S – phase angle of relative vertical motion

This is integrated over the waterline plane and results in

$$R_{aw1} = -2\int_L f^* \frac{dy_w}{dx_b} dx_b$$

$$= -\frac{\rho g \zeta^2}{2} \int_L \left(-1 + \frac{z_x^2}{\zeta^2} + \frac{2scos(-kx_b \cos(\mu) - \epsilon_S}{\zeta} \right) \frac{dy_w}{dx_b} dx_b \qquad \text{Equation 1-4}$$

The contribution of the vertical motion is obtained by

$$R_{aw2} = \frac{1}{2} \rho \nabla {\omega_e}^2 Z_a \theta_a \cos(\epsilon_z - \epsilon_\theta) \qquad \text{Equation 1-5}$$

Thus the total added resistance could be summed up

$$R_{aw} = R_{aw1} + R_{aw2} \qquad \text{Equation 1-6}$$

This method neglects the quadratic velocity term in Bernoulli's equation as well as the term due to the instantaneous wetted surface pressure. The method is also limited to head sea.

Faltinsen et al. (1980) derived a similar formula as Boese (1970). However, this derivation included the quadratic velocity term as well as the pressure term arising from the instantaneous wetted surface. The procedure of Faltinsen et al. (1980) is valid for any wave direction, in contrast to Boese's procedure. They also calculated the transverse drift force and yaw moment. In the same article Faltinsen et al. (1980) derived an asymptotic formula for added resistance in short waves. This will be commented upon in more detail later in this chapter.

1.4.3 Radiated Energy Method

This method equates the work of added resistance to the energy contained in the damping waves radiated away from the ship. This method was first applied by Gerritsma and Beukelman (1972). The method is simple to calculate due to the fact that no boundary value problem needs to be solved. It has proven to be accurate in predicting the added resistance in long waves (Wilson, 1985).

However, the effect of diffracted waves is only considered by correcting the ship motions with one empirical equation. Thus this method cannot predict the added resistance in short waves accurately.

1.4.4 Added Resistance in Short Waves

The focus on the above mentioned methods have been on the energy dissipated through interaction between the incident wave system and the radiated waves related to ship motions. This effect is the dominating effect in the range of wavelengths around the ship length. However, in the short wave length region the diffraction of waves is important. For short waves the ship motions become small, and especially for blunt bows, the major part of the energy dissipation is through reflection of incident waves.

The above-mentioned methods for calculating added resistance in waves have proven poor in short waves (Wilson, 1985, Arribas, 2007). Special methods have been developed for added resistance in short waves.

Fujii and Takahashi (1975) expanded Mauro's method by considering added resistance in short waves. The formula for drift force based on the wave reflection developed by Havelock (1942) was used together with empirical corrections. Modifications and improvements on Fujii and Takahashi's formula have been done by Sakamoto and Baba (1986), Matsumoto et al. (1998) and Ueno et al. (2001). However, these do not provide a significant difference from Faltinsen's asymptotic formula (Guo and Steen, 2010b).

Faltinsen et al. (1980) developed an asymptotic formula for the added resistance in short waves. It uses the incident waves on an infinitely long plane wall to simulate the diffraction problem in

short waves. This method includes the wave reflection effect without consideration of ship motions.

The asymptotic formula can be written as

$$R_{aw} = \int_{L_1} \bar{F}_n \sin(\theta)\, dl \qquad \text{Equation 1-7}$$

Where $\bar{F}_n$ is the force per unit length normal to the hull given as

$$\bar{F}_n = \frac{1}{2}\rho g \zeta_a^2 \left(\left[\frac{k_1}{2k} - \frac{1}{2}\cos^2(\theta + \alpha) \right] + \frac{k_2}{2k}\sin(\theta + \alpha) \right) \qquad \text{Equation 1-8}$$

$$k_1 = \frac{[\omega_e - Vk\cos(\theta + \alpha)]^2}{g} \qquad \text{Equation 1-9}$$

$$k_2 = \sqrt{k_1 - k^2\cos^2(\theta + \alpha)} \qquad \text{Equation 1-10}$$

ζ_a – wave amplitude
θ - angle between the tangent of the waterline and the centreline (x-axis)
α - wave propagation direction with respect to the x-axis
L_1 – non-shadow part of the water plane curve
ω_e - circular frequency of encounter
V – horizontal steady velocity parallel to the ship side
k – wave number

The assumptions that the vessel has vertical sides at the water-plane, the wave-induced ship motion is negligible and the wave energy decays exponentially in depth enable the ship to be replaced by a stationary vertical, infinitely long cylinder with the same cross section in the water-plane as the ship.

Further, the application area of the method is limited to short waves, blunt ships and moderate Froude numbers (F_N <~0.2, (Faltinsen, 1990)). The method has been found to correctly predict the added resistance when these formal conditions of the formula are satisfied. However, it is very sensitive when the conditions are not met, and under-predicts the added resistance when the ship sides are not vertical or the bow is not blunt (Steen and Faltinsen, 1998).

Guo and Steen (2010a) utilized a radiated energy method and the asymptotic formula of Faltinsen et al. (1980) combined with an R-function to predict the added resistance on KVLCC2 in a wider range of wavelengths. They compared the results to experiments conducted on a model of KVLCC2. A new data processing approach in experiments was used due to unstable waves in short waves causing difficulty in testing. They found that the radiated energy method seriously under-predicts the added resistance in short waves, as mentioned earlier. The combined method can predict the added resistance over a range of wavelengths. However, the method slightly under-predicts the added resistance at lower Froude numbers, while it is predicting it well for Froude numbers around 0.142-0.18.

1.4.5 Calculations of Added Resistance with Computational Fluid Dynamics (CFD)

With the increasing computational capacity, computational fluid dynamics is becoming more and more available as a design tool.

Utilizing CFD approach relying on the resolution of the Reynolds Averaged Navier-Stokes (RANS) equation can, as opposed to potential flow, handle effects of viscosity, wave dispersion, nonlinearity and wave breaking (Choi and Yoon, 2009). Turbulence effects can be taken into account through a turbulence model. A much-used approach to handle the free surface is Volume

Of Fluids (VOF). This has proved suitable for flow involving hull shape with section flare and breaking waves (Azcueta, 2004).

Guo et al. (2011) did systematic validation and verification of numerical computation to demonstrate that reliable numerical results can be obtained in calm water as well as head waves on KVLCC2. A comparison between CFD results, the radiated energy method by Gerritsma and Beukelman (1972), and experimental results show that the CFD results have the best agreement with experimental results in most wavelengths. CFD is far better than the radiated energy method in small wavelengths, while fairly better to predict the added resistance at the peak.

Guo et al. (2011) also studied the contribution of ship motions compared to diffracted waves on the added resistance, a division proposed by Fujii and Takahashi (1975), by fixing the ship in CFD calculations. It was found that for wavelengths shorter than $0.63L_{pp}$, the influence of ship motions on added resistance was negligible and the ship could be fixed. Increasing the wavelength increases the difference in added resistance results between a fixed and free ship.

1.5 Discussion of Methods

A calm water resistance method is used to identify changes in the calm water resistance due to changes in the bow section.

For the calm water resistance case, several numerical tools based on potential theory are available. Empirical methods only generates a statistical value based on a database of similar ships and would not be able to capture small changes of the hull shape. To be able to capture the changes of the bow shapes, one of the numerical solvers have to be used.

Due to the focus on large, slow ships in this thesis it is important to have a method that can calculate the short wave added resistance as well as the long wave added resistance. The radiation is expected to be less significant to these types of ships than for smaller ships. The models used are, as an approximation, initially straight walled and blunt. The flare has been removed. This enables the use of Faltinsen's formula in short waves, which have shown reasonably good results if the conditions are met. The formula is also easy to implement in a computer code. In the radiation region several methods are applicable, an integrated pressure method based on Faltinsen's method (refer to chapter 1.4.2) or a radiated energy method based on Gerritsma and Beukelman's method (refer to chapter 1.4.3). A comparison and evaluation of these methods will be done in chapter 5.1.3.

Another possibility is the use of CFD, more specifically RANS with VOF. This is precise for a wide range of wavelengths and bows that are not straight. However, this requires extensive computational time. Taking into account that due to short waves, the mesh will have to be very fine, the computational effort required is significant. However, when investigating the efficiency of unconventional bows CFD is needed to capture higher order effects that may occur when having inclined surfaces above the waterline.

The next chapter will establish the chosen methods that are expected to be able to capture the needs explained above.

2 METHODS

Methods to calculate the calm water and added resistance due to waves will be established in this chapter. The methods will be verified in chapter 5.1 by comparing results with benchmark data given in the literature. A method to implement wave statistics in evaluation of route performance for the ships will also be established as well as a method to evaluate the efficiency of an unconventional bow will also be established.

2.1 CALM WATER RESISTANCE

The calm water resistance needs to be established together with the added resistance for the different bow shapes to be able to evaluate the total performance of the design on a typical voyage.

The goal of the calm water resistance analysis is to establish a resistance curve as an input to the speed-loss calculations done in ShipX.

Empirical methods have been avoided, as much as possible, when estimating the calm water resistance in this thesis. The argumentation is that empirical methods are based on main characteristics of the ship and will not be able to properly account for details in the design of the bow. However, some methods have been used where it is assumed not to distort the results, and when computational effort is either difficult or too time consuming.

The calm water resistance is decomposed into different contributions. Two major components are the viscous resistance and the wave making resistance. The total resistance in calm water can be decomposed as

$$C_{Ts}=C_R+(1+k)(C_{Fs}+\Delta C_F) + C_{Apps} + C_{AAs}+C_{DBs} + C_A \qquad \text{Equation 2-1}$$

C_{Ts} – Total resistance coefficient in ship scale
C_R – Residual resistance coefficient
C_{Fs} - Skin friction coefficient in ship scale
ΔC_F – Hull roughness coefficient
C_{Apps} – Appendix resistance coefficient in ship scale
C_{AAs} – Air resistance coefficient for ship
C_{DBs} – Resistance coefficient of transom stern in ship scale
C_A – Correlation allowance due to model test results

C_A is the correlation allowance which is only added if C_R is found from model tests. The residual resistance is composed of several components. There is no standard decomposition of this coefficient, which may contribute to difficulties in comparison of results. One major component of the residual coefficient is the wave making resistance (C_W), which again can be composed to wave pattern resistance and wave breaking resistance (Larsson and Raven, 2010). The viscous pressure resistance, form effect on pressure, is sometimes accounted for by the form factor, and sometimes in the residual coefficient. This shows that the residual coefficient is not a well-defined component, and one need to be aware of the definition in each case.

In this thesis Friendship-framework with Shipflow integrated has been used to evaluate the wave resistance of the designs. Due to time constraints full CFD calculations of the viscous resistance have not been done with Shipflow. Instead the ITTC ‘57 formula as well as other empirical methods has been used to calculate the different contributions to viscous resistance from e.g. skin friction coefficient, hull roughness and transom stern.

2.1.1 WAVE RESISTANCE

The Friendship-framework is a program that focuses on optimization of flow-related tasks. It is a post-processing tool and provides methods for automatized optimization. It is set up to collaborate with different CFD software, which provides the analyses of the case being worked on. In this thesis the Friendship-framework is combined with Shipflow to calculate the wave resistance of the designs which is a component of the residual resistance coefficient, C_R.

XPAN is the solver used to calculate the wave resistance coefficient. It is a potential solver using a Rankine source panel method. Shipflow calculates the wave resistance in two ways, by transverse wave cuts and with pressure integration. With transverse wave cuts, Shipflow calculates the energy from the wave pattern that radiates from the ship through a transverse boundary behind the vessel. In the other method Shipflow calculates the pressure on the hull and this pressure is integrated over the hull surface, giving the wave resistance.

There are advantages and disadvantages with both methods. The pressure integration is very dependent on a good mesh, and in this case it seems like the low Froude number combined with the standard mesh produces poor results. Therefore the wave resistance coefficient from the wave cuts, which is less dependent on the mesh on the hull, is used to compare the different designs. However, this is sensitive to the mesh size on the free surface, as waves are numerically damped away from the vessel. Details of the results and verification can be seen in chapter 0.

The potential solver is not capable of capturing wave breaking, which can be a significant component of the wave resistance on large blunt ships, and thus leads to an error in the calculations.

2.1.2 VISCOUS RESISTANCE

The skin friction is directly proportional to the wetted surface of the ship, as this is defined as the friction on a plate with the same wetted surface as the vessel. To account for increased velocity over the hull surface due to the displacement of streamlines by the ship the form factor, k_f, has been applied. As mentioned in chapter 2.1 above, the form effect on pressure is sometimes accounted for in the form factor. Thus giving a form factor that is $k = k_f + k_p$.

2.1.2.1 PLATE FRICTION RESISTANCE

The skin friction resistance coefficient is calculated according to the ITTC ’57 formula. It is defined as

$$C_F = \frac{0.075}{(\log(R_N) - 2)^2} \qquad \text{Equation 2-2}$$

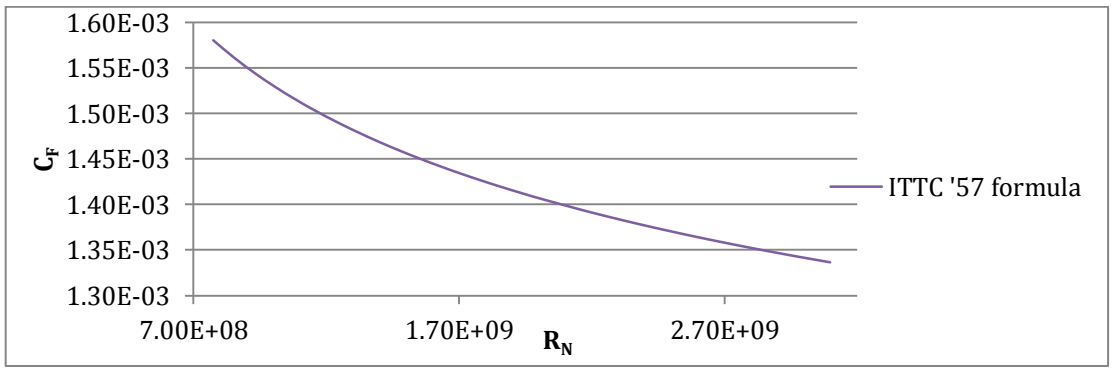

FIGURE 2.1 - ITTC-CURVE FOR FRICTION

2.1.2.2 FORM FACTOR

The form factor can be calculated by different empirical formulas. Such empirical formulas can never represent anything else other than the average of ships used in the analyses. Thus using such empirical methods could give a distorted result that does not represent the actual relative resistance between different designs.

One empirical formula that takes into account both the form effect on pressure and friction is Holtrop's method for predicting the form factor. It is shown below, (Minsaas and Steen, 2008).

$$k = -1 + 0.93 + 0.487118 \cdot C_{14} \left(\frac{B}{L}\right)^{1.06806} \cdot \ldots \left(\frac{T}{L}\right)^{0.46106} \cdot \left(\frac{L}{L_R}\right)^{0.121563} \cdot \left(\frac{L^3}{\nabla}\right)^{0.36486} \cdot (1 - C_P)^{-0.604247} \quad \text{Equation 2-3}$$

$L = L_{wl}$

C_P – Prismatic coefficient

$L_R = L \cdot (1 - C_P + 0.06 \cdot C_P \cdot \frac{L_{CB}}{4C_P - 1})$ = Distance from the bow to the parallel mid ship.

$C_{14} = 1 + 0.011 C_{stern}$

C_{Stern} – Coefficient describing the shape of the stern. C_{Stern}=10 (U-shaped)

This formula uses the prismatic coefficient, C_P, which describes the fullness of the ship towards aft and bow. A large C_P describes a ship with relatively large portion of the volume towards the ends. However, it is not given that this formula will give a correct relation between the different designs as it is very sensitive to main dimensions of the ship.

Prohaska's method is a method used to establish the form factor from experiments, and MARINTEK has developed one empirical formula as well, which does not include the form effect on pressure.

2.1.2.3 HULL ROUGHNESS

The hull roughness is also a significant contribution in resistance. It is calculated as an increase of the skin friction. The hull roughness is dependent on the type of coating, amount of rust, fractures in the coating, fouling etc. For ships in service the hull roughness resistance will increase during the lifetime due to fouling of the hull. Thus the hull roughness allowance calculated here is a first estimate. Results from measurements in wind tunnel, towing tank or cavitation tank have given rise to an approximated formula shown below, (Minsaas and Steen, 2008).

$$\Delta C_F = [110 \cdot (H \cdot V)^{0.21} - 403] \cdot {C_F}^2 \quad \text{Equation 2-4}$$

H ($10^{-3}\ mm$) – roughness

V – ship velocity (m/s)

When the roughness allowance according to Equation 2-4 is below zero, the roughness allowance is taken as zero.

2.1.2.4 TRANSOM STERN

KVLCC2 has a wet transom stern where the flow is separated and creates a suction pressure. This suction pressure arises as a result of the external flow, which carries away the dead water behind the transom. On ships with a large transom and low Froude numbers this component may be considerable. On KVLCC2 it is not very significant, but is still taken into account.

A formula based on experiments with projectiles in air has been made. When formulated using the wetted surface area it becomes (Minsaas and Steen, 2008):

$$C_{DB} = 0.029 \cdot \sqrt{\frac{(\frac{S_B}{S})^3}{C_F}}$$ Equation 2-5

This effect is not taken into account in the form factor due to the special dependence of C_F.

2.2 Added Resistance in Waves

The added resistance is calculated using ShipX. ShipX is a tool developed at MARINTEK in Trondheim. This tool has a plug-in (VERES) for calculating ship responses and motions based on the low speed strip theory formulation by Tuck et al. (1970). The added resistance post processor calculates the added resistance. The software gives a choice between strip theory and pressure integration for calculating responses. Choosing to calculate added resistance based on pressure integration gives a choice of methods in the long wave (radiation) region, either Gerritsma and Beukelmann or a pressure integration approach based on the methods in Faltinsen et al. (1980). Both approaches are combined with Faltinsen's asymptotic formula for added resistance in short wave (diffraction) region. Choosing ordinary strip theory leaves only Gerritsma and Beukelmann's method for calculation of added resistance in the radiation region.

To be able to combine the methods for added resistance due to ship motion induced wave generation and the asymptotic formula for short waves the software use the method of Fujii and Takahashi (1975), by multiplying the asymptotic formula with a correction factor that accounts for finite draft and wavelength. A more detailed explanation can be found in the VERES Theory Manual, (2010).

2.3 Added Resistance due to wind

Added resistance due to wind is not a focus in this thesis. The method used by Sunde (2011) is also adapted in this thesis. In ShipX a standard wind coefficient for a tanker in loaded condition is defined. It varies as a function of wind direction, which is set to the same as wave heading.

The wind speed is calculated by

$$C_X = \sqrt{\frac{9.81 \cdot H_S}{0.21}}$$ Equation 2-6

H_S – Significant wave height of the wave spectrum

The projected area is taken from calculations done by Sunde (2011) and is set to be A_{proj} = 920.8 m^2.

2.4 Route Simulation

ShipX also calculates the involuntary speed-loss on a route, based on engine and propeller characteristics, long term wave statistics, ship motions, calm water and added resistance from VERES.

It takes into account possible reduction in propeller efficiency as the vessel encounter waves due e.g. change in relative submergence of the propeller and corrects the open water diagram. It can also take into account change in engine efficiency due to change in loading.

The calculation of ship motions and added resistance is done in VERES and the results are used as input in the speed-loss calculations.

To calculate the speed-loss in irregular waves the open water diagram is corrected over regular waves. The wave-spectrum realization is cut into successive regular wave parts. Each regular wave has a given probability of occurrence based on Lounget-Higgins joint probability density function applicable to wave amplitude and period.

The speed-loss is calculated for each wave component. The speed-loss in the given sea state is calculated as a weighted average of the speed-losses for each component where the joint probability density is the weighting factor for the wave component.

To find the speed-loss on a given route the weighted average of the speed-loss for each sea-state is calculated. The weighting factor is based on the weighted scatter diagram described in chapter 4.2.1, containing information on the probability of occurrence for each sea state on the route.

2.5 Designing the Models

Variations of the bow have to be designed. The tool used for this is the Maxsurf suite by Formsys. The suite contains tools to do hull design with Maxsurf Pro, and other tools can be used for stability calculations, sea keeping calculations and resistance calculations to mention some.

In this thesis only the hull design features is used. The models are changed according to the methods described in chapter 3. More information on the software can be found here: https://www.formsys.com/maxsurf.

3 CHANGING BOW DESIGN

Evaluating the trade-off between calm water resistance and added resistance due to waves when changing the sharpness of the bow is not as straight forward as it might seem. The design is based on a finished design of a VLCC. Thus the base design is already designed for certain requirements and speed. Such requirements could be a ship owner's demand to load capacity and length due to size restrictions in ports or on special legs of voyages in canals etc.

3.1 RESISTANCE CONSIDERATIONS

When changing the bow design, it is important to evaluate all the aspects of the resistance. One can risk decreasing the efficiency of the design due to focusing on only one parameter. This section will look into the different resistance components and how they presumably will change with entrance angle. The resistance components that are assumed to not or to a small degree be influenced by the changes in the bow are not discussed, e.g. the wet transom stern resistance.

The friction component is ruled by the wetted surface of the underwater hull as well as the hull surface roughness. Thus a design that increases the wetted surface will increase the skin friction. It is not dependent on the shape of the hull, and thus it is difficult to avoid, other than minimizing the wetted surface. A sharp bow will by mathematical considerations have a larger wetted surface compared to a blunt bow, of the same displacement. The friction resistance is one of the major resistance components and a percentage change thus contributes more to an increase or decrease of the total resistance than other components. However, considering the large wetted surface area on KVLCC2, the change in wetted surface due to changes in the bow may not be significant.

The form factor is dependent on the shape of underwater hull. As explained in 2.1 it incorporates the increase of velocity over the hull due to the displacement of the streamlines as well as the form effect on the pressure. A longer, more slender bow increases the overall slenderness of the vessel, and thus the form factor should be decreased for a longer bow.

The wave making resistance is small for the large, slow ships compared to viscous resistance due to the low Froude number. It is very dependent on the shape of the hull. In theory the wave resistance could potentially increase drastically with changes in the bow shape due to e.g. interaction effects between the bow wave system and the fore shoulder wave system. Due to the low significance of this component, it is not a major concern. However, it should be monitored because it may be relatively simple to avoid such effects, thus avoiding unnecessary increase in the resistance.

The added resistance due to reflection of waves in head seas will decrease when the bow is sharpened, as found in Guo and Steen (2010b). The degree of change in the bow is a trade-off between the ratio of time spent in calm water and wave conditions and the severity of the wave conditions. If the vessels encounters short waves most of the time, a sharper bow may be optimal. However, if the encountered waves are in the radiation regime the majority of the operating time a sharper bow is expected to be less, as the motion characteristics are most important in this range. The sharpness also rules the amount of reduction of added resistance in waves. Thus, a sharper bow will in theory have less added resistance, but the trade-off with calm water resistance will restrict an extremely long bow.

3.2 LENGTH AND DISPLACEMENT CONSIDERATIONS

Sharpening of the bow shape can be done in basically two ways. This is schematically shown in Figure 3.1 below. The black line represents a half-circle shaped bow. The blue line is a sharpening of the bow when keeping the length fixed. The volume is removed from the shoulders. This will

require the displacement to decrease, which in turn will require the available cargo space to decrease. This might be a problem for the ship owners wanting to carry as much cargo as possible for a given length. This way of sharpening the bow will possibly decrease the wetted surface, considering skin friction resistance, though sacrificing volume.

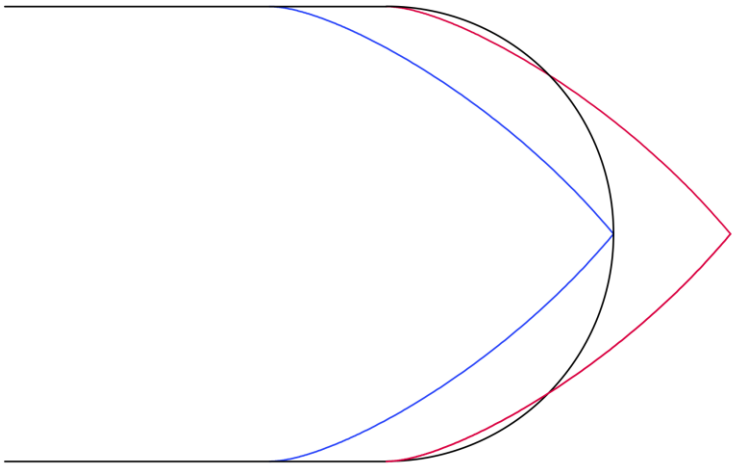

FIGURE 3.1 - SCHEMTAICALLY OPTIONS OF CHANGING THE BOW SHAPE. BLACK LINE IS ORIGINAL BOW SHAPE, BLUE LINE IS DECREASED DISPLACEMENT AND RED LINE IS LENGTHENED SHIP.

Increasing the length as shown in the red line will increase the displacement, of the ship. However, this may cause issues regarding length requirements in ports or on certain parts of a route such as canals.

Keeping the displacement fixed can be done by shifting volume from the shoulders to the front of the bow as shown in Figure 3.2. Here the volume in 1 and 2 are shifted to 3. This will maintain the displacement. It is basically a combination of the extremes shown in Figure 3.1. However, the length will in this case also necessarily be increased. Regarding resistance, the wetted surface to volume ratio of this transformation will increase.

When changing the bow shape from the base-case, hydrostatic values may also change. One important hydrostatic value is the Longitudinal Centre of Buoyancy (LCB). The original design has an LCB that is coordinated with the Longitudinal Centre of Gravity (LCG). Shifting the LCB will induce a change in trim on the ship.

When designing alternatives the LCB is monitored closely and an effort is put into keeping it as constant as possible. However, shifting volume forward will induce some change in the LCB and an assumption has to be made that the trim can be compensated by shifting weights. Due to the sheer size of KVLCC2 the change in percentages of L_{PP} is small as can be seen if one compares KVLCC2A and KVLCC2C in Table 3.1 and Table 3.3.

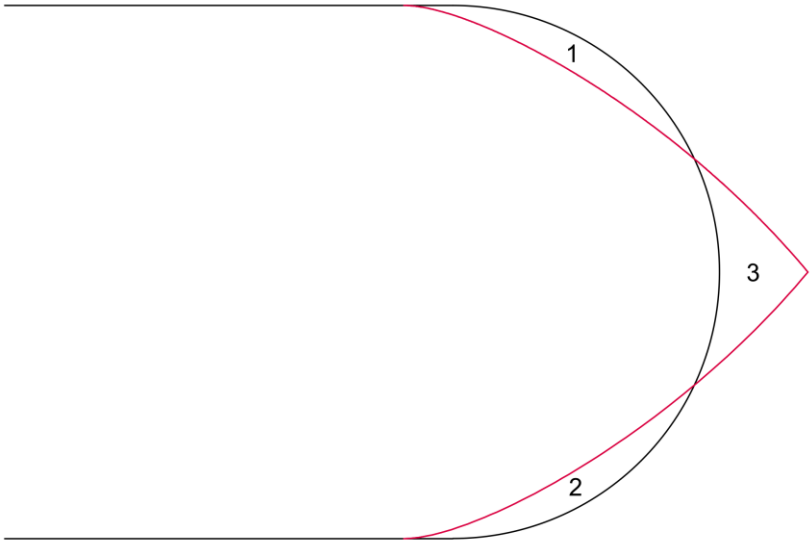

FIGURE 3.2 - COMBINATION OF THE TWO DESIGNS. THE VOLUME MOVED FROM 1 AND 2 IS EQUAL TO VOLUME 3

The original KVLCC2 is designed with a bulb extending 8 meters in front of the fore perpendicular. Regarding the length of the ship as $L=L_{PP}+L_{bulb}$ it is possible to move volume from the shoulders and forward over the bulb as seen in Figure 3.3.

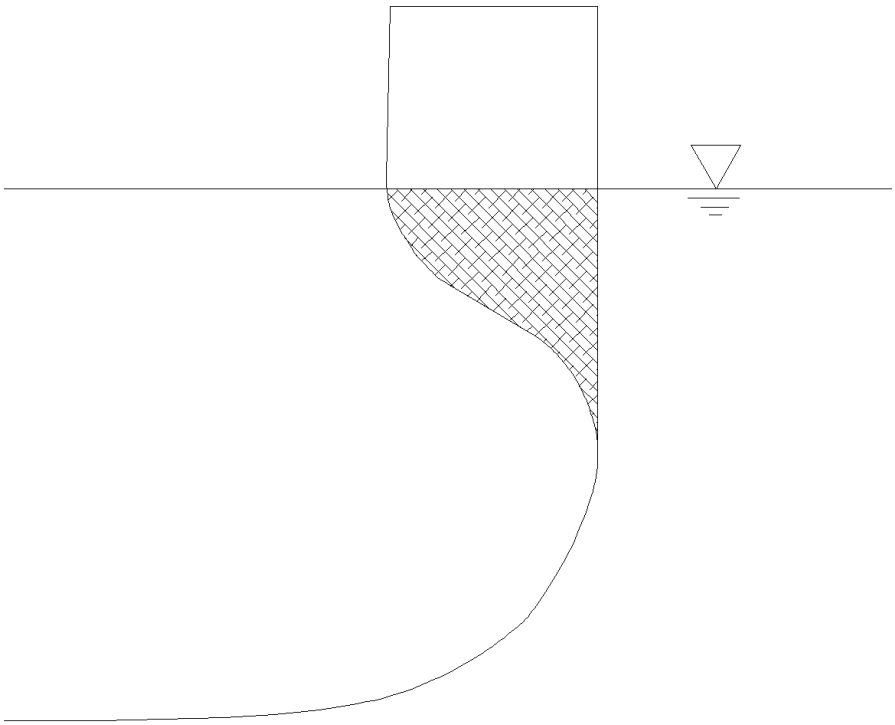

FIGURE 3.3 - THE HATCHED AREA CAN BE USED TO MOVE VOLUME FORWARD AND MAKING THE BOW SHARPER

3.3 THE DESIGNS

Several designs have been made for this thesis. They represent different waterline curves and approaches to changing the bow. A short explanation of the design and characteristics are presented below.

3.3.1 KVLCC2A

KVLCC2 is the second variant of the MOERI tanker that has been used as an academic standard within CFD validation. The additional notation A means, in this thesis, that it is the original design with bulb. This has been used for verification of the methods used to analyse the calm water and added resistance. To fulfil the requirement in Faltinsen's method for added resistance in short waves, the flare in the bow has been removed such that the sides are more or less straight in the waterline. The body plan of the ship can be seen in Figure 3.4.

The iges-file provided on Simman2008 (2008) had many surfaces that produced poor offsets in Shipflow and thus it had to be redesigned in Maxsurf to get at smooth surface. Due to this, the main particulars of this ship, shown in Table 3.1 are slightly different from the given in Table 1.1.

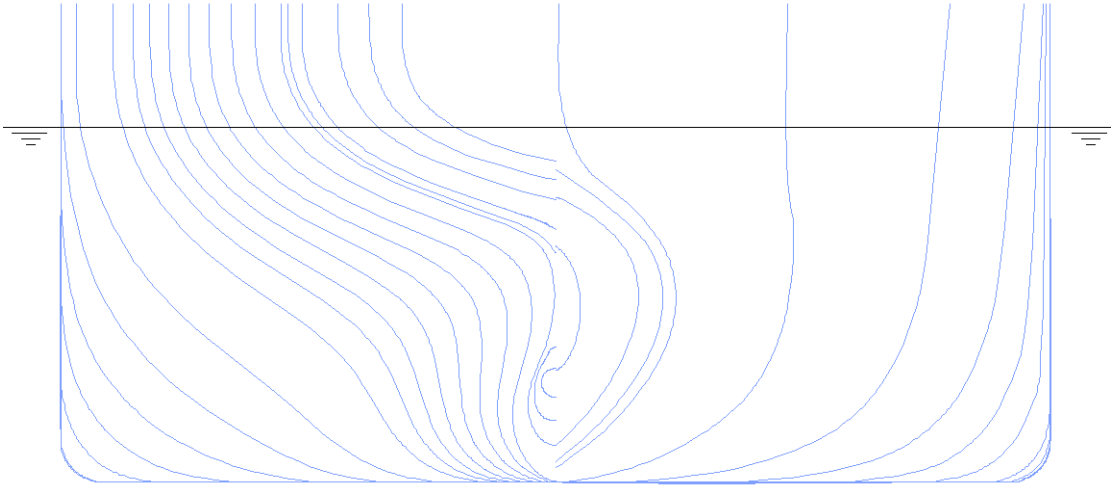

FIGURE 3.4 - KVLCC2A BODY BLAN

TABLE 3.1 - MAIN DIMENSIONS KVLCC2A

Main Particulars	KVLCC2A
L_{pp} (m)	320.0
L_{wl} (m)	325.5
B_{wl} (m)	58.0
D (m)	28.0
T (m)	20.8
Displacement ∇ (m^3)	312948.6
S excl. rudder (m^2)	27663.4
C_B	0.797
C_M	0.999
LCB (%). fwd+ from amidship	3.46
LCB (m) from AP	171.3

3.3.2 KVLCC2B

KVLCC2B in this thesis is similar to KVLCC2B used in Guo (2011). However, due to lack of a 3D model the version in this thesis was designed in Maxsurf based on the description and main dimensions given in Guo (2011).

The main concept of this design is the straight sides all the way down with a small bilge radius. The bulb is removed and it has the same curvature in the waterline as KVLCC2A. The wetted surface area of this is considerably larger and thus is expected to produce poor overall results. It is used in the analysis to study the effect of wetted surface area on the overall performance.

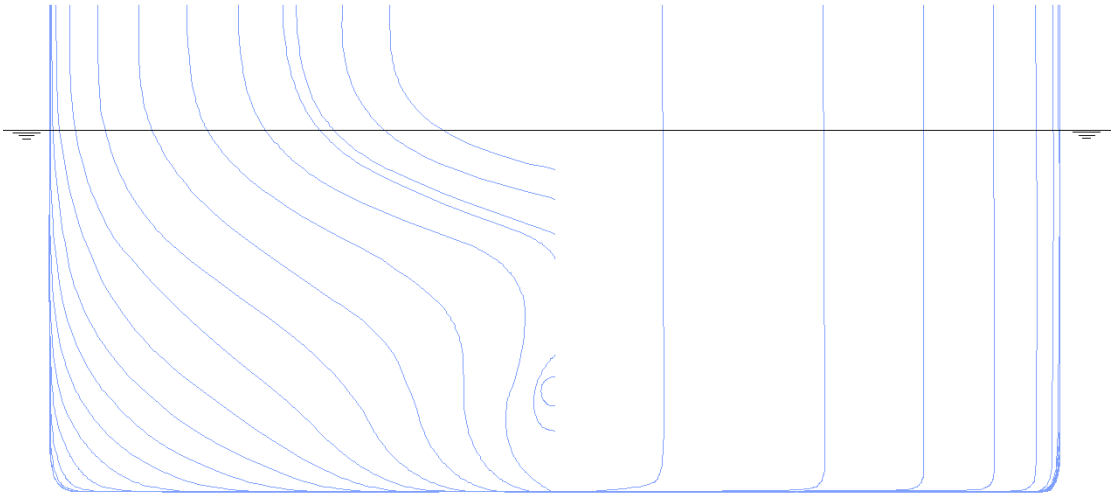

FIGURE 3.5 - KVLCC2B BODY PLAN

TABLE 3.2 - MAIN DIMENSIONS KVLCC2B

Main Particulars	KVLCC2B
L_{pp} (m)	320
L_{wl} (m)	325.5
B_{wl} (m)	58
D (m)	28
T (m)	20.8
Displacement ∇ (m^3)	314373.1
S excl. rudder (m^2)	28146.4
C_B	0.8
C_M	0.999
LCB (%). fwd+ from amidship	3.559
LCB (m) from AP	171.6

3.3.3 KVLCC2C

KVLCC2C was also produced by Guo (2011). It is based on line drawings provided by Professor Sverre Steen. It has a sharper entrance angle than KVLCC2A and KVLCC2B. It is designed by the principle of moving volume from the shoulders to fill in the volume above the bulb, thus the L_{PP} is lengthened by 8 m and the C_B is slightly reduced. However, the overall length is maintained. The bow is slightly trimmed down below the waterline to keep the displacement and LCB as constant as possible.

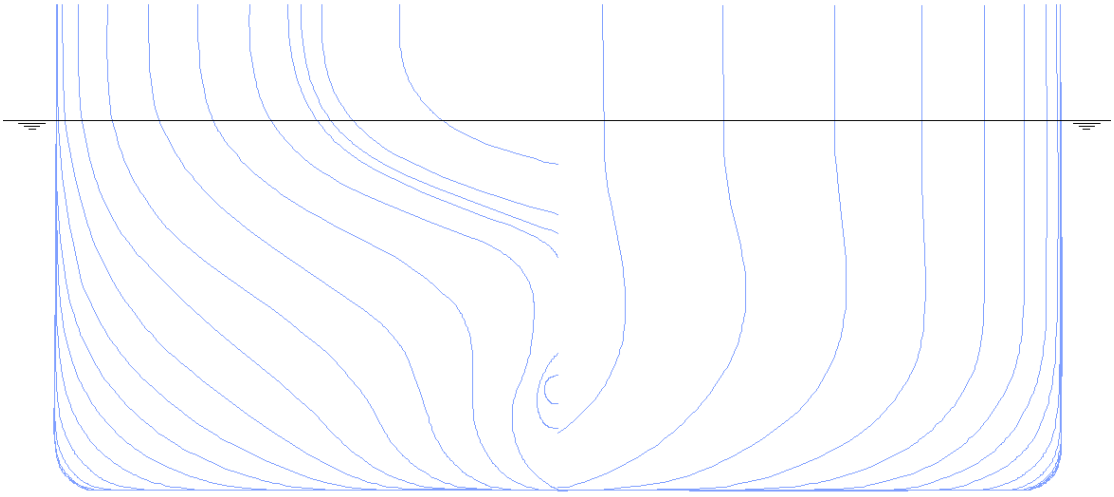

FIGURE 3.6 - KVLCC2C BODY PLAN

TABLE 3.3 - MAIN DIMENSIONS KVLCC2C

Main Particulars	KVLCC2C
L_{pp} (m)	328.0
L_{wl} (m)	333.5
B_{wl} (m)	58.0
D (m)	30.0
T (m)	20.8
Displacement ∇ (m^3)	313049.4
S excl. rudder (m^2)	27787.7
C_B	0.776
C_M	0.998
LCB (%). fwd+ from amidship	2.169
LCB (m) from AP	171.2

3.3.4 KVLCC2D

KVLCC2D is a blunter version of KVLCC2A, however, without bulb. It is made to get even more extreme results from the analyses. KVLCC2A is blunt, but has a sharp angle in the bow, thus this is made to get a more continuous curve at the bow. The length of 320 m is kept constant and the displacement is increased and thus the C_B is also larger. The lines under the waterline are somewhat slimmer than KVLCC2A to reduce the displacement and wetted surface that increases due to the fattening of the bow. The LCB is further forward from the Aft Perpendicular (AP) than for KVLCC2A and an assumption is made that it is possible to move weights forward due to the increased volume in the bow.

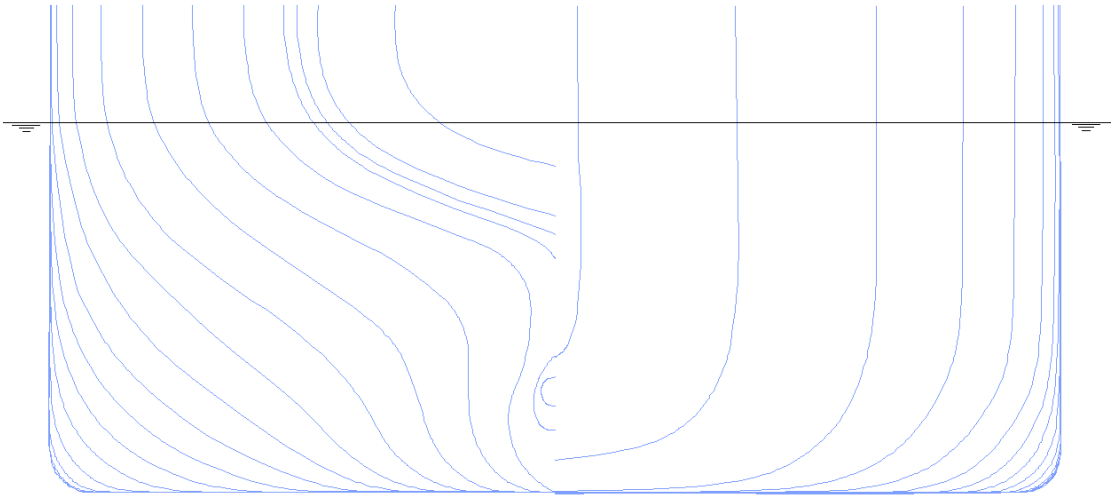

FIGURE 3.7 - KVLCC2D BODY PLAN

TABLE 3.4 - MAIN DIMENSIONS KVLCC2D

Main Particulars	KVLCC2D
L_{pp} (m)	320
L_{wl} (m)	325.5
B_{wl} (m)	58
D (m)	28
T (m)	20.8
Displacement ∇ (m^3)	314992.6
S excl. rudder (m^2)	27691.8
C_B	0.8
C_M	0.999
LCB (%). fwd+ from amidship	3.647
LCB (m) from AP	171.9

3.3.5 KVLCC2E

KVLCC2E is an elongated version of KVLCC2C, without any bulbous curvature in the bow. It is on the other side of the extremes compared to KVLCC2D. The bow is elongated by 8 m to 336 m compared to KVLCC2C. Due to the elongation of the bow, the C_B is reduced and the LCB is moved forward.

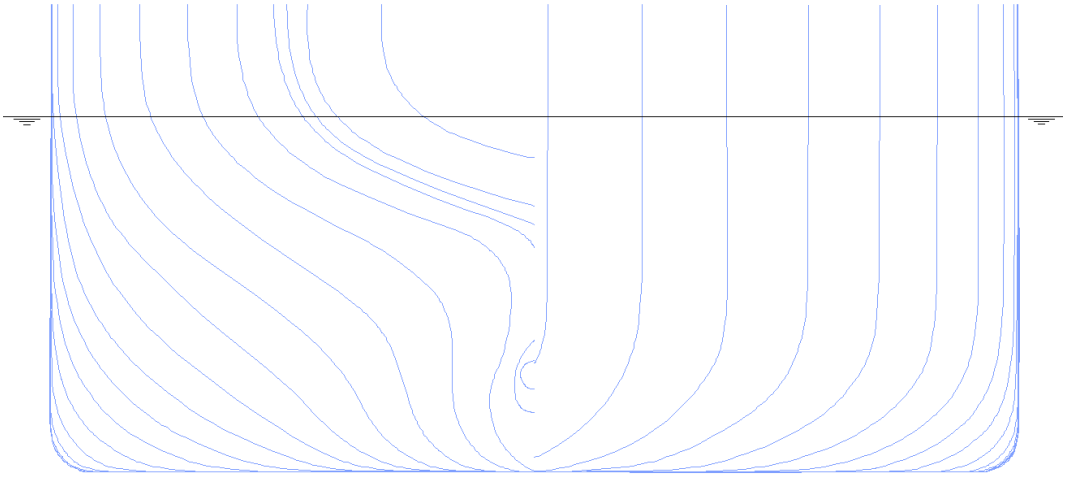

FIGURE 3.8 - KVLCC2E BODY PLAN

TABLE 3.5 - MAIN DIMENSIONS KVLCC2E

Main Particulars	KVLCC2E
L_{pp} (m)	336
L_{wl} (m)	341.5
B_{wl} (m)	58
D (m)	28
T (m)	20.8
Displacement ∇ (m^3)	314026.6
S excl. rudder (m^2)	27982.8
C_B	0.774
C_M	0.998
LCB (%). fwd+ from amidship	1.212
LCB (m) from AP	172.1

3.3.6 WATERLINES

In Figure 3.9 below the waterlines of the different designs are shown as well as the half angle of entrance in the bow. As seen in the figure, KVLCC2E is longer and sharper, and should thus reduce the added resistance, at least the diffraction component in head seas. However, due to the increased wetted surface and frictional resistance one can expect a decreased benefit.

It can be seen by the tables above that KVLCC2D has more volume than KVLCC2A, but the wetted surface is more or less the same. As mentioned this was achieved by slightly slimming down the underwater hull at the bow compared to KVLCC2A. The removal of the bulb also influences to reduce the wetted surface, as the bulb has a high surface area to volume ratio.

In the figure the lines of KVLCC2A and KVLCC2B coincide.

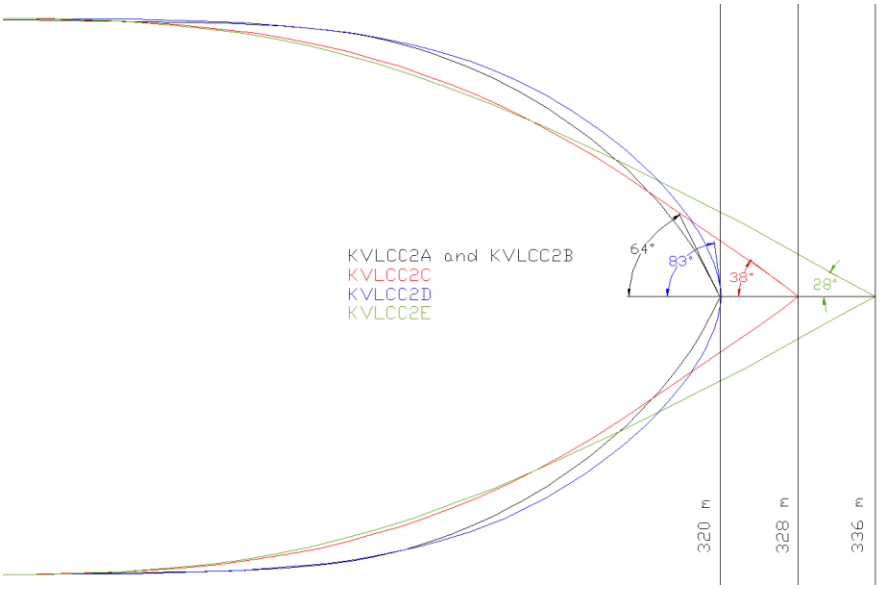

FIGURE 3.9 - WATERLINES OF THE DESIGNS

3.3.7 SECTIONAL AREA CURVE

The sectional area curve for KVLCC2A and a detail of the bow area of all the designs are shown in Figure 3.10 and Figure 3.11.

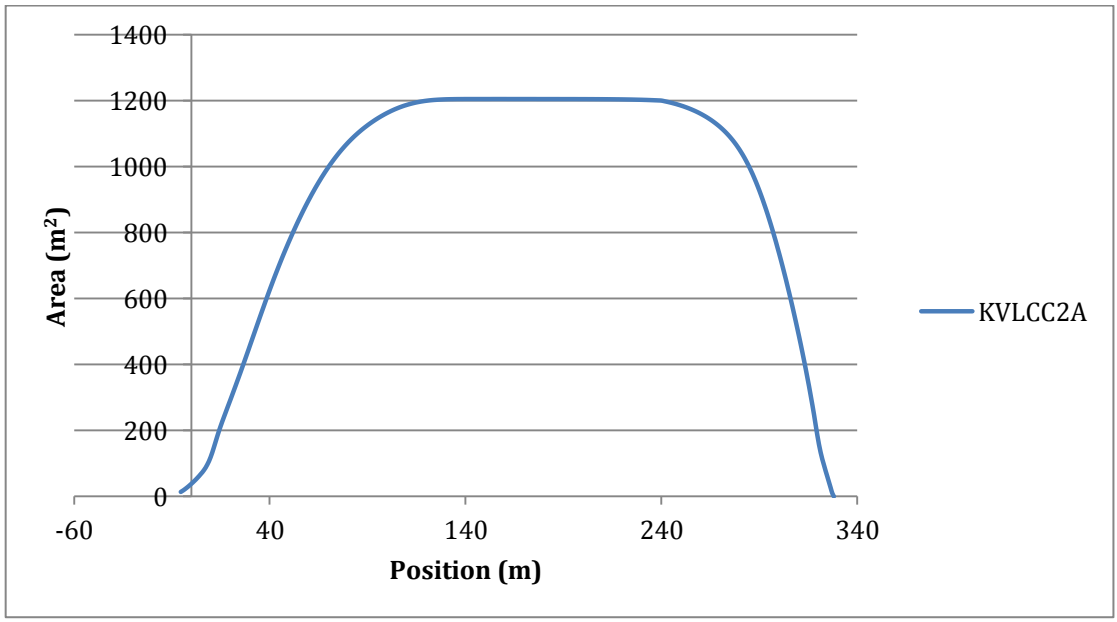

FIGURE 3.10 - SECTIONAL AREA CURVE OF KVLCC2A

KVLCC2B has more volume between 260 m and ~300 m due to the straight sides all the way down. It is also without bulb, as all the designs except KVLCC2A which makes it shorter than KVLCC2A. Both KVLCC2C and KVLCC2E have some volume cut from the shoulders between 270 m and 310 m. However, these are longer in the waterline and thus this volume is moved forward. KVLCC2D is the bluntest of the designs and this is seen by the steeper ending of the sectional area curve. It has more area than KVLCC2A between 250 m and 315 m because the shoulders have been moved forward and thus has a higher displacement.

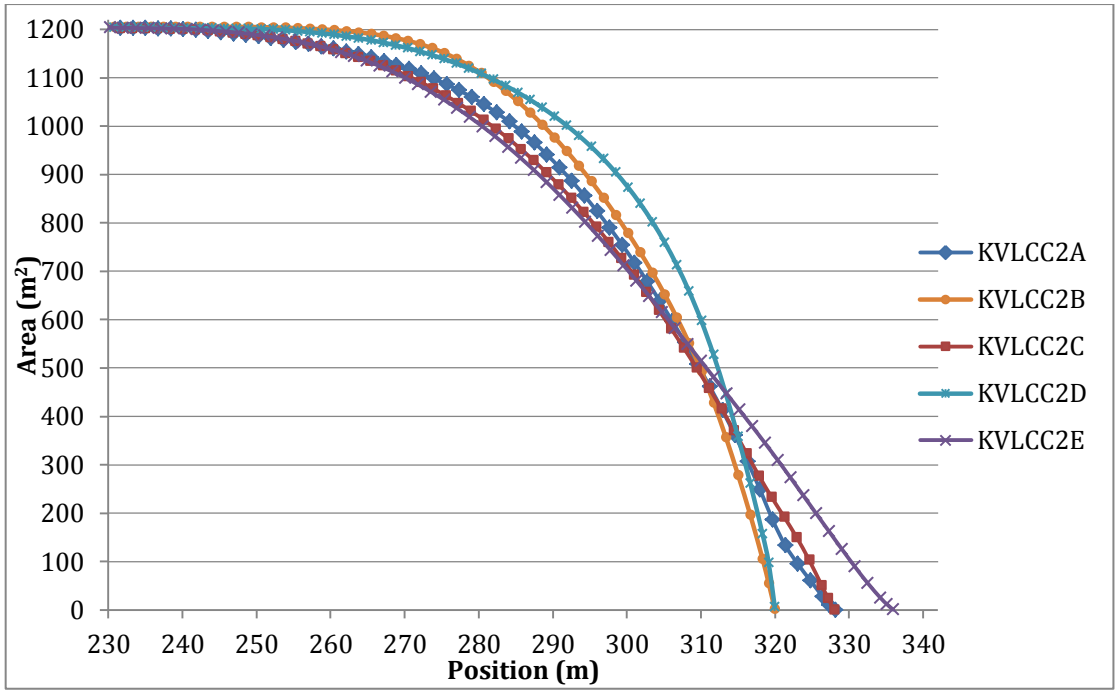

FIGURE 3.11 - SECTIONAL AREA CURVE OF THE BOW AREA OF ALL DESIGNS

3.3.8 EXPECTED PERFORMANCE

The relative expected performance on a route between the different designs regarding key parameters frictional resistance and added resistance can be seen in Figure 3.12. The frictional resistance is the major component of the calm water resistance and is thus used as a parameter here. This chart shows the relative performance in added resistance based on bow shape, and the frictional resistance based on wetted surface. It is only a graphical presentation of the personal perception of level of performance and not weighted by the significance of added resistance and frictional resistance on the total performance. The difference in added resistance is based mostly on the diffraction effect as the motions and radiation is more difficult to intuitively range.

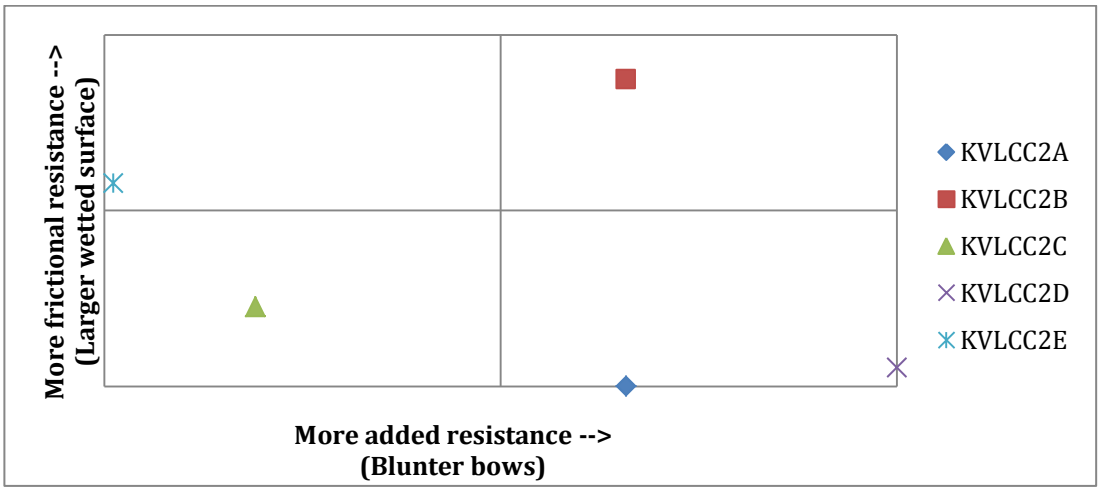

FIGURE 3.12 - RELATIVE PERFORMANCE BETWEEN DESIGNS REGARDING FRICTIONAL RESISTANCE AND ADDED RESISTANCE

Figure 3.12 shows that the expected performance of KVLCC2B is poor both with regards to added resistance and frictional resistance, due to the blunt bow and straight sides.

KVLCC2D is expected to perform well with regard to frictional resistance, however, the worst to added resistance.

KVLCC2C has bigger a wetted surface than KVLCC2A, but not nearly as much as KVLCC2E or KVLCC2B. The increase in wetted surface due to the longer bow, is not as big as one might expect compared to KVLCC2A and KVLCC2E. This may be ascribed to the fact that KVLCC2A has a bulb, and thus some area in front of the fore perpendicular that does not represent an increase in the wetted surface area when designing KVLCC2C. The added resistance of KVLCC2C is expected to be good. Overall the vessel is a compromise between KVLCC2A and KVLCC2E.

KVLCC2E is the extreme design with regard to added resistance. It has the worst performance in frictional resistance of the naturally shaped bows, i.e. excluding KVLCC2B which has a large wetted surface due to the inconvenient design.

It is difficult to give an expected best performer as it depends on the relative significance between the different resistance components, and for added resistance the severity of the sea states the vessel will encounter.

4 ROUTES AND WAVE STATISTICS

The calm water conditions most ship designs are optimized for is a rare event for the large ocean going vessels. To be able to get a realistic evaluation of the performance of ships, the operating profile should be taken into account. Due to time restriction, a full operational profile will not be evaluated in this thesis, which is recommended if a design study is carried out. In this thesis only the fully laden case with 100% DWT utilization will be investigated. This chapter will establish typical routes and wave statistics for these.

4.1 ROUTES

The report on Triality (2010), by DNV, considers the main trade routes for VLCC's world-wide. They point out that most VLCCs originate in the Arabian Gulf and have three main markets; East Asia, US and Europe. Based on this, two routes have been chosen as a typical voyage for a VLCC in this thesis.

In addition a route across the North Atlantic, which hosts some of the most severe sea conditions in the world, is chosen to get a variation of characteristic sea states.

Even though KVLCC2 is designed as a VLCC, the size and shape of the hull is close to a typical large bulk carrier. Therefore one bulk route has been chosen in this thesis.

Typical bulk routes are dependent on the type of trade that is being considered. Cape size vessels are focused on long haul iron ore and coal trade routes (Genco, 2012). Typical iron ore trade routes are from Port Hedland in Australia or Brazil to China with e.g. Qingdao as discharge port. Iron ore supply from Australia and Brazil accounted for 64.4% of the imported iron ore to China in 2009 (China-Daily, 2010). Due to lack of wave statistics in the Java Sea, Banda Sea and Arafura Sea only the route from Brazil to China has been chosen as a bulk route. The routes can be seen in Figure 4.1.

4.1.1 ARABIAN GULF – GULF OF MEXICO

The first route originates in the Arabian Gulf. The origin port is typically Ras Tanura, one of the largest ports in the world for crude oil (Saudi-Aramco, 2012). The voyage goes south down and around the Cape of Good Hope, across the South Atlantic Ocean and ends in the Gulf of Mexico. Louisiana Offshore Oil Port (LOOP) is the largest point of entry for crude oil coming in to the U.S.

4.1.2 ARABIAN GULF - JAPAN

The other route and a route that is expected to grow in the future is the route from the Arabian Gulf to the Far East. Ras Tanura is again the origin port. The destination port is Chiba, Japan. This is the largest port in Japan and handles large crude oil tankers.

4.1.3 WESTERN EUROPE – EAST COAST, NORTH AMERICA

North America, including west and east coast, imported about 682 million tonnes of oil in 2005. In 2004 the seaborne trade from the North Sea to North America was 46 million tonnes of a total seaborne trade from the North Sea of 62 million tonnes (Stopford, 2009). Mongstad in Norway is one of the largest export ports of crude oil in the North Sea and is used as loading port, while New York is used as a discharge port on the East Coast of North America.

4.1.4 BRAZIL – CHINA

Vale S.A. is a Brazilian mining company, second largest in the world, and the largest producer of iron ore. The company is one of the largest logistics operators in Brazil and owns the port of Tubarão, which is the largest iron ore export port in the world (Løvstad, 2008). The port of Qingdao in China has a terminal for handling large iron ore bulk carriers.

4.2 WAVE STATISTICS

This chapter will briefly describe the basics of wave statistics and establish the wave statistics for the typical routes chosen in the last section.

The wave conditions on a location will vary significantly over time. Even during hours the wave conditions can change. Thus to evaluate the vessels for regular waves will have no value when trying to estimate the best performance in a realistic scenario other than establishing the characteristics of the vessel responses in waves over a range of wave periods. Irregular waves, waves of different periods and heights, are the case in the real world and often the waves are also spread out in direction, making the surface chaotic.

Typically, wave characteristics are measured by buoys or reported by ships. The measurements of buoys are used to establish wave spectra. These spectra contain information about the energy distribution over wave frequency and are more or less specific for a certain ocean area and several spectra have been defined throughout the years. They are defined as an energy distribution over period or frequency given by certain spectral parameters like the significant wave height and a characteristic period (H_S and T_Z for Pierson-Moskowitz spectrum). Since the waves in real life are spread out over the direction, the energy is too. A directional wave spectrum describes not only how the energy varies with wave period, but also how it varies with direction.

Short term statistics utilizes these spectra to describe the sea surface within a certain period of time, where the parameters can be assumed constant, called a sea state. A widely used time period is 3 hours. Thus one assumes that the sea state is constant for 3 hours. However, during a year, or the lifetime of the vessel, the vessel will encounter a wide range of sea states that can be described by changing the characteristic spectral parameters. However, some sea states appear more often than others in an area. Thus some sea states have a higher probability of occurrence when thinking statistics. To utilize long term statistics a probability distribution of the sea states is thus needed. This will be described in the next chapter.

4.2.1 LONG TERM STATISTICS

The long term statistics are defined by a scatter diagram. This diagram shows the probability of occurrence of a combination of significant wave height and a characteristic period. In this thesis it is the zero crossing period, T_Z. An example of the scatter diagrams used in this report can be seen in Appendix A.

To generate the needed scatter diagrams for the routes RouteSim by DNV is used. It contains wave data for specified zones around the world.

The routes have to be defined with area number and the length ratio of the route segment in the specified area. In Figure 4.1, the map of the predefined areas in RouteSim is shown. The red lines in the map are the VLCC routes and the yellow are the iron ore bulk route described above. The green is the North Atlantic route.

RouteSim contains information about scatter diagrams in each zone. These will be extracted and weighted with respect to the length ratio of each area and a weighted scatter diagram for the total route will be used as input to ShipX. The input to RouteSim is shown in Table 4.1. The area number in Table 4.1 corresponds to an area on the map in Figure 4.1. The ratio is the length in each area divided by the total length of the route in percentage. Table 4.2 shows the corresponding length in nautical miles.

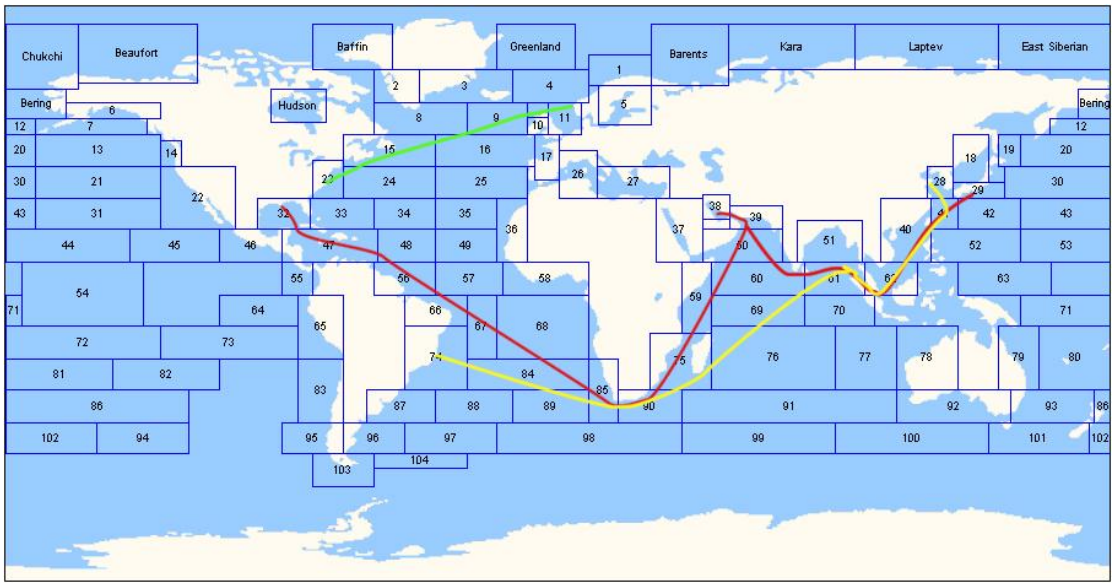

FIGURE 4.1 - MAP OF PREDEFINED AREAS AND ROUTES. RED LINES IS VLCC ROUTES AND YELLOW IS THE IRON ORE BULK ROUTE. THE GREEN IS FROM MONGSTAD TO NEW YORK

TABLE 4.1 - AREA AND RATIOS USED AS INPUT TO ROUTESIM

Ras Tanura - LOOP		Ras Tanura - Chiba		Tubarão - Qingdao		Mongstad - New York	
Area Number	Ratio (%)	Area Number	Ratio (%)	Area Number	Ratio (%)	Area Number	Ratio (%)
32	4.09	29	9.86	28	2.39	9	29.63
38	3.43	38	6.42	40	7.26	11	9.09
39	3.58	39	6.70	41	5.34	15	35.02
47	12.46	40	11.73	61	11.21	16	11.03
48	1.99	41	9.00	62	8.79	23	7.62
50	5.28	50	12.08	69	8.21	24	7.62
56	8.13	60	10.29	74	5.88		
59	6.04	61	17.81	75	6.62		
60	6.04	62	16.11	76	11.67		
66	4.09			84	10.14		
67	5.14			85	4.99		
68	7.13			89	6.37		
75	9.62			90	11.12		
84	8.18						
85	4.89						
90	9.91						

TABLE 4.2 - TOTAL DISTANCES (SOURCE: HTTP://WWW.SEA-DISTANCES.COM/)

Route	Total distance (nm)
Ras Tanura - LOOP	12299
Ras Tanura - Chiba	6608
Mongstad - New York	3365
Tubarão - Qingdao	11086

In order to do long term statistics calculations in ShipX assumptions on the wave spectrum for each route have to be made. ShipX gives a choice between Pierson-Moskowitz spectrum, JONSWAP spectrum and Torsethaugen spectrum.

The JOint North Sea WAve Project (JONSWAP) spectrum is based on measurements in the North Sea. The peak in the spectrum is more pronounced than in the Pierson-Moskowitz spectrum. This is a characteristic of the waves in the North Sea.

The Pierson-Moskowitz spectrum describes a fully developed sea. This means that the wind has been steady long enough for the waves to come to a sort of equilibrium with the wind. The spectrum was developed from measurements in the North Atlantic during 1964.

The Torsethaugen spectrum is a double peak spectrum that has frequently been used for design purposes at the Norwegian Continental Shelf, both in connection with numerical analyses and model tests. The spectrum was established by fitting two JONSWAP shaped models to average measured spectra from the Norwegian Continental Shelf (Torsethaugen and Haver, 2004).

Due to the limited availability of area specific spectra in ShipX, a simplification is made, and only one type is assumed for the whole route. The most general for open ocean areas is the Pierson-Moskowitz spectrum and this one is thus applied on all routes.

4.2.2 Validity of Faltinsen's Formula

In Faltinsen (1990) it is stated that there for a two parameter Pierson-Moskowitz spectrum is no significant energy for

$$\frac{\omega T_Z}{2\pi} < 0.5 \qquad \text{Equation 4-1}$$

And by using the dispersion relation and requirements for short waves it is found that long term statistics in combination with Faltinsen's formula for added resistance in short waves can only be used when

$$T_Z < 0.9\left(\frac{L}{g}\right)^{\frac{1}{2}} \qquad \text{Equation 4-2}$$

This requirement gives that for a vessel of 320 m T_Z<5.14 s.

4.2.3 Scatter Diagrams

The weighted scatter diagrams are presented below. There are no specified directions in these diagrams as this is not provided by RouteSim, they are so-called omnidirectional. Hence, a simplification has been made to be able to utilize the information in the wave statistics.

In the input file to ShipX the period utilized has to be specified, and ShipX then computes other spectrum periods from this if needed. The scatter diagrams are given by H_S and T_Z, and thus T_Z will be specified in the input file of ShipX.

In Figure 4.2 the weighted scatter diagram for the route from Ras Tanura to Chiba is shown. The floor axes show H_S and T_Z and the vertical axis shows the probability of the occurrence for a combination of H_S and T_Z. As seen the probability of a sea state with a H_S>6.5 m or T_Z>10 s is very low.

In Figure 4.3 the Cumulative Distribution Function (CDF) is shown. The cumulative distribution function used is defined as

$$\hat{F}_{T_Z}(T_Z) = \frac{n_{T_Z}}{n+1} \qquad \text{Equation 4-3}$$

n – total number of observations
n_{T_Z} – number of observations lower or equal to (T_Z)

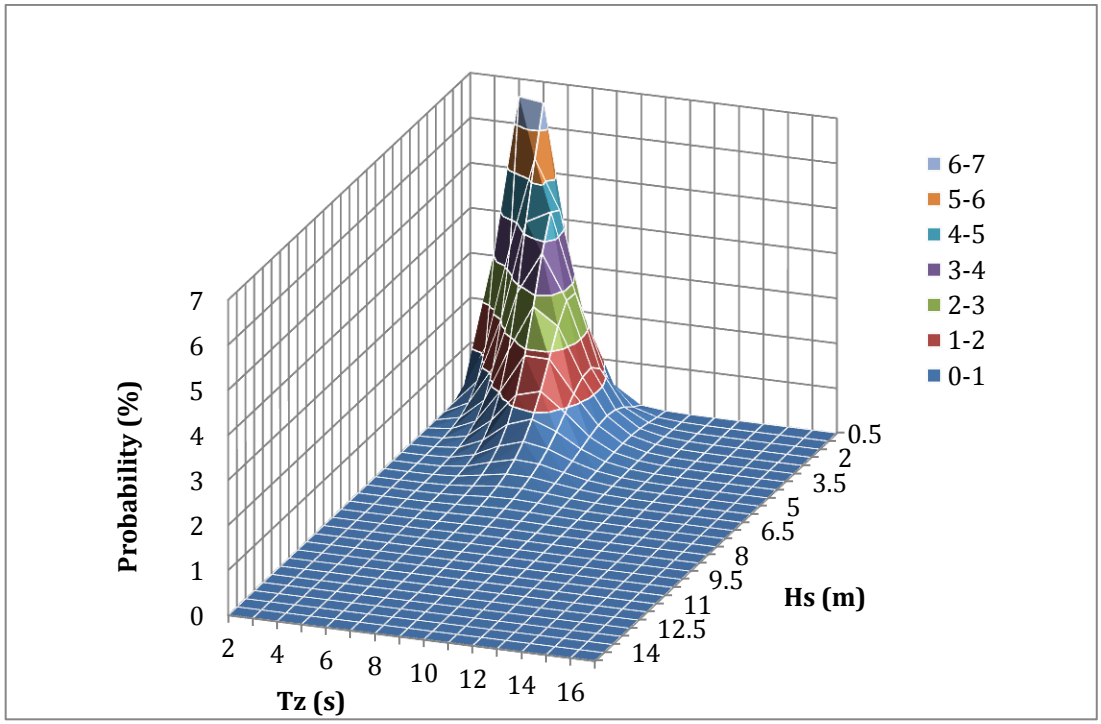

FIGURE 4.2 - WEIGHTED SCATTER DIAGRAM FROM RAS TANURA TO CHIBA

By using the requirement given by Equation 4-2 we can see from Figure 4.3 that on the route from Ras Tanura to Chiba about 50% of the sea states are below T_Z=5.14 s. This shows that a large portion of the encountered waves are within the short wave assumption of Faltinsen's formula and thus the diffraction effect cannot be neglected, and will be a significant contribution to the speed-loss. Corresponding values for the other routes are shown in Table 4.3.

TABLE 4.3 - PERCENTAGE OF SEA STATES WITHIN THE LIMITATIONS OF FALTINSEN'S FORMULA FOR ADDED RESISTANCE IN SHORT WAVES

Route	$\hat{F}_{T_Z}(T_Z < 5.14\ s)$
Ras Tanura to LOOP	~20%
Ras Tanura to Chiba	~50%
Mongstad to New York	~11%
Tubarão to Qingdao	~20%

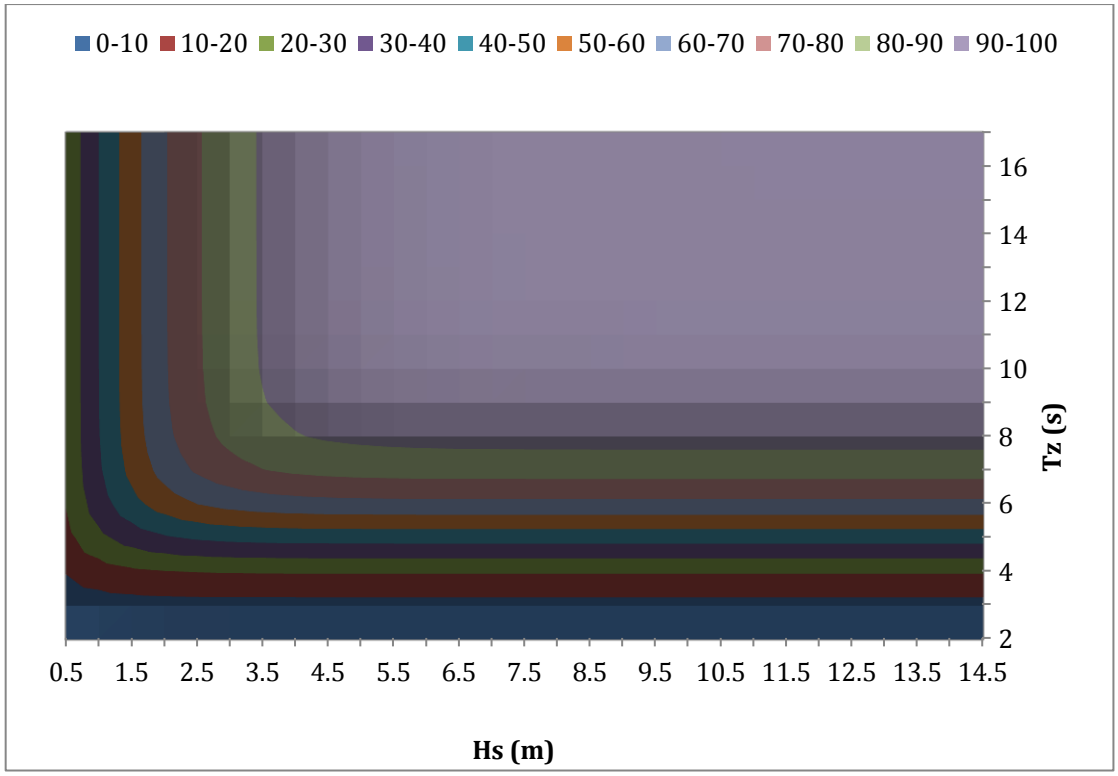

FIGURE 4.3 - THE CUMULATIVE DISTRIBUTION FUNCTION IN PERCENT – RAS TANURA – CHIBA

From Table 4.3 it can be noted that the route across the North Atlantic is the one with least sea states below the criteria for Faltinsen's formula. This is as expected, as the North Atlantic is known to be one of the harsher oceans in the world. This means also that added resistance due to diffraction is of less significance in this area compared to the other routes and that the sharper bows may be less effective on this route.

The scatter diagrams for the rest of the routes can be seen below. It can be noted that the two routes departing from Ras Tanura have about 90% of the sea states below $H_S \cong 3.5$ m, whilst Mongstad – New York being the extreme case with 90% of the sea states below $H_S \cong 5.25$ m, with just ~70% under $H_S \cong 3.5$ m (Figure 4.7).

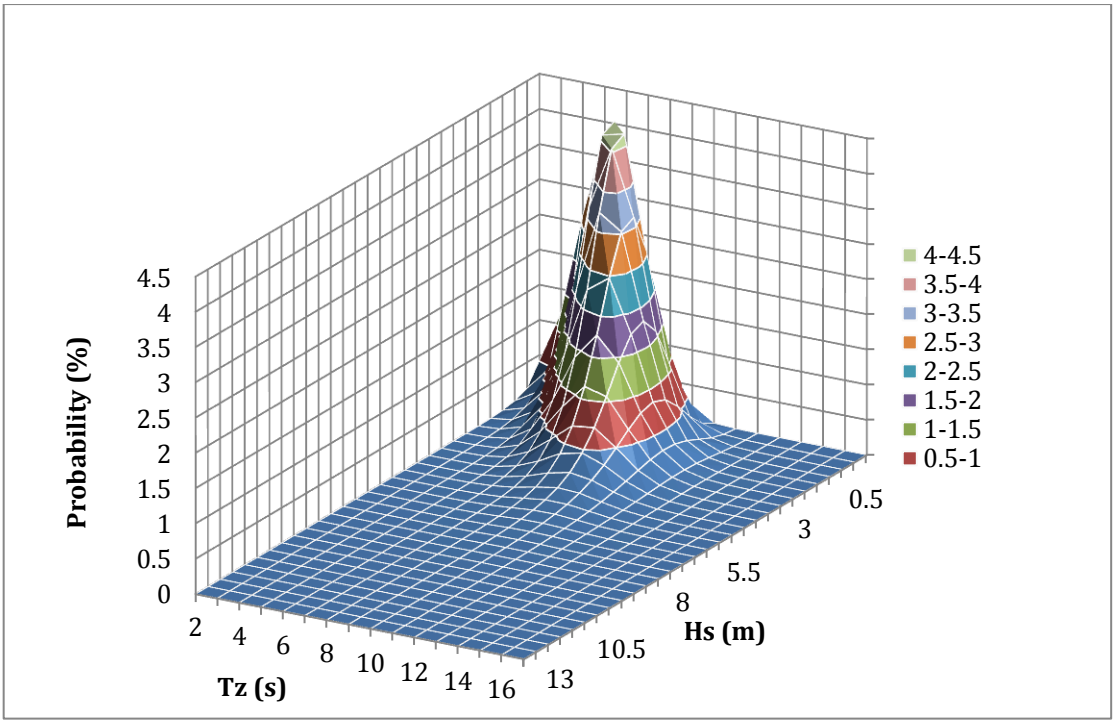

FIGURE 4.4 – WEIGHTED SCATTER DIAGRAM FROM RAS TANURA TO LOOP

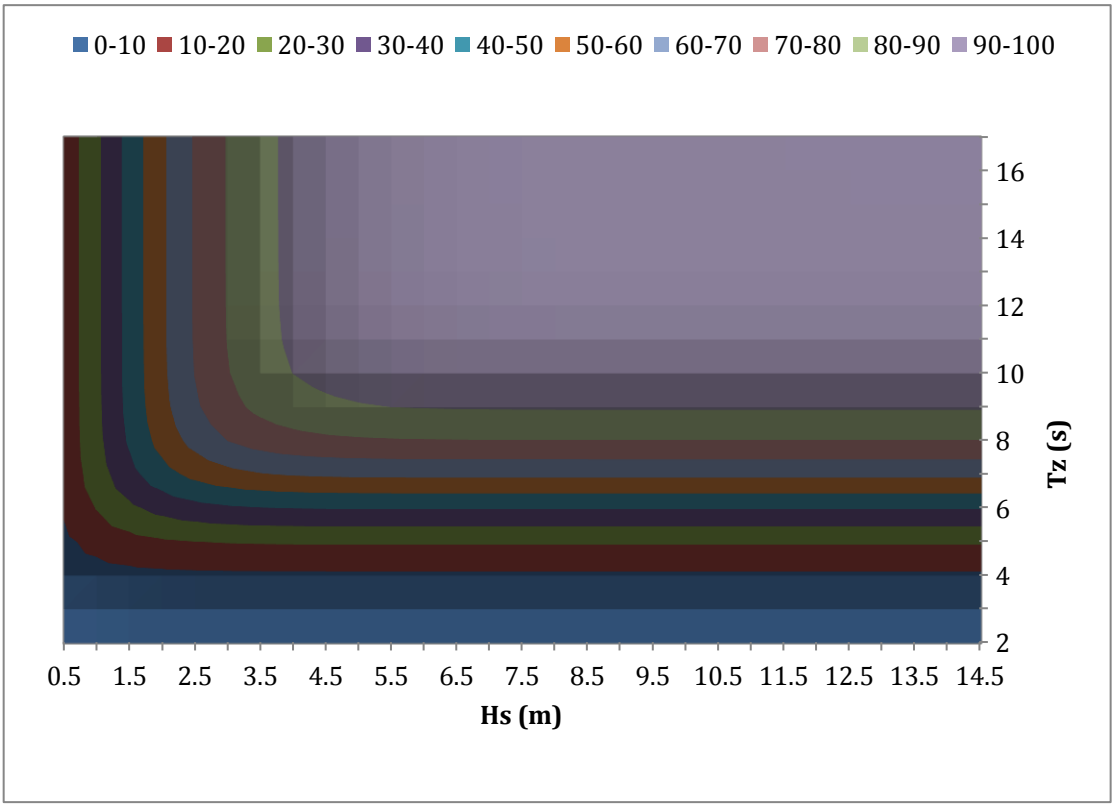

FIGURE 4.5 – THE CUMULATIVE DISTRIBUTION FUNCTION IN PERCENT – RAS TANURA TO LOOP

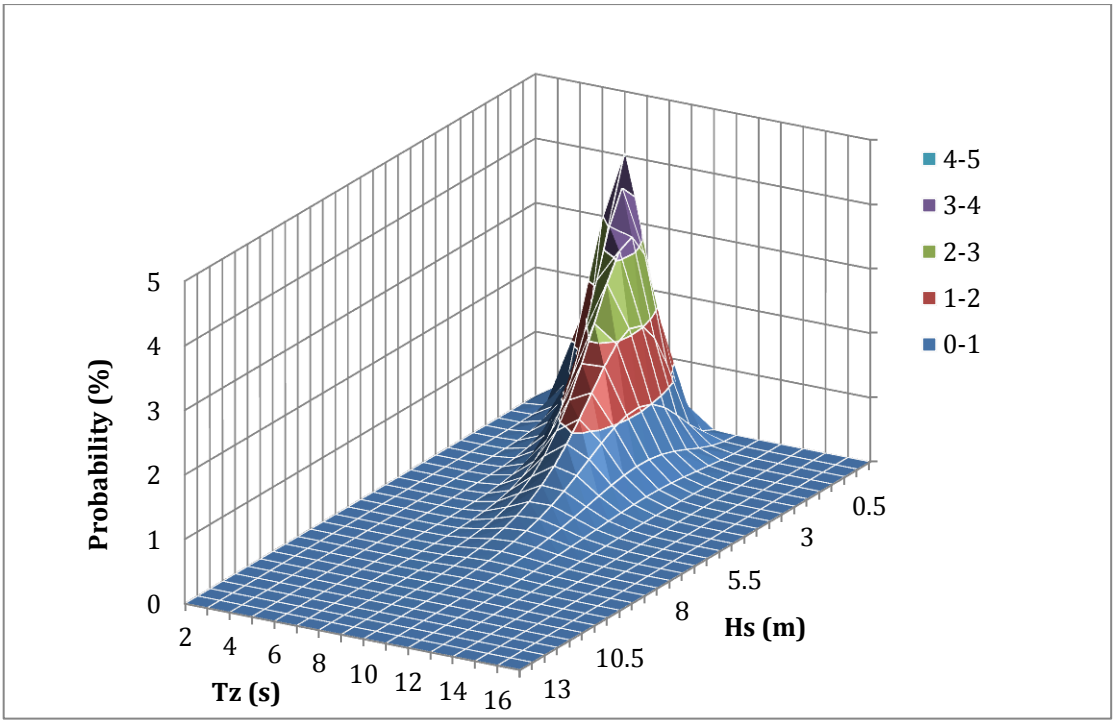

FIGURE 4.6 – WEIGHTED SCATTER DIAGRAM FROM MONGSTAD TO NEW YORK

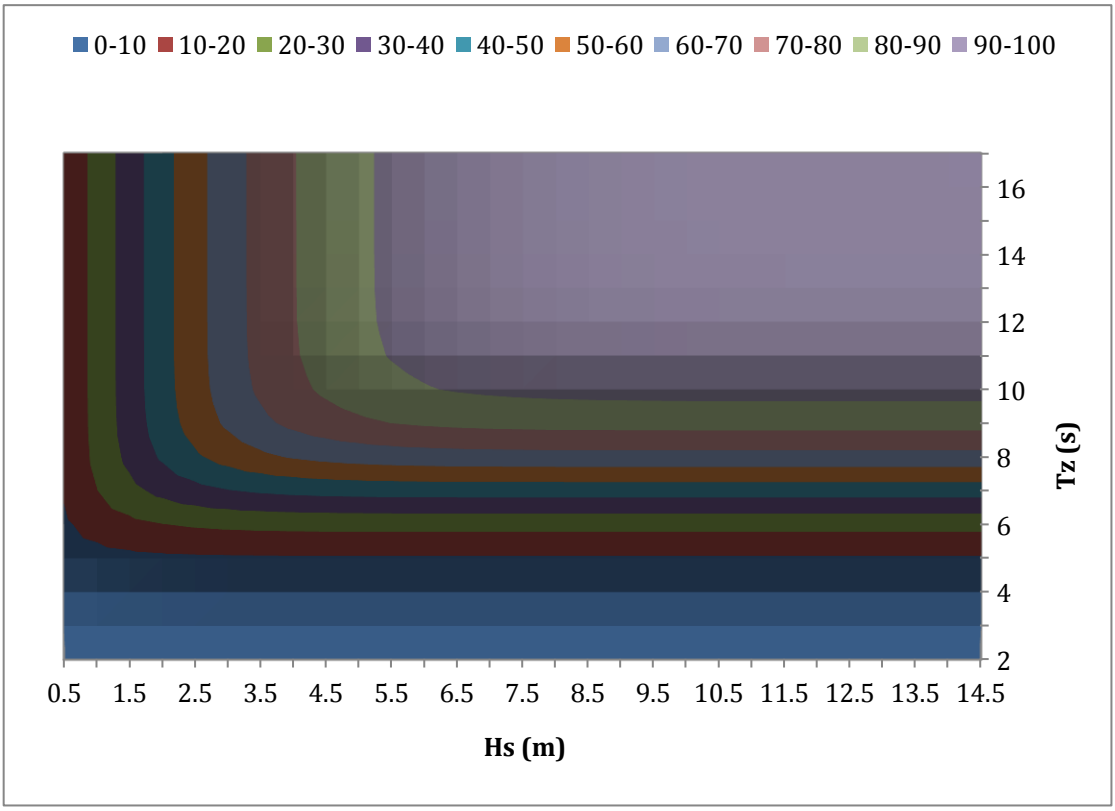

FIGURE 4.7 - THE CUMULATIVE DISTRIBUTION FUNCTION IN PERCENT – MONGSTAD TO NEW YORK

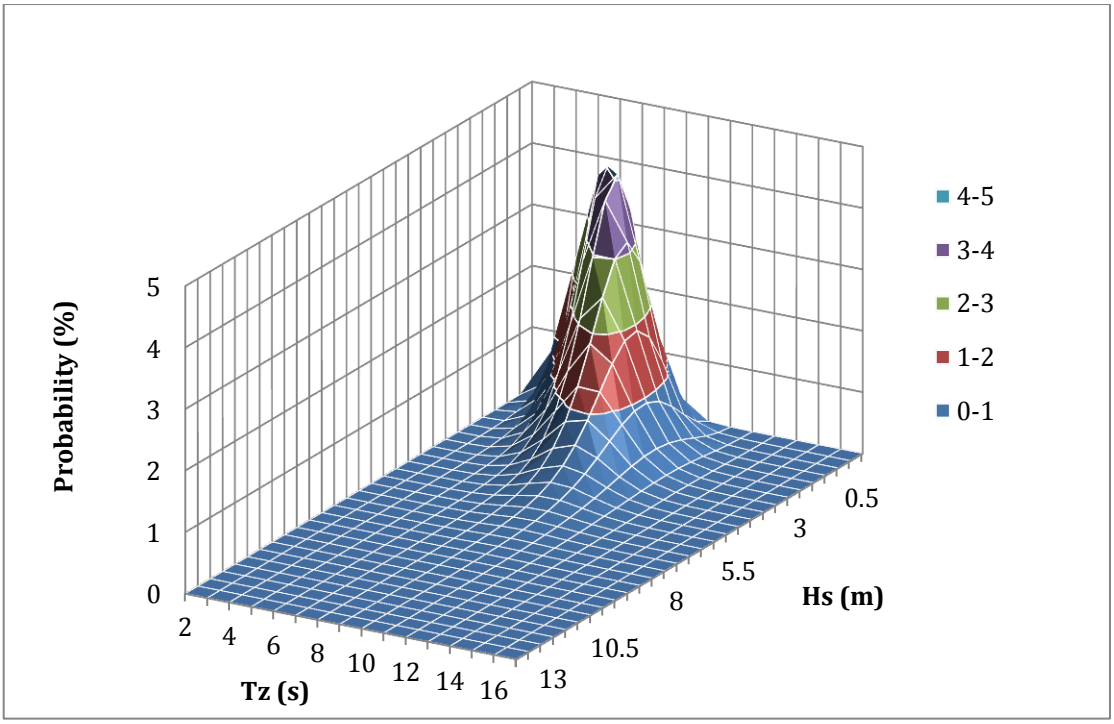

FIGURE 4.8 - WEIGHTED SCATTER DIAGRAM FROM TUBARÃO TO QINGDAO

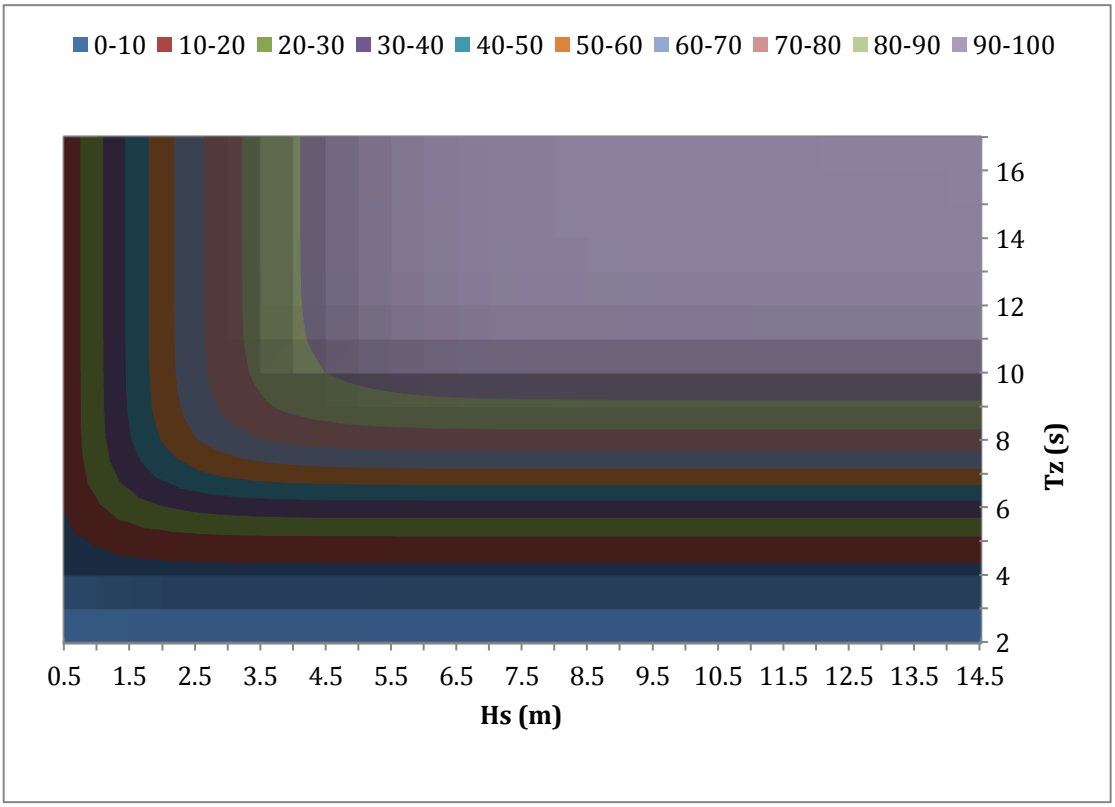

FIGURE 4.9 - THE CUMULATIVE DISTRIBUTION FUNCTION IN PERCENT –TUBARÃO TO QINGDAO

5 ANALYSIS AND RESULTS

This chapter describes the set up and program of the different analyses and present the results. Verification of the methods used for Shipflow is performed and presented. Three parts have been evaluated, the calm water resistance and the added resistance in waves, which are the input to the evaluation of designs on typical routes.

5.1 VERIFICATION

MARINTEK have done experiments on KVLCC2 in relation with the work of Guo (2011). Resistance curves have been developed and these results will be used to verify the calculations done with Shipflow.

The original model test results can be seen in Table 5.2. Characteristics of the model are given in the table below.

TABLE 5.1 - MAIN DIMENSIONS OF SHIP AND MODEL USED IN MARINTEK EXPERIMENTS

	Model scale	**58**
	Ship	**Model**
L_{pp} (m)	320	5.517
L_{wl} (m)	325.503	5.612
B_{wl} (m)	58.021	1
T (m)	20.8	0.359
S excl. rudder (m^2)	27800.68	8.264
S transom stern	13.48	0.004
Displacement ∇ (m^3)	312677.38	1.603
C_B	0.796	0.796
Water density	1025	998.82
Kinematic viscosity	1.19E-06	1.10E-06

TABLE 5.2 - RESULTS FROM MARINTEK EXPERIMENTS, FORM FACTOR K = 0.2021

Model

F_N	R_{Nm}	C_{Tm}	C_{Fm}	C_{Appm}	C_{BDm}	C_R
0.101	3.80E+06	5.81E-03	3.58E-03	0.00E+00	5.00E-06	1.50E-03
0.121	4.56E+06	5.23E-03	3.46E-03	0.00E+00	5.00E-06	1.07E-03
0.143	5.39E+06	5.34E-03	3.36E-03	0.00E+00	5.00E-06	1.31E-03
0.157	5.91E+06	5.29E-03	3.29E-03	0.00E+00	5.00E-06	1.33E-03
0.161	6.07E+06	5.14E-03	3.28E-03	0.00E+00	5.00E-06	1.19E-03
0.181	6.83E+06	5.54E-03	3.21E-03	0.00E+00	5.00E-06	1.67E-03

Ship

F_N	R_{Ns}	C_R	C_{Fs}	C_{Vs}	C_{BDs}	C_{Apps}	C_{Ts}
0.101	1.56E+09	1.50E-03	1.45E-03	1.87E-03	8.00E-06	0.00E+00	3.25E-03
0.121	1.87E+09	1.07E-03	1.42E-03	1.87E-03	8.00E-06	0.00E+00	2.83E-03
0.143	2.21E+09	1.31E-03	1.39E-03	1.87E-03	8.00E-06	0.00E+00	3.06E-03
0.157	2.43E+09	1.33E-03	1.38E-03	1.87E-03	8.00E-06	0.00E+00	3.08E-03
0.161	2.49E+09	1.19E-03	1.37E-03	1.87E-03	8.00E-06	0.00E+00	2.94E-03
0.181	2.80E+09	1.67E-03	1.35E-03	1.87E-03	8.00E-06	0.00E+00	3.42E-03

The division of the resistance components from MARINTEK is that the viscous pressure resistance is taken into C_R. Thus the form factor used by MARINTEK is $k=k_f$ (refer to chapter 2.1.2). In this thesis, the viscous pressure resistance is taken into account by the form factor, thus the MARINTEK form factor is too low.

To recalculate the resistance coefficients with a new form factor the following procedure is used.

The new residual resistance coefficient is calculated from the model scale results by

$$C_R = C_{Tm} - (1+k) \cdot C_{Fm} - C_{BDm} \qquad \text{Equation 5-1}$$

k – the new form factor

In full scale the skin friction coefficient is not altered from the original results, but the viscous resistance $C_{Vs} = (1+k)(C_{Fs} + \Delta C_{Fs})$ has to be recalculated with the new form factor. Below, calculations with two different form factors have been performed. In Table 5.3 a form factor of k=0.391 is applied, taken from numerical calculations in Steen et al. (2010) and a form factor calculated by Holtrop's method of k=0.3435. The residual resistance is now decreased and the viscous resistance increased. The form factors used can be seen in the table. The hull roughness is calculated by Equation 2-4.

TABLE 5.3 - RESULTS FROM MARINTEK EXPERIMENTS WITH FORM FACTOR FROM NUMERICAL CALCULATIONS (STEEN ET AL., 2010) AND EMPIRICAL FORM FACTOR BY HOLTROP.

Model							
F_N	R_{Nm}	C_{Tm}	C_{Fm}	C_{Appm}	C_{BDm}	C_R	
0.101	3.80E+06	5.81E-03	3.58E-03	0.00E+00	5.00E-06	8.26E-04	
0.121	4.56E+06	5.23E-03	3.46E-03	0.00E+00	5.00E-06	4.21E-04	
0.143	5.39E+06	5.34E-03	3.36E-03	0.00E+00	5.00E-06	6.63E-04	
0.157	5.91E+06	5.29E-03	3.29E-03	0.00E+00	5.00E-06	7.07E-04	
0.161	6.07E+06	5.14E-03	3.28E-03	0.00E+00	5.00E-06	5.72E-04	
0.181	6.83E+06	5.54E-03	3.21E-03	0.00E+00	5.00E-06	1.07E-03	
Ship	**Form factor**	**(Steen et al., 2010)**	**0.391**				
F_N	R_{Ns}	C_R	C_{Fs}	C_{Vs}	C_{BDs}	C_{Apps}	C_{Ts}
0.101	1.56E+09	8.26E-04	1.45E-03	2.17E-03	8.00E-06	0.00E+00	3.00E-03
0.121	1.87E+09	4.21E-04	1.42E-03	2.16E-03	8.00E-06	0.00E+00	2.59E-03
0.143	2.21E+09	6.63E-04	1.39E-03	2.16E-03	8.00E-06	0.00E+00	2.83E-03
0.157	2.43E+09	7.07E-04	1.38E-03	2.16E-03	8.00E-06	0.00E+00	2.88E-03
0.161	2.49E+09	5.72E-04	1.37E-03	2.16E-03	8.00E-06	0.00E+00	2.74E-03
0.181	2.80E+09	1.07E-03	1.35E-03	2.16E-03	8.00E-06	0.00E+00	3.24E-03
	Form factor	**Holtrop**	**0.3435**				
0.101	1.56E+09	9.96E-04	1.45E-03	2.17E-03	8.00E-06	0.00E+00	3.17E-03
0.121	1.87E+09	5.85E-04	1.42E-03	2.16E-03	8.00E-06	0.00E+00	2.76E-03
0.143	2.21E+09	8.22E-04	1.39E-03	2.16E-03	8.00E-06	0.00E+00	2.99E-03
0.157	2.43E+09	8.63E-04	1.38E-03	2.16E-03	8.00E-06	0.00E+00	3.03E-03
0.161	2.49E+09	7.28E-04	1.37E-03	2.16E-03	8.00E-06	0.00E+00	2.90E-03
0.181	2.80E+09	1.22E-03	1.35E-03	2.16E-03	8.00E-06	0.00E+00	3.39E-03

5.1.1 WAVE MAKING AND RESIDUAL RESISTANCE VERIFICATION

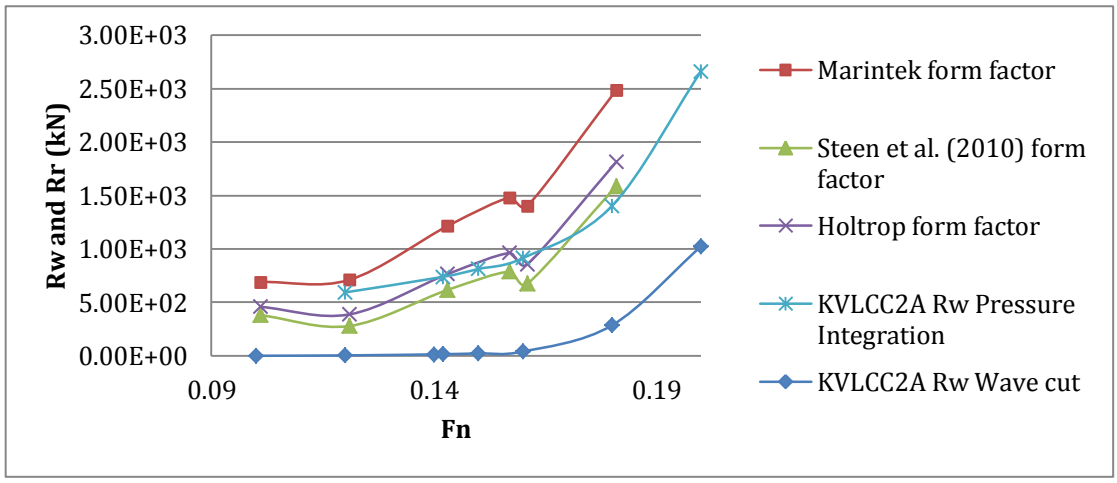

FIGURE 5.1 - R_W FROM NUMERICAL CALCULATIONS AND R_R FROM EXPERIMENTS

In Figure 5.1 the results for the residual resistance from experiments and the wave resistance from Shipflow for KVLCC2A are plotted. The wave resistance is expected to go to zero as the Froude number approaches 0.1. The result from the wave cut approaches zero in the area of Froude numbers between 0.14-0.16, while the wave resistance from pressure integration approaches ~500 kN.

It can be seen from the experimental values representing the residual resistance that components other than the wave resistance seem to dominate when the Froude number is low. When talking to Shipflow support and Jaeouk Sun in DNV it seems to be difficult to calculate the wave resistance at low Froude numbers. They recommended using the wave cut value, as this is less dependent on the mesh. Somewhat lower results than the actual should be expected due to numerical damping of waves. However, they commented that for comparison purposes it would be the most reliable parameter.

The XPAN solver in Shipflow has been run with the finest standard mesh on the hull and free surface. The mesh in Shipflow is optimized with regards to a standard case. After consulting with Magnus Östberg at Shipflow support it was decided there should be no need to change the mesh with regard to the specific case in this thesis. Thus the standard mesh was used.

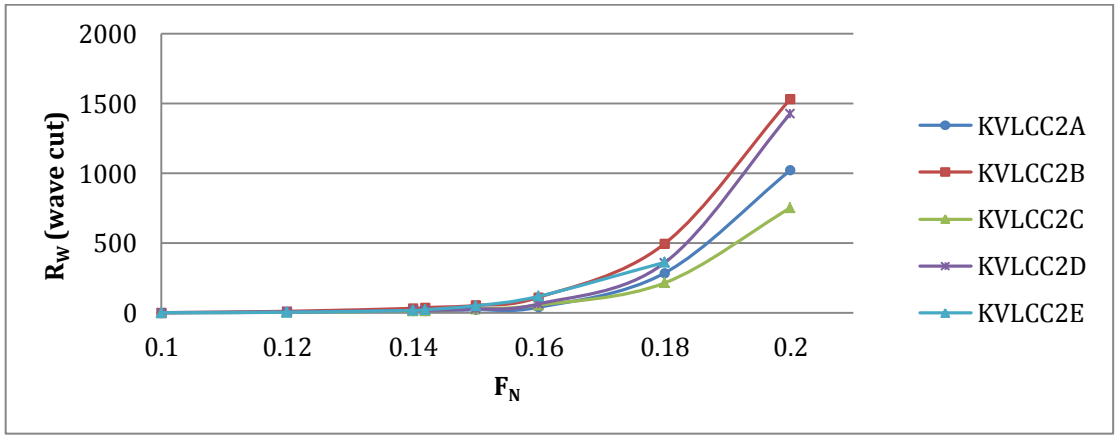

FIGURE 5.2 - R_W FROM WAVE CUTS IN SHIPFLOW

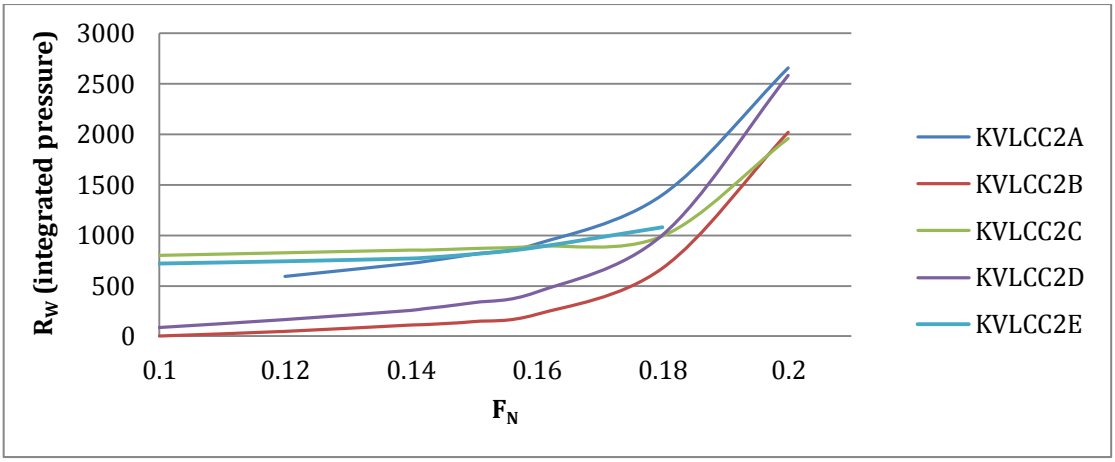

FIGURE 5.3 - R_W FROM INTEGRATED PRESSURE IN SHIPFLOW

In Figure 5.2 and Figure 5.3 the results from the wave making resistance calculations in Shipflow are shown for each design, wave cuts and integrated pressure respectively. The results from the integrated pressure method are not consistent. It seems like the sharp designs have an effect, a hydrostatic force, which should not be there. The results for KVLCC2B and KVLCC2D both approach zero on low Froude numbers, and seem to be describing the physics better. However, due to the inconsistency in these results they cannot be used further in the calculations.

The results from the wave cuts seem more reasonable in relative terms between the designs. However, they do not capture the effects that make the experimental residual results go to around 500-700 kN at low Froude numbers in Figure 5.1.

The total calm water resistance will be too small when using the wave cut results, which will influence the results of the route simulation

5.1.1.1 MODIFICATION OF WAVE RESISTANCE RESULTS

The wave making resistance calculated by wave cuts in Shipflow is too low (refer to model test results). This will influence the results as the added resistance will be relatively larger.

The non-zero residual resistance from model tests at $F_N \leq 0.1$ is a pressure force that should be independent of velocity and should be equal for all the designs as the aft ships are identical. Thus a possible modification of the results can be to add or subtract a constant value on coefficients to get the same residual resistance coefficient for all designs at $F_N=0.1$.

With basis in the model test results calculated with Holtrop's form factor the target residual coefficient at $F_N=0.1$ is $C_R=9.96E-04$ are found in Table 5.3. The difference between the calculated results and the target value at $F_N=0.1$ will be added to the wave resistance for each design. The new resistance coefficient for the designs is from now on named as the modified residual resistance. The coefficients calculated for each design can be found in Appendix B.

The modified residual resistance, seen in Figure 5.4, becomes somewhat larger than the model test results. However, the modified residual resistance is a better fit to the model test results than the wave cut calculations. Thus the modified residual resistance will be used in further calculations.

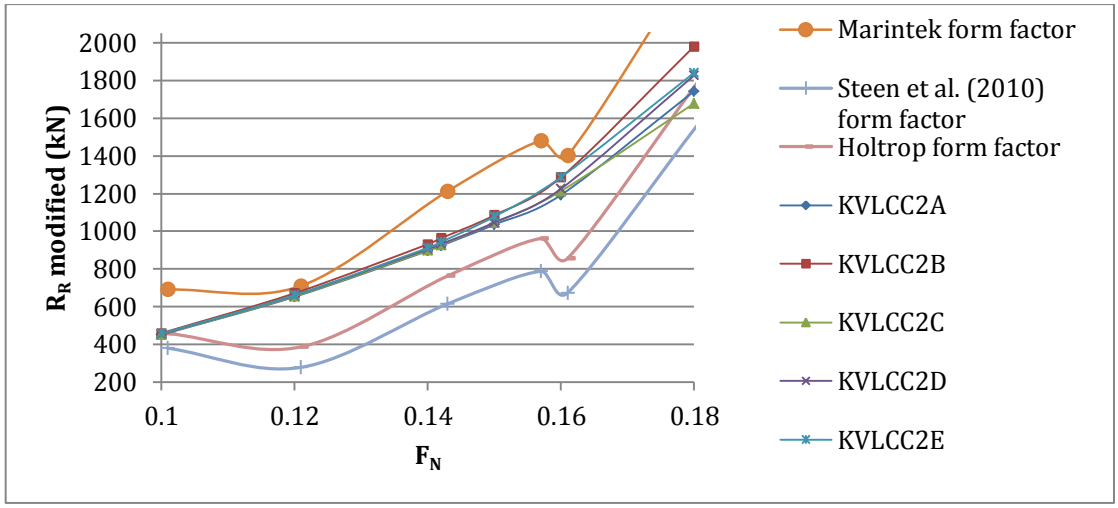

FIGURE 5.4 – COMPARISON OF THE MODEL TEST RESIDUAL RESISTANCE AND MODIFIED RESIDUAL RESISTANCE

5.1.2 VISCOUS RESISTANCE VERIFICATION

The viscous resistance is calculated in the same manner by MARINTEK as explained in chapter 2.1.2, with the exception of the form factor which is calculated by MARINTEK's formula. In Table 5.3 the viscous results from MARINTEK is recalculated with new form factors. These values are used to verify that the method used is correct.

In Table 5.4 the viscous resistance for the model designed in Maxsurf, and used in calculations, are shown. The vessel used in MARINTEK's experiments should be the same, but some deviations in wetted surface, small deviation in length in waterline, transom stern area and volume displacement create deviations in the results.

TABLE 5.4 - VISCOUS RESISTANCE FOR KVLCC2A, FORM FACTOR = 0.3435

F_N	$(1+k)\cdot(C_F+\Delta C_F)$	C_{DB}
0.1	2.09E-03	8.524E-06
0.11	2.09E-03	8.573E-06
0.12	2.09E-03	8.618E-06
0.13	2.09E-03	8.659E-06
0.142	2.09E-03	8.705E-06
0.145	2.09E-03	8.716E-06
0.155	2.09E-03	8.750E-06
0.16	2.09E-03	8.766E-06

The transom stern coefficient is somewhat larger for KVLCC2A than in MARINTEK's results. This is at least partially because of a smaller ratio between transom stern area and wetted surface area, and maybe round off errors in MARINTEK's results. However, this deviation is small, on the order of 10^{-7}, and is tolerated.

The viscous resistance is smaller than for MARINTEK. This deviation is also relatively small and the method for calculating viscous resistance is assumed to be verified.

5.1.2.1 CHOICE OF METHOD FOR CALCULATING FORM FACTOR

Two methods for calculating the form factor of the designs is available. The first is Holtrop's formula, based on empirical values. This gives results as shown in Table 5.5.

TABLE 5.5 - FORM FACTORS CALCULATED BY HOLTROP'S METHOD

Design	1+k
KVLCC2A	1.343517
KVLCC2B	1.344976
KVLCC2C	1.330679
KVLCC2D	1.345783
KVLCC2E	1.311831

The fact that KVLCC2A, KVLCC2B and KVLCC2D have the largest and similar form factor seems reasonable. It is hard to say if the decrease in form factor for KVLCC2C and KVLCC2E is realistic.

A possible alternative is to use numerical calculations to derive the form factor. KVLCC2A and KVLCC2C were run in the XCHAP solver in Shipflow. The result was a form factor of 0.309 and 0.32 for KVLCC2A and KVLCC2C respectively. This does not seem reasonable and was a time consuming analysis. Therefore, Holtrop's method has been chosen and the values presented in Table 5.5 are the ones used.

5.1.3 Verification of Added Resistance In Waves

The added resistance in waves is verified against results calculated in Guo (2011). Calculations with both pressure integration and Gerritsma and Beukelmann combined with Faltinsen's asymptotic formula in short waves are performed and compared to results from Guo and Steen (2011).

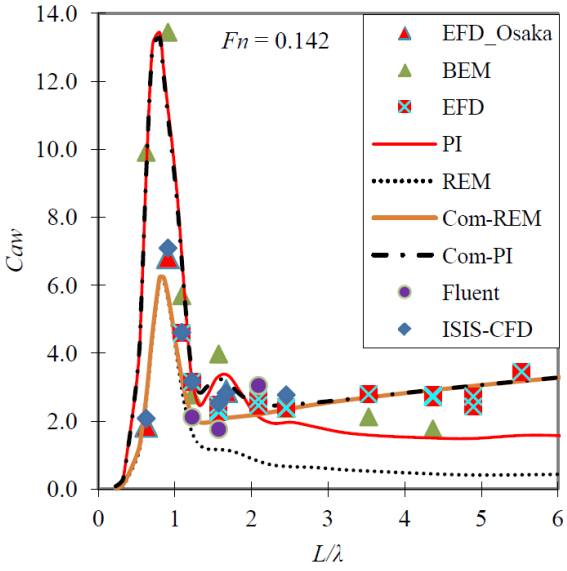

FIGURE 5.5 - EXPERIMENTAL AND NUMERICAL RESULTS FOR ADDED RESISTANCE FOR KVLCC2A (GUO, 2011)

In Figure 5.5 experimental and calculated results for the added resistance of KVLCC2A are shown, taken from (Guo and Steen, 2011). "EFD" are the experimental results from the towing tank at MARINTEK, while "EFD_Osaka" are experimental results from Osaka. Of interest is the "Com-REM" and "Com-PI", which is the radiated energy method and the pressure integration method combined with Faltinsen's asymptotic formula, respectively.

It can be seen that the pressure integration method over-predicts the added resistance in the radiation region. The radiation energy method under-predicts in the radiation region, but not as

much as the over-prediction by the pressure integration method. It can also be seen that Faltinsen's asymptotic formula predicts well the added resistance in short waves.

The methods used by ShipX, both shown below, are the same as the methods used in Figure 5.5. The radiation energy method fits best with the experimental results. Thus this will be used in the calculations.

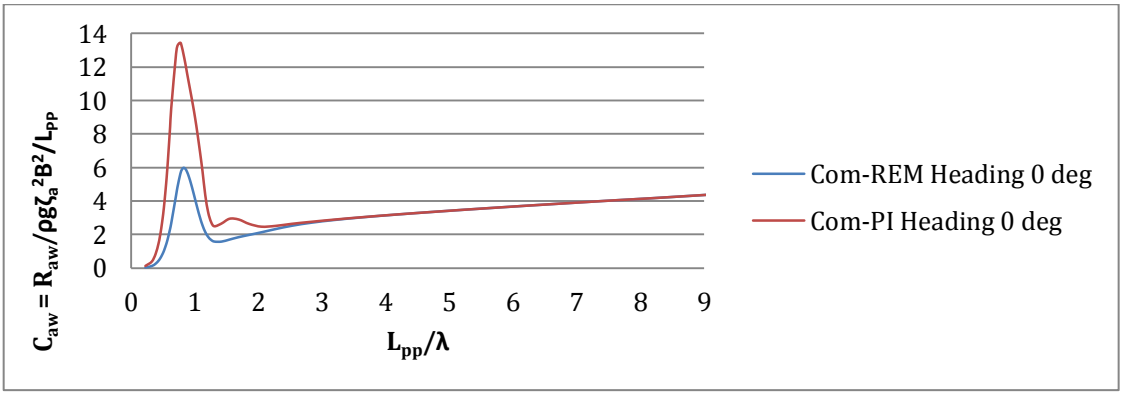

FIGURE 5.6 - ADDED RESISTANCE COEFFICIENT FOR KVLCC2A FROM SHIPX AT F_N=0.142

5.2 RESULTS

The results from calm water resistance of the ships as well as the added resistance amplitude operator for each design and the results of the route simulation will be presented and commented on.

5.2.1 CALM WATER RESISTANCE

Resistance coefficients calculated by the methods in chapter 2 are presented in Appendix B.

5.2.1.1 WAVE RESISTANCE

The wave resistance is one of the major components that are highly dependent on details in the design. However, for low Froude numbers as the case is for KVLCC2, it is of low significance compared to the viscous resistance. As seen in chapter 5.1.1, Shipflow is not able to represent the wave resistance at these low Froude numbers accurately. In any case the relative wave resistance between the different designs should be evaluated for comparison.

In Figure 5.7 the wave resistance from transverse wave cuts in Shipflow is presented for each design. The figure only shows a small range of Froude numbers to make it possible to separate the different designs.

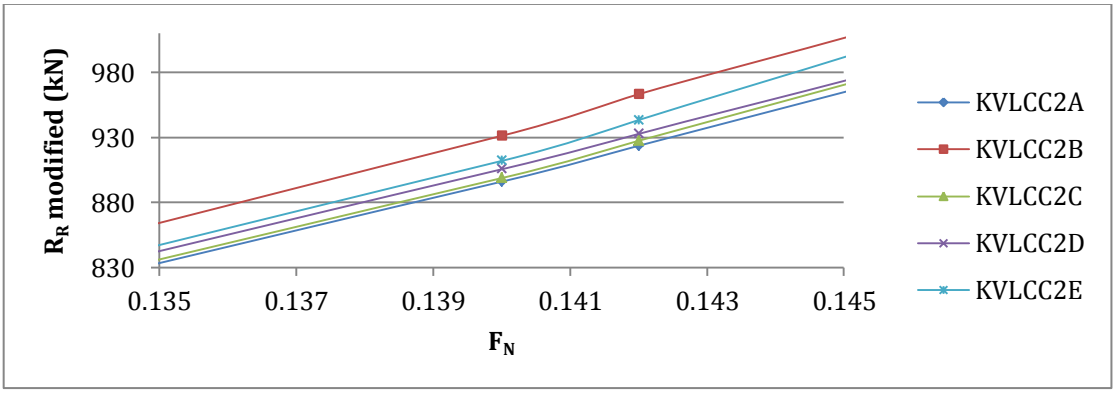

FIGURE 5.7 - MODIFIED RESIDUAL RESISTANCE FOR A SMALL RANGE OF FROUDE NUMBERS

5.2.1.2 VISCOUS RESISTANCE

The results for viscous resistance are presented in Figure 5.8 below.

It is difficult to differentiate between the designs from Figure 5.8. The change in viscous resistance from KVLCC2A to the other designs at F_N=0.142 is shown in Table 5.6. The change is calculated from;

$$\frac{(C_{VS})_i-(C_{VS})_A}{(C_{VS})_A} = \frac{(C_{TS}-C_R)_i-(C_{VS})_A}{(C_{TS}-C_R)_A} = \frac{\left((1+k)\cdot(C_{FS}+\Delta C_{FS})+C_{DBS}\right)_i-(C_{VS})_A}{\left((1+k)\cdot(C_{FS}+\Delta C_{FS})+C_{DBS}\right)_A} \qquad \text{Equation 5-2}$$

i – index of design (B, C, D, and E)

It can be seen that the change is rather small. KVLCC2E has a 2.93% increase in resistance compared to KVLCC2A at a given Froude number. The increase in skin friction is larger, but is compensated by the lower form factor of KVLCC2E.

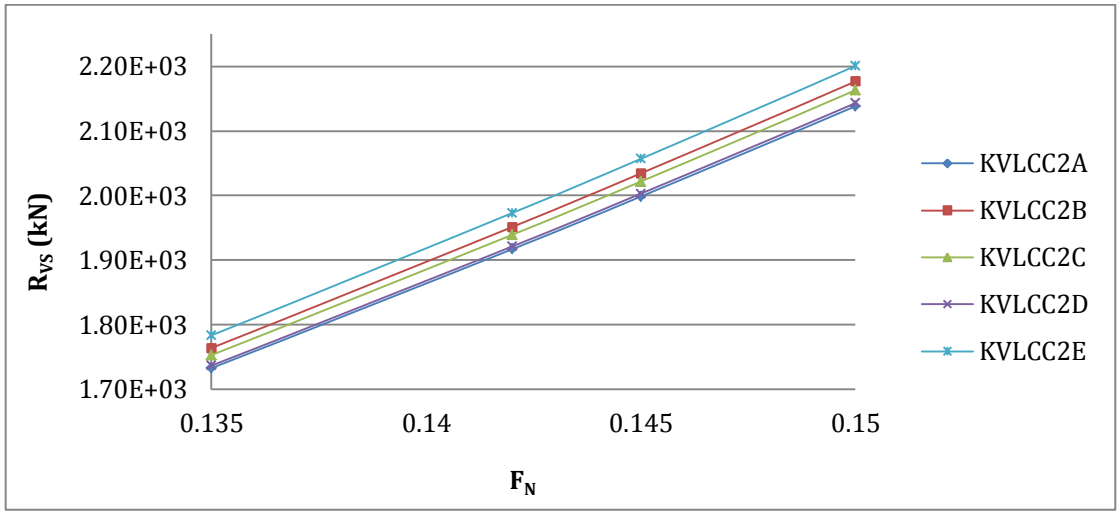

FIGURE 5.8 - VISCOUS RESISTANCE FOR THE DESIGNS

KVLCC2B has a larger increase in the viscous resistance than KVLCC2C, which is mainly due to the large increase in wetted surface.

TABLE 5.6 - PERCANTAGE CHANGE IN VISCOUS RESISTANCE CALCULATED IN NEWTON AT F_N=0.142, WITH KVLCC2A AS BASE CASE

Design	% change
KVLCC2B	1.80 %
KVLCC2C	1.17 %
KVLCC2D	0.22 %
KVLCC2E	2.93 %

5.2.1.3 TOTAL CALM WATER RESISTANCE

The total calm water resistance is shown in Figure 5.9 for a small range of Froude numbers. These results will be the input to the route simulation in ShipX.

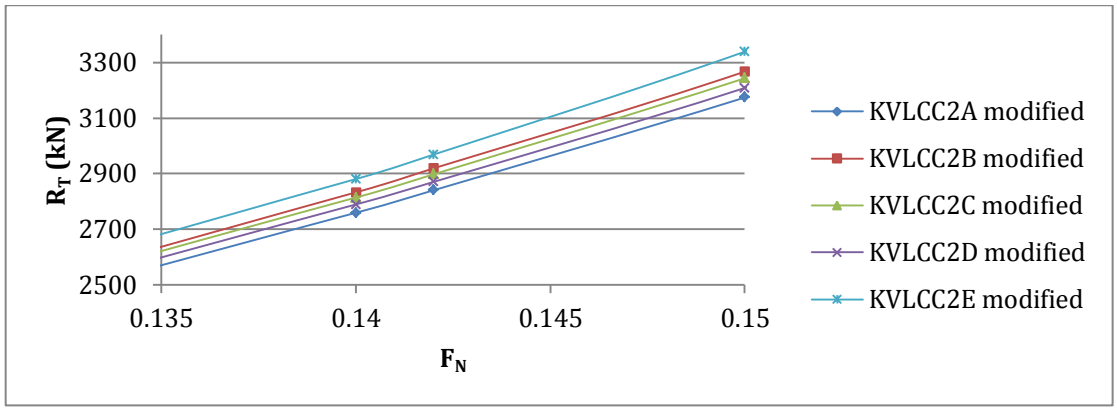

FIGURE 5.9 – TOTAL CALM WATER RESISTANCE

KVLCC2E has the highest calm water resistance against Froude number. The total viscous resistance coefficient is lower for the longer designs due to a longer water line length would that result in a higher Reynolds number at constant speed. Remembering the ITTC curve for friction a higher Reynolds number results in a lower plate friction coefficient for a given speed. Thus some of the increased wetted surface will be compensated for by a lower friction coefficient as well as a lower form factor. The resistance curves plotted against Froude number will for the longer designs, KVLCC2C and KVLCC2E, will shift to the right when plotted against speed because these designs will have a higher speed corresponding to a Froude number. For a given Froude number one can find the relation between the speeds for the short designs and longer designs.

$$\frac{V_{C,E}}{V_A} = \sqrt{\frac{L_{C,E}}{L_A}} \qquad \text{Equation 5-3}$$

This ratio is 1.0122 for KVLCC2C and 1.0243 for KVLCC2E. Figure 5.10 shows the total resistance plotted against velocity instead of Froude number. Thus the expected increase in calm water resistance for the sharper designs is not the case by these calculations. Due to the relatively low increase in wetted surface for KVLCC2C it is not punished as much as expected. KVLCC2E also has a low calm water resistance but it seems like the benefit of the length is punished by a larger increase in the wetted surface.

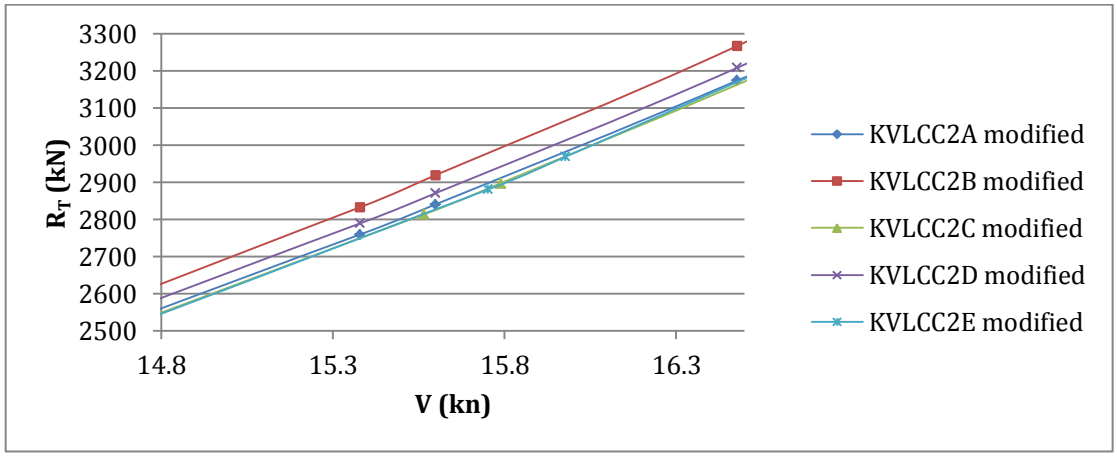

FIGURE 5.10 - TOTAL CALM WATER RESISTANCE PLOTTED AGAINST KNOTS

5.2.2 Added Resistance In Waves

The added resistance in waves for headings 0°, 45°, 90°, 135° and 180° is shown in Figure 5.11. In the radiation region 45° heading has the largest added resistance. However, it has lower added resistance in the diffraction region than head sea waves. Thus what is the most critical heading, in terms of added resistance, is dependent on the wave conditions. The same tendency is seen for all the other designs as well, but not presented here. Plots for all headings at F_N=0.142 is given for all designs in 8Appendix C.

In Figure 5.12 the added resistance for each design at F_N=0.142 in head sea is shown. It can be seen that KVLCC2C and KVLCC2E has a slightly higher added resistance coefficient, C_{aw}, in the diffraction region. However, it is pronouncedly lower in the diffraction region, as expected. The difference between KVLCC2C and KVLCC2E is, however, not as significant.

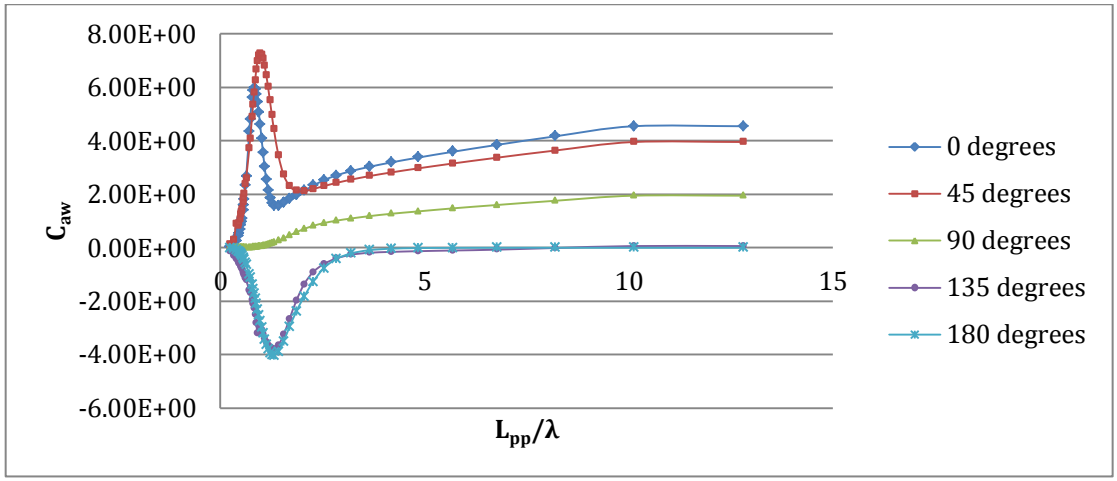

FIGURE 5.11 - RAO IN ADDED RESISTANCE FOR KVLCC2A AT DIFFERENT HEADINGS, F_N=0.142

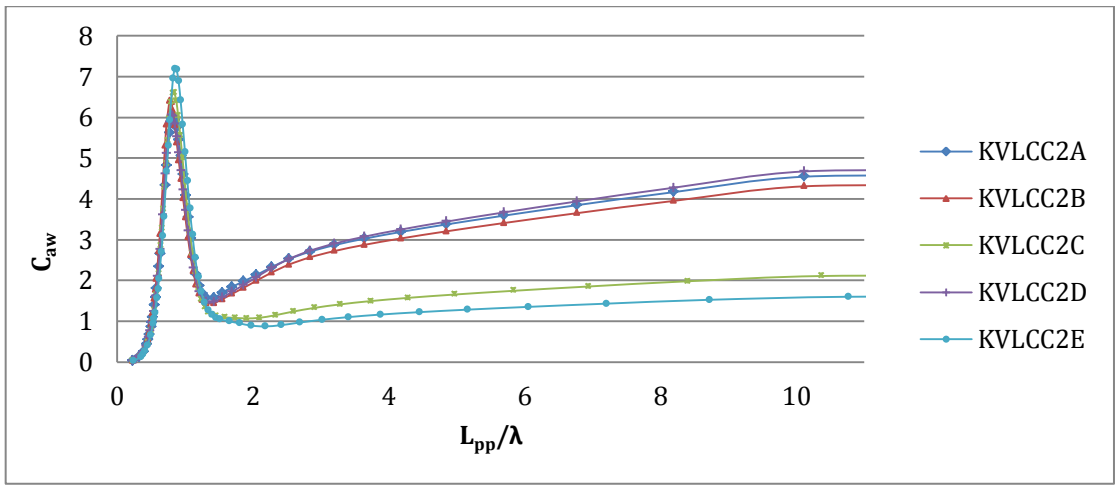

FIGURE 5.12 - ADDED RESISTANCE RAO AT HEAD SEAS AT F_N = 0.142

It can be seen that KVLCC2A has more similar results compared to KVLCC2D than KVLCC2B. KVLCC2B should have the same waterline curve as KVLCC2A and they were thus expected to have the same results in the diffraction region. One explanation might be that the bulb of KVLCC2A influences the calculations even though it is below the design water line in calm water. Another possibility is that the ShipX model, which was the same used by Bingjie Guo in (Guo, 2011), is slightly different from KVLCC2A waterline, which had to be redesigned in Maxsurf. A test with the model used to calculate the calm water resistance has been done. This design has

the same water line curve as KVLCC2A. The results comparing KVLCC2A, KVLCC2B (from Guo) and KVLCC2B (designed in Maxsurf without line drawings) are shown in Figure 5.13.

It should be emphasized that the redesign was done without any line drawings, and thus the results are not expected to be exactly the same for the two models. However, one can see that the redesigned model has even lower added resistance than KVLCC2B from (Guo, 2011). The redesigned model has the same water line curve as KVLCC2A, which thus indicates that the bulb of KVLCC2A influences the results even at short waves.

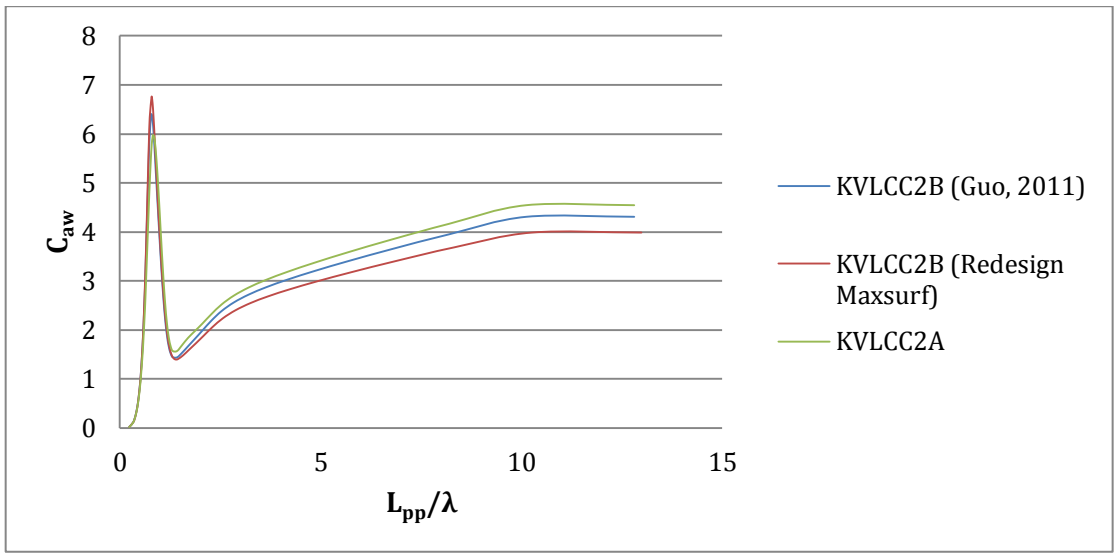

FIGURE 5.13 - COMPARISON OF ADDED RESISTANCE CALCULATIONS IN SHIPX FOR KVLCC2B MODELS, F_N=0.142

5.2.3 Simulation of Routes

With the scatter diagrams, calm water resistance and added resistance in waves established the propeller and engine characteristics are the last properties to establish before evaluating each design over the routes.

5.2.3.1 Propeller and Engine Characteristics

For ShipX to calculate the speed-loss the propeller and engine characteristics have to be established. ShipX calculates a corrected open water diagram, loss of propeller efficiency, due to variable loading in waves.

The propeller characteristics are given for experiments to standardize the experiments performed all over the world for CFD validation (Simman2008, 2008). The given propeller characteristics have been used on a Wageningen B-series propeller, a widely used propeller series, which is included in the ShipX library.

From Sea-web (Sea-Web, 2012), statistics for the fleet of ships can be found. A search on engine and propulsion configuration for tankers and bulk carriers between 290 and 330 meters long gives a basis for statistically determine the most used configurations. It shows that ~92% of the vessels fulfilling the criteria of the search have 1 propeller, and even more have fixed pitch as well.

The propeller characteristics given by Simman2008 (2008) are shown in Table 5.7.

TABLE 5.7 - PROPELLER CHARACTERISTICS

Type	Fixed
No. of blades	4
D (m)	9.86
P/D (0.7R)	0.721
A_e/A_0 (m)	0.431
Rotation	Right hand
Hub ratio	0.155

ShipX also needs input on the propulsion characteristics. That is the wake coefficient, w, thrust deduction coefficient, t, rotational efficiency, η_R, mechanical efficiency, η_M, and gear box reduction ratio. The first coefficients are taken from Kim et al. (2001), the mechanical efficiency is assumed to be 0.97 and the gearbox reduction ratio is assumed to be one, as the comparison ships from Sea-Web had a majority of direct drive propulsion systems. Values are presented in Table 5.8. They are assumed equal for all the designs as the aft hull has major influence on the values and are equal for all the designs.

TABLE 5.8 - PROPULSION SETTINGS

RPM	80
w	0.305
t	0.19
η_R	1.005
η_M	0.97

A typical engine size for a ship of similar dimensions as KVLCC2 can be found by using the same Sea-web search. A plot of the length and engine power for tankers and bulk carriers is shown in Figure 5.14. It can be seen that the engine size is between 22 000 kW and 27 000 kW. Since the KVLCC2 designs are in the upper range of the vessels here 27 000 kW is chosen as engine size in the analyses in ShipX.

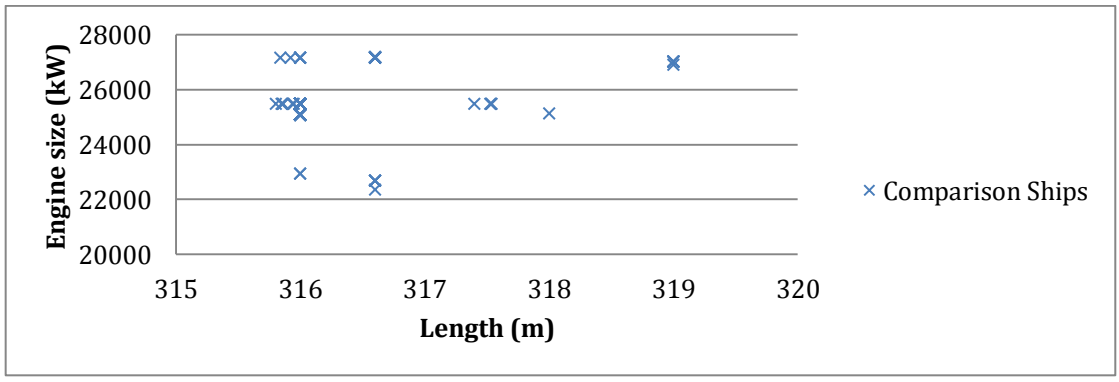

FIGURE 5.14 - ENGINE SIZE OF COMPARISON SHIPS FROM SEA-WEB.

5.2.3.2 SPEED-LOSS RESULTS

The speed-loss calculations are calculated for each design over each route. As mentioned the scatter diagrams do not contain any information on wave direction. Thus the results are first presented as speed-loss over headings 0°-180° with 45° intervals. Average speed-loss results, where each heading is weighted equally, are also presented.

Due to different calm water resistance, each ship has a different attainable speed in calm water presented in Table 5.9. The table shows that both KVLCC2C and KVLCC2D have a higher

attainable speed for the engine and propulsion configuration presented above in calm water than the blunter designs.

TABLE 5.9 - ATTAINABLE SPEED IN CALM WATER BASED ON ENGINE AND PROPULSION CONFIGURATION PRESENTED IN CHAPTER 5.2.3.1.

Design	V_{attCW} (kn)
KVLCC2A	13.4
KVLCC2B	13.26
KVLCC2C	13.53
KVLCC2D	13.33
KVLCC2E	13.44

Speed-loss on each route for each design over headings is presented in Figure 5.15-Figure 5.19.

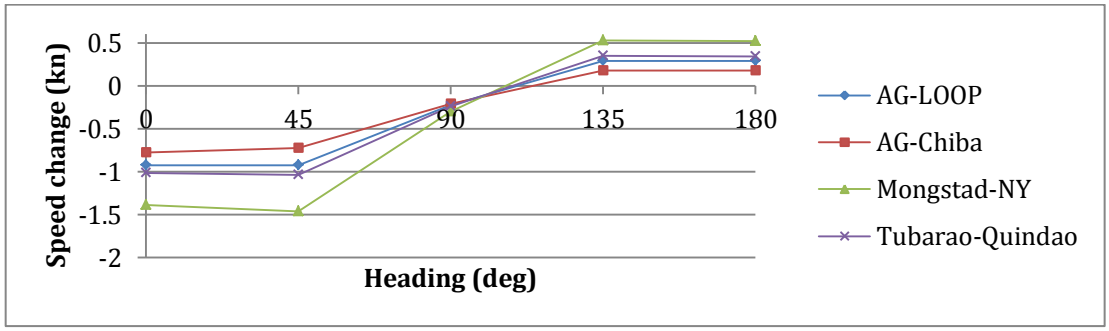

FIGURE 5.15 - KVLCC2A: SPEED-LOSS OVER HEADINGS FOR EACH ROUTE

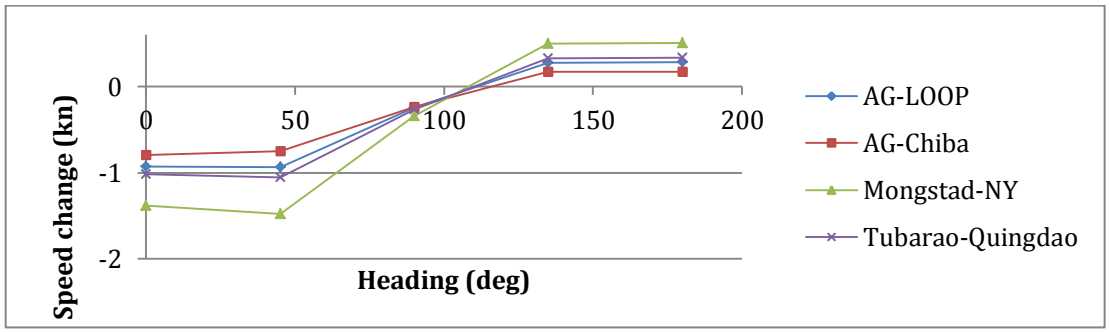

FIGURE 5.16 - KVLCC2B: SPEED-LOSS OVER HEADINGS FOR EACH ROUTE

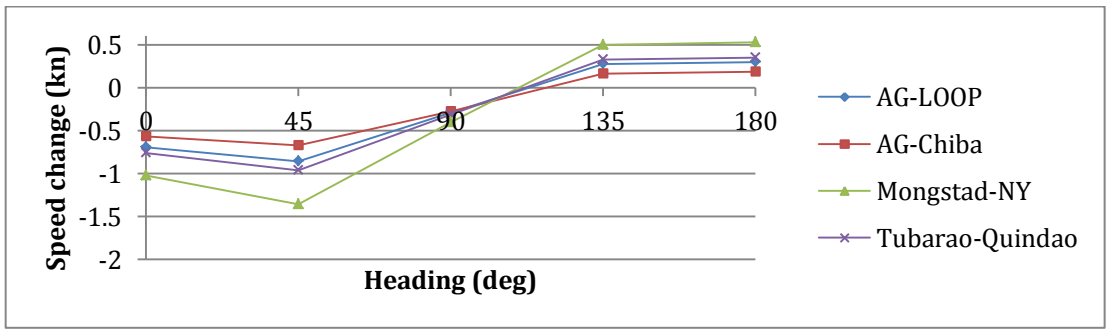

FIGURE 5.17 - KVLCC2C: SPEED-LOSS OVER HEADINGS FOR EACH ROUTE

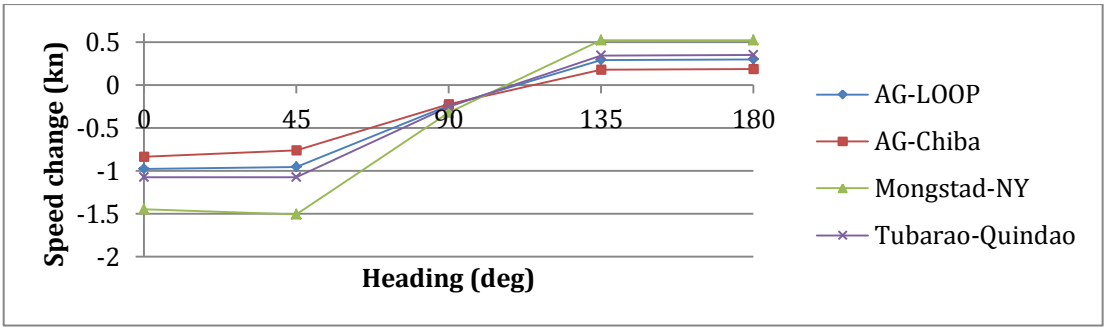

FIGURE 5.18 - KVLCC2D: SPEED-LOSS OVER HEADINGS FOR EACH ROUTE

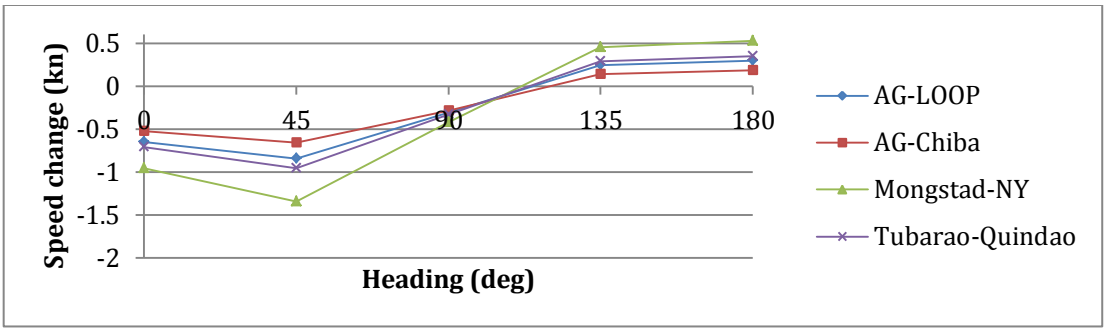

FIGURE 5.19 - KVLCC2E: SPEED-LOSS OVER HEADING FOR EACH ROUTE

For comparison purposes the speed-loss over each heading for all the designs on the route Arabian Gulf to LOOP has been plotted in Figure 5.20. The other routes have the same trends seen in the figures above.

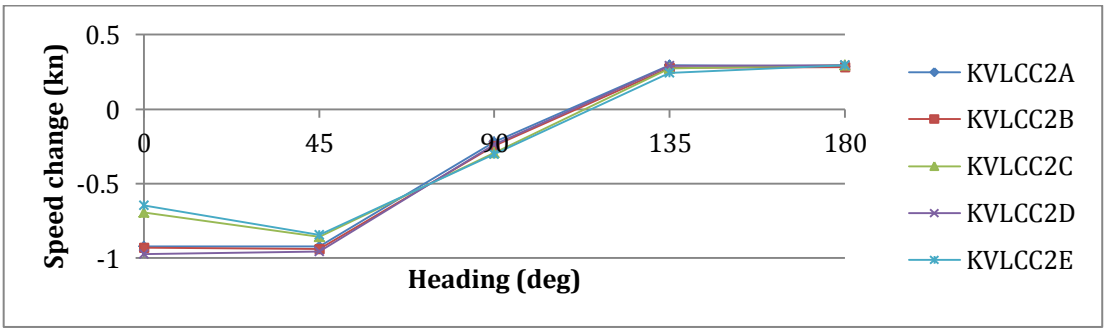

FIGURE 5.20 – SPEED-LOSS FOR EACH DESIGN ON THE ROUTE FROM THE ARABIAN GULF TO LOOP

As expected the route from Mongstad to New York gives the largest effect on the speed-loss calculations. The benefit of the sharper bow is also, as expected, greatest in head seas. Comparison of these two designs to the three other designs shows that at 45° heading the difference in speed loss is not very significant.

At 90° heading the speed-loss is actually larger for the sharpest designs. This might be due to the longer bow creating a larger wall surface for the waves to reflect off. However, the difference is very small and on larger headings the effect of a sharper bow can be neglected. This is no surprise as the waves will not face the bow part of the vessel.

Figure 5.21 and Figure 5.22 show the speed-loss averaged over headings for each design on each route. The weighting factor is assumed to be one for each heading, i.e. the vessel will experience sea states equally from all sides.

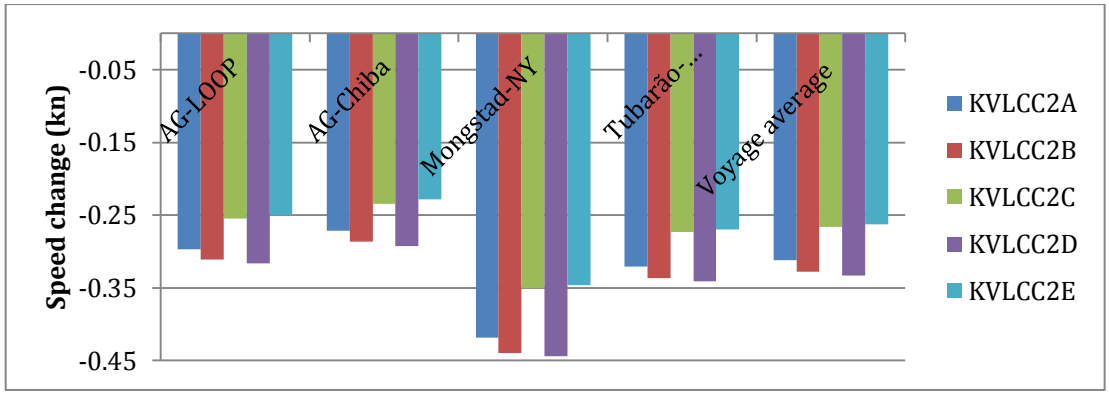

FIGURE 5.21 – SPEED-LOSS AVERAGED OVER HEADINGS GROUPED BY ROUTE

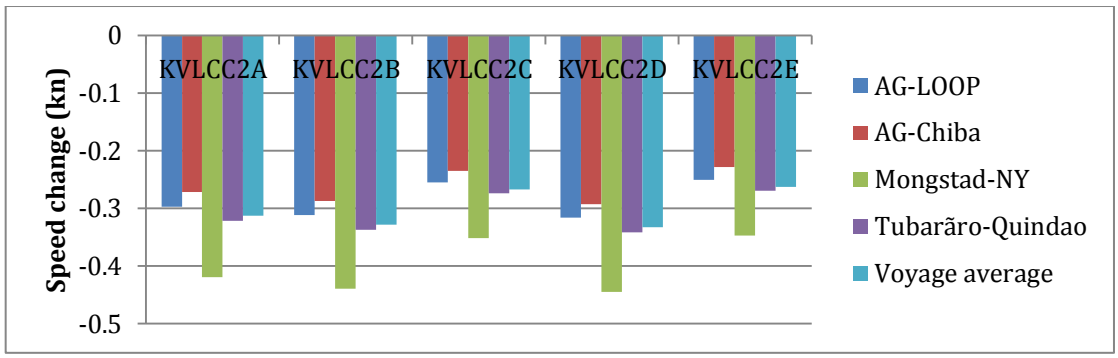

FIGURE 5.22 - SPEED-LOSS AVERAGED OVER HEADINGS GROUPED BY DESIGN

The voyage average shown in Figure 5.21 and Figure 5.22 is the average speed loss over the routes, as if a vessel were to trade the same 4 routes in cycle, weighted by the route length. The short route of Mongstad to New York compared to the routes departing from the Arabian Gulf has little influence on the overall average.

To investigate if there is a difference in the benefit of a sharper bow on the different routes, representing a range in typical sea states the speed-loss of KVLCC2C has been compared to the speed-loss of KVLCC2A. This shows that the speed loss of KVLCC2C is 14.2 % lower on the route from the Arabian Gulf to LOOP, 13.8% from the Arabian Gulf to Chiba and 16.2% lower on the route from Mongstad to New York across the North Atlantic. The route from Tubarão to Qingdao shows a 14.9% lower speed-loss for KVLCC2C.

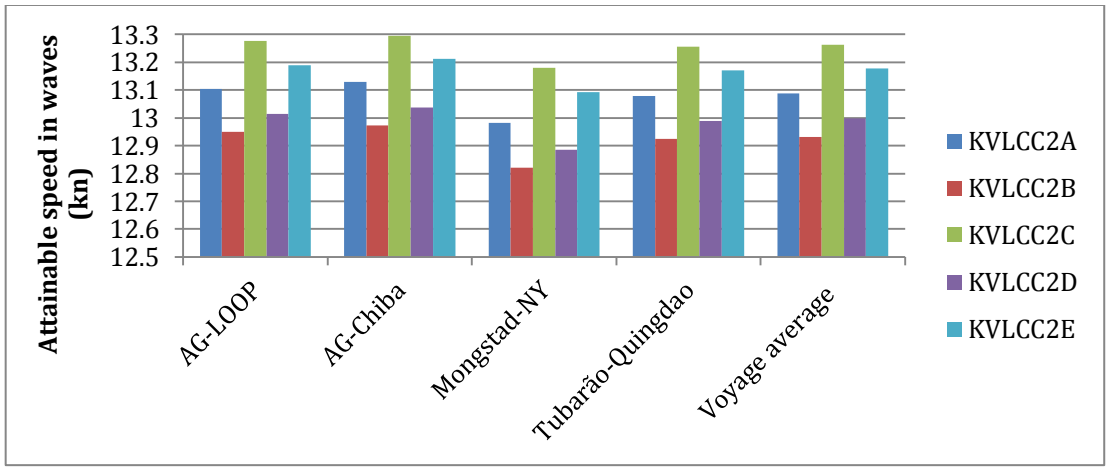

FIGURE 5.23 - ATTAINABLE SPEED IN WAVES AVERAGED OVER HEADINGS GROUPED BY ROUTE

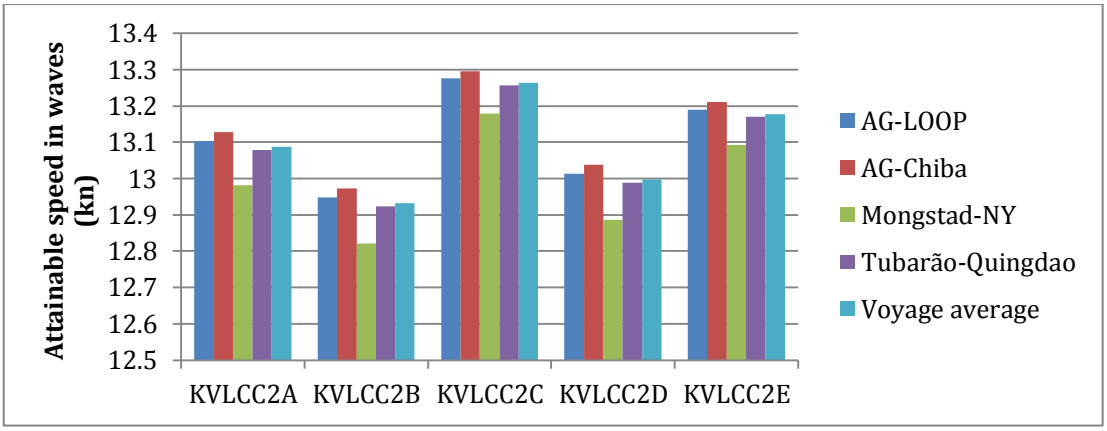

FIGURE 5.24 - ATTAINABLE SPEED IN WAVES AVERAGED OVER HEADINGS GROUPED BY DESIGN

Figure 5.23 and Figure 5.24 shows the attainable speed for each design with added resistance and the open water diagram corrected for waves included. It should be noted that both KVLCC2C and KVLCC2E have a higher attainable speed in calm water. However, to see the effect of the added resistance on each design the percentage speed-loss of the attainable speed in calm water for each design is presented in Table 5.10.

KVLCC2C and KVLCC2E have more or less the same results. The slightly lower head sea added resistance of KVLCC2E in the diffraction regime is not enough to make KVLCC2E significantly better than KVLCC2C. The blunter designs and KVLCC2D especially are the one affected the most by waves, as expected. However, KVLCC2B has overall lowest performance due to both a high calm water resistance and a large influence from waves.

TABLE 5.10 - PERCENTAGE SPEED-LOSS OF ATTAINABLE SPEED IN CALM WATER

	AG-LOOP	AG-Chiba	Mongstad-NY	Tubarão-Qingdao	Voyage average
KVLCC2A	2.22 %	2.03 %	3.12 %	2.39 %	2.33 %
KVLCC2B	2.35 %	2.16 %	3.32 %	2.54 %	2.47 %
KVLCC2C	1.88 %	1.73 %	2.59 %	2.02 %	1.97 %
KVLCC2D	2.37 %	2.20 %	3.33 %	2.56 %	2.50 %
KVLCC2E	1.86 %	1.70 %	2.58 %	2.01 %	1.95 %

6 CONCLUSION

From the calculations performed in this thesis it can be concluded that

- KVLCC2C is the overall best performer when both calm water resistance and influence of the wave environment is included. Even though the water line length of the design has been increased by 8 m, the calm water resistance is relatively low and the benefit of the sharper bow also contributes to better performance in waves than the blunter designs.
- KVLCC2E has the second highest attainable speed. It has smaller added resistance in the diffraction regime than all the other designs. However, the benefit of this is decreased by a higher calm water resistance than KVLCC2C thus giving a lower attainable speed. A design like KVLCC2E, which is extended further than the overall length of the original KVLCC2 design, may not be desired from an owner's point of view because it may violate length restrictions in ports and thus reduce the number of possible ports to visit.
- Of the designs presented KVLCC2B has the lowest attainable speed on each route. This is not a surprise as the vertical sides all the way down to the bottom create a large viscous resistance. It was expected that the speed-loss of KVLCC2B was going to be similar to KVLCC2A due to the equal water line curve of the bow. However, the results show that the speed-loss of KVLCC2B is very similar to KVLCC2D. This is despite the results from added resistance calculations showing that KVLCC2B design has a lower added resistance coefficient in the diffraction regime than KVLCC2A.
- KVLCC2D has the lowest attainable speed of the designs with a naturally shaped under water hull, excluding KVLCC2B. The speed loss is not substantially much greater than for KVLCC2A. However, a larger calm water resistance contributes to a poor overall performance.
- The fact that the effect is greatest for head seas shows that a sharper bow will reduce the added resistance in waves for head seas, which is the primary goal of the sharper entrance angle. Also the sharper entrance angle does not influence the performance in the radiation regime or in oblique waves too much. It also shows that the reflection effect on added resistance, despite the low magnitude of the effect compared to radiation, is a major component of the total added resistance. Thus the majority of wave conditions experienced are small (short) compared to KVLCC2 design.
- The dominating wave heading on a route seems to play a crucial role when evaluating different designs. The benefit of a sharper bow will be smaller if the vessel travels in oblique waves most of the time. However, a merchant vessel will seldom trade the same cycle its entire operating time. Thus an assumption of equal importance of all headings is not that far-fetched.

  Following the argumentation of headings above the results indicate that a sharpening of the bow would be beneficial even though the gain of a sharper bow is mostly within wave headings of 45°.
- A small increase in benefit is seen on routes with more severe wave conditions as in the North Atlantic. However, it does not influence enough to give a different optimal design.

The calm water resistance did not turn out as was expected in chapter 3.3.8. The conclusions stated above have to be based on the results calculated in this thesis. However, as discussed in the previous chapter several aspects of the calm water resistance have to be assessed in more detail and to a higher precision to be able to confidently state the benefits of a sharper bow. As it turns out, the difference between the designs is not extreme, and thus the precision requirement for a calm water resistance analysis is high.

The wave making resistance calculation is one of the factors that should be calculated with other methods as Shipflow was not able to give reasonable results. The form factor calculated by Holtrop's empirical method is also an uncertain parameter in the calculations. A precise division of the calm water resistance between the designs is dependent on these two parameters.

7 INNOVATIVE BOW DESIGNS

There are several bow designs developed with the objective of reducing the added resistance in waves. In this thesis they are referred to as innovative bow designs, as they have features not found on most bow designs today with special consideration on added resistance in waves. The last decade some segments have opened up to unconventional bows, and some designs have become a relatively common feature in the fleet. This is probably most noticeable in the offshore service segments, where X-Bow from Ulstein Design and the STX OSV's relatively novel design has become the standard bow design on ships built at Ulstein Shipyard and STX' yards in Norway. Designs with these bows are also sold to yards and ship owners all over the world.

In other segments and especially the larger segments of merchant ships the trend of highly innovative bow has not been the same. The offshore service fleet is generally small compared to the merchant ships supplying the world trade. Still some designs have been developed especially for large segments, and at least one has been built and tested in full scale.

This chapter will review some innovative bows and discuss their working principles and evaluate their applicability to large, slow ships. Most bow designs are hard to review as they are subject to patent protection and information from experiments and such are often confidential. The efficiency of such bows can only be concluded by model tests, CFD calculations or full scale tests. However, an evaluation of the working principles and how well they fulfil the objectives according to theory will be carried out.

7.1 X-BOW

FIGURE 7.1 - THE X BOW CONCEPT

It is not easy to acquire experimental data on this bow. However, the patent application provides some information on the reasoning for developing this bow, and the effects that are aimed for by the bow design. The website of Ulstein Group provides some information, however, rather superficially.

7.1.1 BACKGROUND

The objective of the X bow design is not merely to reduce added resistance in waves. It aims at improving several aspects of the operation of offshore vessels. Offshore service vessels often

have the wheelhouse and superstructure in front of the mid ship. Thus motions are a critical point in this case for the accommodation and resting of the crew. Motion characteristics are also an important aspect of the operability of offshore vessels, which Ulstein Design claims to have improved with X bow. The patent application sums up advantages of X bow as (amongst others)(Kvamsvåg, 2006):

- Lower accelerations and retardations, which give higher average speed at sea, thereby reducing power requirement and consumption of fuel.
- Reduction in the amount of or elimination of green water on deck.
- Lower risk of heavy weather damage to the foreship because the reflection of waves is reduced.
- Improved working environment on board with regard to;
    - The above mentioned lower accelerations and retardations, improving safety during navigation and higher operability.
    - Reduction of noise and vibration because of gentle motions and reduced slamming. Increasing comfort and better environment with regard to resting time of the crew.

Even though the patent application states validity in general for displacement ships, it focuses on vessels intended for marine operations. It states that when offshore service vessel are waiting on the weather, they will normally have their bow turned upwind and into the waves. Typical bows on offshore ships have raked bow above the waterline resulting in reflection of waves to a great degree, heavily subject to slamming of waves against the ship side, generation of spray and occurrence of green water on deck in front of the superstructure, (Kvamsvåg, 2006).

7.1.2 WORKING PRINCIPLES

The design is briefly described as a backward sloping bow above the water line as seen in Figure 7.1. The underwater hull is similar to conventional hulls, thus the concept focus on the hull shape above the waterline.

Volume has been moved from the shoulders and the common flare forward and up resulting in smoother volume distribution in the bow. The conventional flare is designed mainly to reduce green water on deck. With the X-bow, the waves are allowed to creep up on the bow and thus the tall enclosed bow structure of the design is needed.

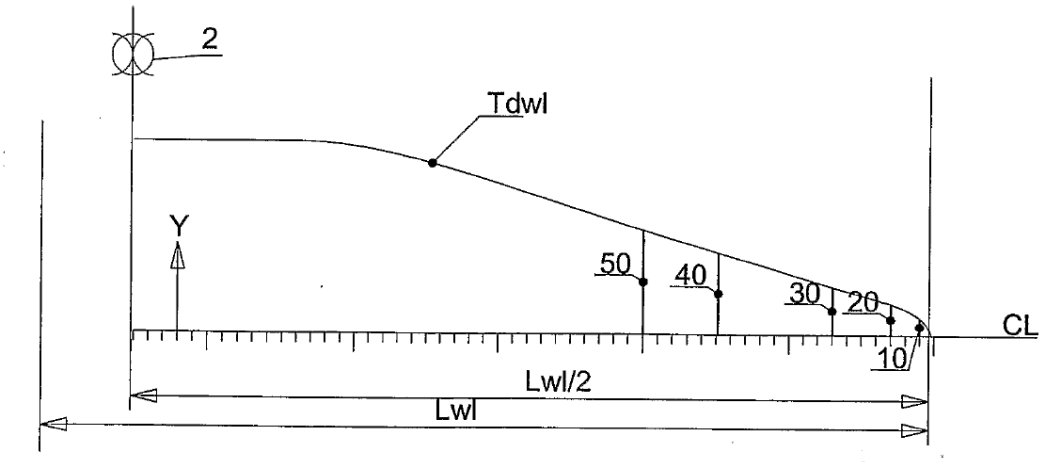

FIGURE 7.2 - WATERLINE OF X-BOW, (KVAMSVÅG, 2006).

The relocation of volume from the shoulders and forward allows for a sharper entrance angle and thus less reflection of waves. The waterline is shown in Figure 7.2.

For conventional bows, when encountering incident waves, the submerged volume increases rapidly, buoyancy increases correspondingly, which results in the waves being thrown back causing large accelerations and retardation forces. The smoother lines of the X bow above water allow the wave to follow the ship side and be directed to the sides, resulting in smoother motions and less throwback of water in large waves.

7.2 STX DESIGN

FIGURE 7.3 - STX OSV - PSV 08 (HTTP://WWW.STXOSV.COM/NEWSANDMEDIA/PAGES/DEFAULT.ASPX)

7.2.1 BACKGROUND

STX OSV designs and builds offshore and specialized vessels used in the offshore oil and gas exploration and production and oil services industries. They have also developed an innovative bow concept, obviously focused on the segments mentioned above. This bow design is proprietary information and therefore, test results are not available. The patent application, (Tvete and Borgen, 2012), has been used as the main source of information.

On the same basis as for the X-bow, the bow is developed to improve performance in marine operations. The patent application states that the objective of the new bow is to reduce the added resistance in waves, as well as reducing the level of accelerations, motions in seaway and slamming in the bow region. This should result in less fuel consumption and more comfort for the crew, (Tvete and Borgen, 2012).

7.2.2 WORKING PRINCIPLES

The bow concept is divided into three sections, dealing with three different aspects of the resistance regime.

On the lower part, section A in Figure 7.4, the hull shape is kept more or less as conventional hulls to minimize the calm water resistance. This part contributes to a lesser degree to the added resistance in waves.

The middle part, B, comprises a blunt shaped surface curving inwards and backwards from the transition area and back to a recessed blunt shaped section, designed to reflect smaller waves to the sides. This is as opposed to having a very sharp curve in this area which, according to Tvete and Borgen (2012), will make the small waves follow the hull shape further aft and induce

friction resistance. It is argued that the short time period of handling the reflection of waves will generate less speed-loss than the friction resistance of following waves.

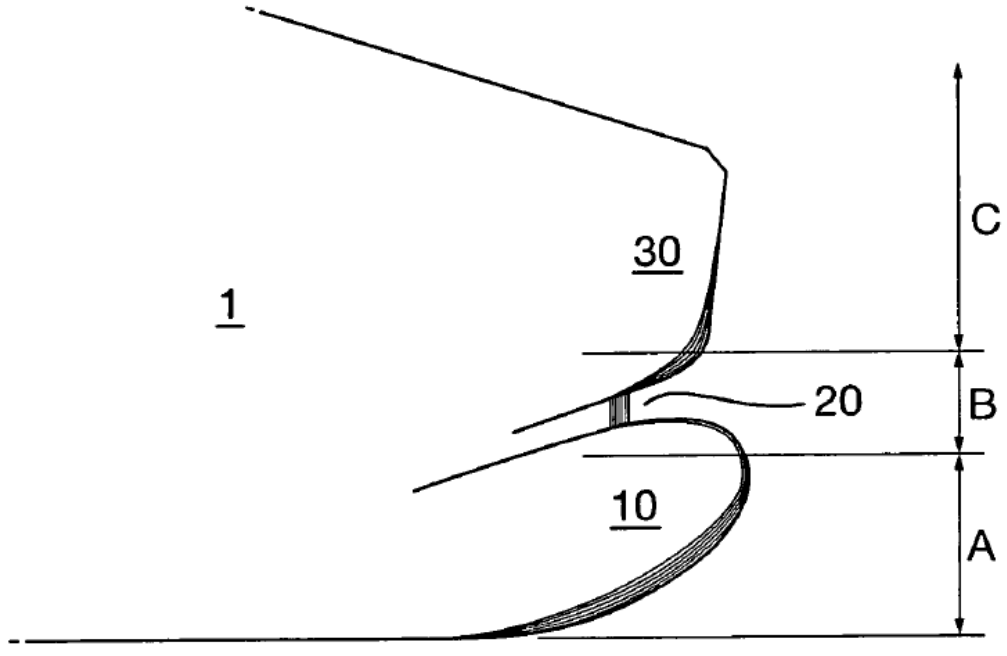

FIGURE 7.4 - PROFILE VIEW OF THE STX BOW, (TVETE AND BORGEN, 2012).

The upper bow portion, C, is stretched forward making it sharper. This makes it possible to reduce the flare angles, seen on conventional bows, and shoulder of the bow obtaining some of the same characteristics as the X bow with slower volume increase when piercing into the large waves. The sharpening is based on the same reasoning as the X-bow, making the bow pierce through the waves and split them instead of hitting the waves with a blunt bow design.

7.3 Ax-Bow

7.3.1 Background

The Ax-bow is as bow concept designed by NKK. NKK is a Japanese steel manufacturer and ship builder. The Ax-bow concept was developed because the energy saving measures in later years have led to a smaller power supply on merchant ships, thus the speed-loss of these energy-saving ships is crucial compared to ships with a large sea margin implemented. Hence, a ship with better performance in waves even with smaller installed propulsion power was desired, (Matsumoto, 2002).

The bow concept was installed on “Kohyohsan”, a 172 000DWT Cape size bulk carrier with overall length of 289 m and breadth 45 m. A sister ship was fitted with an ordinary bow and full scale measurements have been done.

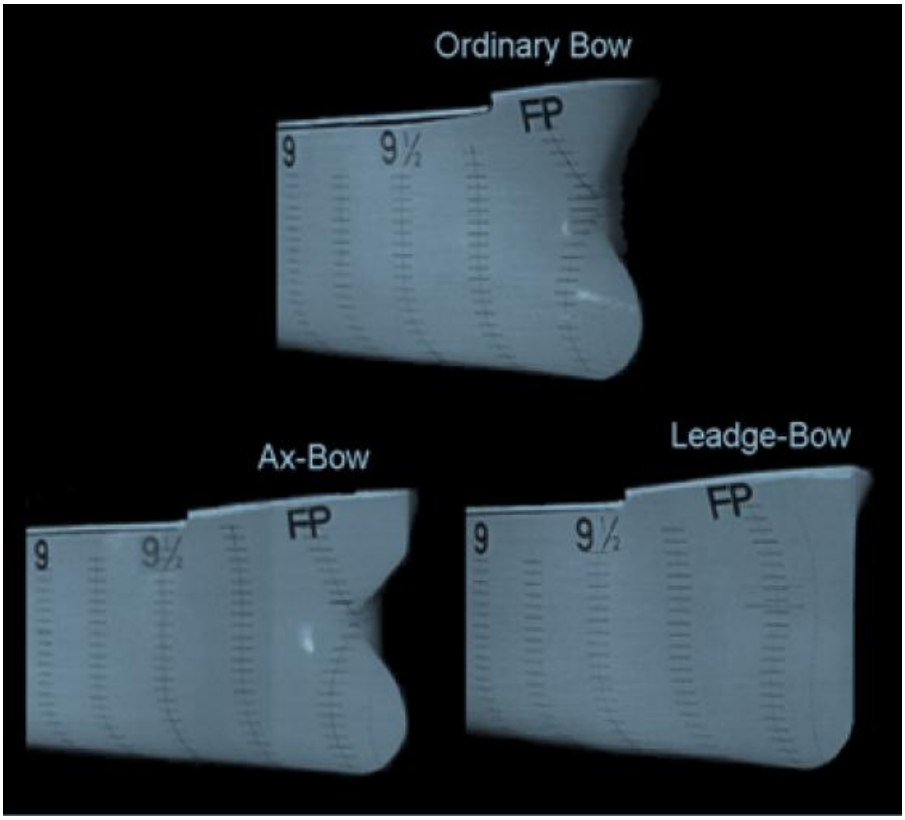

FIGURE 7.5 - THE AX-BOW CONCEPT COMPARED TO THE ORDINARY BOW AND LEADGE-BOW (ITTC, 2008).

7.3.2 WORKING PRINCIPLES

The design focuses on the shape above the waterline. The hull shape below the waterline is the same as for the ordinary bow maintaining the calm water performance of the ordinary ship. The bow has been sharpened above the waterline, like a beak, to reflect incident waves more to the sides than forward. To satisfy the length requirements in ports the bow had to be sharpened as much as possible within the regulations. A requirement of 289 m maximum overall length in a European port was the dimensioning requirement, (Hirota et al., 2005).

Model tests have been performed with the bow. Figure 7.6 shows the results as the non-dimensional resistance increase in regular waves. The figure indicates a 20 to 30 % reduction in almost the entire range of wavelength, (Matsumoto, 2002). However, the reduction seems to be largest in the small (short) waves where a reduction of almost 50 % is measured.

Full scale measurements are summed up in Hirota et al. (2005), see Figure 7.8. They show that the Ax-bow reduces the speed-loss, especially in the higher sea states compared to a conventional ship. Values are given in Table 7.1. From track records of the Kohyohsan it is shown that the required horse power is reduced by 3-4 % compared to the sister ship (Sea-Japan, 2006).

TABLE 7.1 - REDUCTION RATIOS OF SPEED-LOSS, (HIROTA ET AL., 2005).

(a) Short Term Prediction by Tank Test

H(m)	3	4	5	6
Te(sec.)	6.5	7.8	8.5	8.8
Ax-Bow(knot)	-0.75	-1.29	-1.80	-2.38
Ord. Bow(knot)	-1.16	-1.93	-2.67	-3.48
Reduction(%)	*64%*	*67%*	*68%*	*68%*

(b) Result of Full Scale Measurement

H(m)	3	4	5	6
Te(sec.)	6.5	7.8	8.5	8.8
Ax-Bow(knot)	-0.57	-0.87	-1.20	-1.50
Ord. Bow(knot)	-0.68	-1.20	-1.88	-2.63
Reduction(%)	*84%*	*73%*	*64%*	*57%*

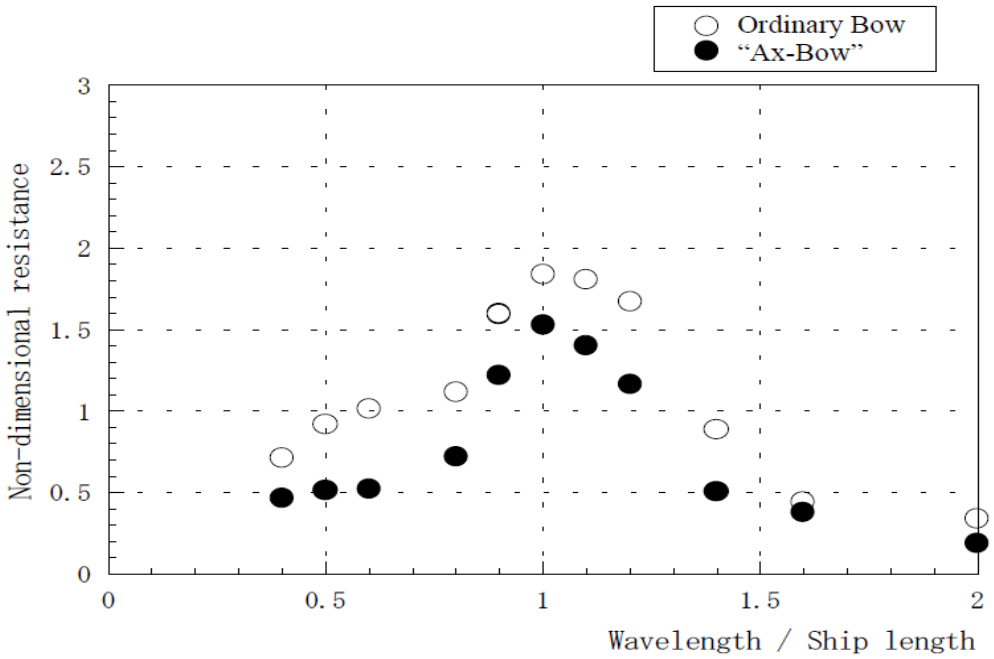

FIGURE 7.6 - ADDED RESISTANCE RESULTS FROM MODEL TESTS WITH AX-BOW

7.4 BEAK BOW

The Beak bow is a predecessor of the Ax-bow. It is designed as a longer and pointy beak, seen in Figure 7.7. Due to the mentioned length restrictions the Ax-bow was developed. The Beak bow tested in Hirota et al. (2005) would give a ship with overall length of 300 m.

There is not much difference in the measured added resistance coefficient between the Beak bow and the Ax bow, hence approximately 20-30% reduction in resistance increase in waves compared to conventional bows.

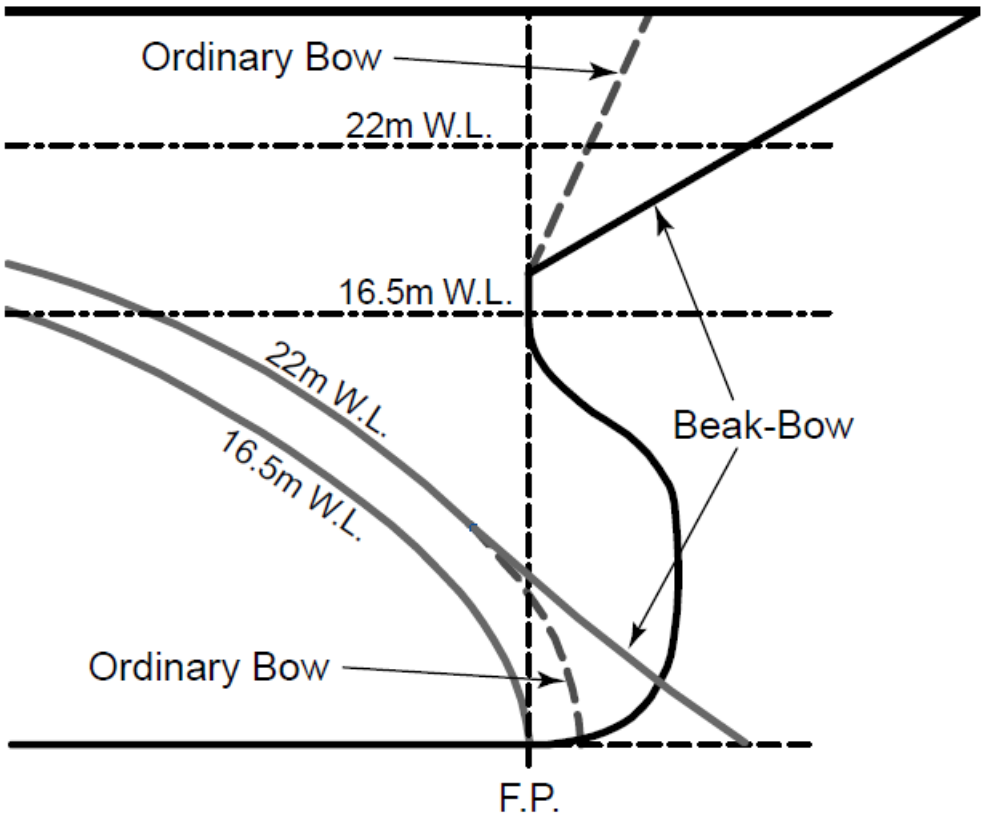

FIGURE 7.7 - BEAK BOW PROFILE AND WATERPLANE VIEW, (Hirota et al., 2005).

7.5 LEADGE BOW

The Leadge bow is a further development of the Ax-bow, shown in Figure 7.5. The working principles of the bow are the same as the Ax-bow, reflecting waves to the sides. However, the stem has been straightened filling up the gap between the "Ax" and the bulb. This eliminates the bulbous bow in the profile view. The whole stem line is sharpened, also under the waterline hull. Due to this the bow was expected to reduce the added resistance in both ballast and full load conditions. The design approach of the Leadge bow is very similar to that of KVLCC2C and KVLCC2E, thus a confirmation on the performance regarding added resistance can be made.

According to Sea-Japan (2006) the bow shape has been confirmed to give the same calm water wave making resistance as the conventional hull with bulbous bow. Due to the relative low speed of the vessel, the wave making resistance is a small part of the total resistance and a change would not contribute much to the overall calm water resistance. Thus an increase in wave making resistance is not crucial to the overall performance, (Hirota et al., 2005).

A curious result is given in (Hirota et al., 2005). It states that Ax-bow has a reduction of 20-30% in one part of the paper. However, in another part treating the Leadge bow, it states that the reduction is 12% in head seas for the Ax bow, and the Leadge bow has a reduction of 19%. Two different models have been used in the cases and the ordinary bow seems to be different in the efficiency regarding added resistance. In any case, the latter results seem to point to the increased efficiency of the Leadge bow regarding added resistance in waves.

7.6 Evaluation of Designs Implemented on KVLCC2

The X-bow and STX's bow are designed with the offshore service segments in mind. These ships are typically 70-140 m long. Thus, the amount of waves in the short wave region is considerably lower than for a VLCC.

The conventional bows in the offshore segments are also considerably less blunt than the large tanker and bulk segments, probably due to a higher Froude number. The wave making resistance is more significant than for large slow ships, and a sharper bow may be beneficial for the calm water resistance. Thus the gain of sharpening the bow of these ships is expected to be less for two reasons. The conventional bow is considerably sharper and the amount of waves that can be included in the short wave region is considerably less than for large tankers.

The argumentation from STX that if the shape of the mid-section is too sharp the waves will not be reflected off the ship, but rather guided along the ship side seems reasonable. However, the significance of the friction resistance compared to the reflection in this case is questionable and difficult to evaluate without any test results. Without much information it is also assumed that the bluntness of the section is not in the range of tankers and bulk carriers, rather a relative term considering conventional bows on offshore service vessels. Thus, it is probably sharper than the average VLCC bow.

The exposure time to waves inducing added resistance through heaving and pitching is larger than for ships like KVLCC2, due to the significant difference in size. Thus the X-bow and STX' bow have a great focus on this region. The pointy shaped section of the bows are primarily to split the large waves, instead of throwing them back, which requires a lot of energy and creates speed-loss.

The X-bow allows waves to creep up on the bow as it slopes backwards. This requires a relatively tall bow. On the X-bow and for STX it is a benefit as the superstructure can be incorporated in this tall bow. On a VLCC this would probably require a taller bow than customary today due to issues with green water on deck. The implementation of this may not be beneficial as more wind is captured by the bow.

On the other hand, a sharper bow on a VLCC would work in a similar way, splitting the waves reducing the throwback caused by the rake and flare on a conventional bow. Thus the large waves may cause issues with green water on deck, and a taller bow may be necessary.

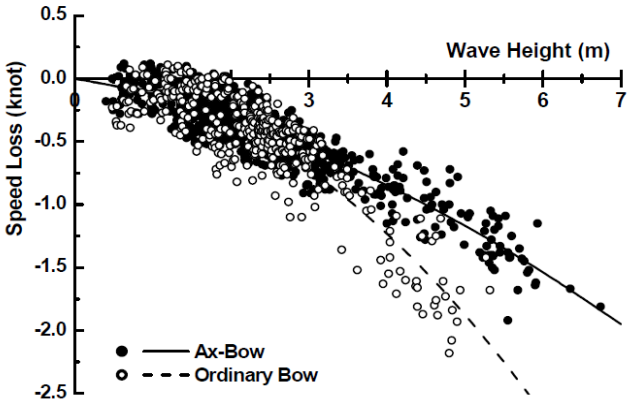

FIGURE 7.8 - FULL SCALE MEASUREMENTS OF AX BOW FITTED ON A CAPE-SIZE BULK CARRIER, (Hirota et al., 2005)

For large, slow ships the exposure time to the range of relatively short waves is larger and thus the reflection of waves is more important. As seen in the full scale measurements of the Ax-bow

in Figure 7.8 the trending benefit of the Ax-bow is increasing with wave height. Thus it seems like the sharpening above the waterline also influences the added resistance in the radiation region as well as in the reflection region.

Universal Shipbuilding Corp. applied for the patent on the Leadge-Bow in 2002, (Sea-Japan, 2006). However, Financial Times states that the patent was denied on the basis that it looks too similar to old-fashioned, low-tech hulls, (Dickie, 2011). This shows that improvement in performance in seaway can be improved by simple, not necessarily drastically innovative means.

8 FURTHER WORK

As discussed in the results and conclusion several aspects of the calm water analysis needs to be taken a closer look at. A method for calculating the wave making resistance of each design precisely, with effects like wave breaking, should be found. A possibility is to use RANS calculations with VOF. Another possibility would be to run model tests on several designs. Both methods could give a resistance curve more precisely than the XPAN solver in Shipflow. The methods could also provide form factors that are based on the actual hull shape and not on empirical formulas. However full scale CFD calculations are extremely time consuming and access to a cluster or similar is preferable.

The last time dependent objective of the problem definition for this thesis which deals with a numerical study of innovative bow shapes is a natural extension of this thesis. Effort should be made on searching for even more developed innovative bow designs for large, slow ships to be able to compare different approaches to reduce the added resistance. Possibly developing a new design from scratch could be an interesting, but time consuming task. CFD will have to be utilized to evaluate the efficiency of designs without vertical sides. This is time consuming and another issue is to get access to patented designs to compare with.

Several simplifications and assumptions have been made in this thesis. One expansion of the problem could be to include an operational profile and direction distribution of the wave environment to get an even more realistic evaluation of the performance of each design.

Another could be to include more detailed engine characteristics such that fuel consumption can be calculated and a study of how different bow designs influence the economics. This diverges from a hydrodynamic study, but is none the less interesting.

References

ARRIBAS, F. P. 2007. Some Methods to Obtain the Added Resistance of a Ship Advancing in Waves. *Ocean Engineering,* 34**,** 946-955.

AZCUETA, R. Steady and Unsteady RANS Simulations for Littoral Combat Ship. Proceedings of the 24th Symposium on Naval Hydrodynamics, 2004 St. Johns, Newfoundland and Labrador, Canada.

BOESE, P. 1970. Simplified Method of Calculation of Increased Ship Resistance in Waves (Eine einfache methode zur berechnnung der winderstansershohung eines schiffes im seegang). *Shiffstechnik,* 17 (86).

CHINA-DAILY. 2010. *China's iron-ore imports from South Africa, Ukraine, Canada up in 2009* [Online]. China Daily. Available: http://www.chinadaily.com.cn/china/2010-02/16/content_9471501.htm [Accessed 22.03 2012].

CHOI, J. & YOON, S. B. 2009. Numerical Simulations Using Momentum Source Wave-maker applied to RANS Equation Model. *Coastal Engineering,* 56**,** 1043-1060.

DICKIE, M. 2011. Japanese Yards Claim to Have Edge Over Rivals. *Financial Times* Tokyo Financial Times.

DNV 2010. Triality - Taking Environmental and Economical Performance a Long Step Forward. *Tanker Update, DNV.* DNV.

FALTINSEN, O. M. 1990. *Sea Loads On Ships And Offshore Structures,* Cambridge, Cambridge University Press.

FALTINSEN, O. M. 2010. *Hydrodynamics of High-Speed Marine Vehicles,* Cambridge New York, Cambridge University Press.

FALTINSEN, O. M., MINSAAS, K. J., LIAPIS, N. & SKJØRDAL, S. O. Prediction of Resistance and Propulsion of a Ship in a Seaway. Proceeding of the 13th Symposium on Naval Hydrodynamics, 1980. 505-529.

FALTINSEN, O. M. & SVENSEN, T. Incorporation of Seakeeping Theories in CAD. *In:* OORTMERSSEN, G. V., ed. Proceedings of the International Symposium on CFD and CAD in ship design, 1990 Wageningen, the Netherlands. Elsevier Science Publishers B.V.

FATHI, D. & HOFF, J. R. 2010. ShipX Vessel Responses (VERES) - Theory Manual. Trondheim: MARINTEK A/S.

FUJII, H. & TAKAHASHI, T. Experimental Study on the Resistance Increase of a Ship in Regular Oblique waves. Proceedings of the 14th ITTC, 1975 Ottawa, Canada. 351-360.

GENCO. 2012. *Industry* [Online]. Available: http://www.gencoshipping.com/industry.html [Accessed 22.03 2012].

GERRITSMA, J. & BEUKELMAN, W. 1972. Analysis of the Resistance Increase in Waves of a Fast Cargo Ship. *International Shipbuilding Progress,* 19**,** 285-292.

GUO, B. 2011. *Numerical and Experimental Investigation of Added Resistance in Waves.* PhD, Norwegian University of Science and Technology.

GUO, B. & STEEN, S. Added Resistance of a VLCC in Short Waves. Proceedings of the ASME 2010 29th International Conference on Ocean, Offshore and Arctic Engineering, 2010a Shanghai, China.

GUO, B. & STEEN, S. 2010b. Experiment on Added Resistance in Short Waves. *28th Symposium on Naval Hydrodynamics.* Pasadena, CA, USA.

GUO, B. & STEEN, S. 2011. Comparative Study of Sea-Keeping Prediction of Ships in Head Sea Waves. Trondheim: Norwegian University of Science and Technology.

GUO, B., STEEN, S. & DENG, G. B. 2011. Sea-keeping Prediction of KVLCC2 in Head Waves with RANS. *Doctoral Thesis: Numerical and Experimental Investigation of Added Resistance in Waves***,** 126-139.

HAVELOCK, T. H. 1942. Drifting Force on a Ship among Waves. *Philosophical Magazine.*

HIROTA, K., MATSUMOTO, K., TAKAGISHI, K., YAMASAKI, K., ORIHARA, H. & YOSHIDA, H. Development of Bow Shape to Reduce the Added Resistance due to Waves and Verification on Full Scale Measurement. International Conference on Marine Research and Transportation, 2005 The Island of ISCHIA (Gulf of Naples) Italy.

ITTC, S. C. Final Report and Recommendation to the 25th ITTC. Proceedings of the 25th ITTC. The Seakeeping Committee. 2008 Fukuoka City.

JOOSEN, W. P. A. Added resistance in waves. Proceeding of the Sixth Symposium on Naval Hydrodynamics, 1966 Washington.
KASHIWAGI, M. Impact of Hull Design on Added Resistance in Waves - Application of the Enhanced Unified Theory. Proceedings of the 10th International Marine Design Conference, 2009 Trondheim, Norway. 521-535.
KASHIWAGI, M., IKEDA, T. & SASAKAWA, T. 2010. Effect of forward speed of a ship on added resistance in waves. *International Journal of Offshore and Polar Engineering,* 20**,** 196-203.
KIM, W. J., VAN, S. H. & KIM, D. H. 2001. Measurement of flows around modern commercial ship models. *Experiments in Fluids,* 31**,** 567-578.
KVAMSVÅG, U.-D.-A. Ø. G. 2006. *The Foreship Arrangement for a Vessel of the Displacement Type*. PCT/NO2006/000073.
LARSSON, L. & RAVEN, H. C. 2010. Principles of Naval Architecture Series - Ship Resistance and Flow. Society of Naval Architects and Marine Engineers (SNAME).
LAURSEN, W. 2001. Efficient New Bow Shapes Get Sexy. *Baird Maritime* [Online]. Available: http://www.bairdmaritime.com/index.php?option=com_content&view=article&id=11612&Itemid=208 [Accessed 20.05.2012].
LØVSTAD, M. 2008. *Where iron ore is king - Port Complex of Tubarão* [Online]. Available: http://www.dnv.com/industry/maritime/publicationsanddownloads/publications/updates/bulk/2008/2_2008/whereironoreiskingportcomplexoftubaro.asp [Accessed 22.03 2012].
MARUO, H. 1957. The Excess Resistance of a Ship in Rough Seas. *International Shipbuilding Progress,* 4(35).
MARUO, H. 1960. The Drift of a Body Floating on Waves. *Journal of Ship Research,* 4 (3).
MATSUMOTO, K. 2002. "Ax-Bow" : A New Energy-saving Bow Shape at Sea. *NKK Technical Review,* 86**,** 46-47.
MATSUMOTO, K., NAITO, S., TAKAGI, K., HIROTA, K. & TAKAGISHI, K. Beak-bow to Reduce the Wave Added Resistance at Sea. 7th International Symposium on practical design of ships and mobile units., 1998 The Hague, The Netherlands. 527-533.
MINSAAS, K. & STEEN, S. 2008. *Lecture Notes - Ship Resistance*, Department of Marine Technology - NTNU.
SAKAMOTO, T. & BABA, E. Minimization of resistance of slowly moving full hull forms in short waves. Proceedings of the 16th Symposium on Naval Hydrodynamics, 1986 Berkely, USA. 598-612.
SAUDI-ARAMCO. 2012. *Ras Tanura Terminal* [Online]. Available: http://www.saudiaramco.com/en/home.html#our-operations%257C%252Fen%252Fhome%252Four-operations%252Fports-and-terminals%252Ffacilities%252Fras-tanura-terminal.baseajax.html [Accessed 22.03 2012].
SEA-JAPAN 2006. Universial Applies New Energy-aving Type Leadge Bow to 81,000DWT Bulker. *SEA-Japan,* 318.
SEA-WEB. 2012. *Fairplay Database* [Online]. Available: www.sea-web.com [Accessed 18.04.2012 2012].
SIMMAN2008. 2008. *Moeri Tanker KVLCC2* [Online]. Available: http://www.simman2008.dk/KVLCC/KVLCC2/kvlcc2_geometry.html [Accessed 15.02 2012].
STEEN, S., DENG, G. B. & GUO, B. 2010. RANS Prediction and Experiment on Ship Resistance and Flow Field of KVLCC2.
STEEN, S. & FALTINSEN, O. M. Added Resistance of a Ship Moving in Small Sea States. Practical Design of Ships and Mobile units, 1998 Hague, The Netherlands.
STOPFORD, M. 2009. *Maritime Economics,* 2 Park Square, Milton Park, Abingdon, Oxon OX14 4RN, Routledge.
SUNDE, C. A. 2011. *The Importance of Added Resistance and Speed of Ships Due to Waves for Ships Designed for Slow-Steaming.* MSc, Norwegian University of Science and Technology.
TORSETHAUGEN, K. & HAVER, S. Simplified double peak spectral model for ocean waves. The Fourteenth (2004) International OFFSHORE AND POLAR ENGINEERING CONFERENCE, 2004 Toulon, France. International Society of Offshore and Polar Engineers (ISOPE), 76-84.
TUCK, E. O., SALVESEN, N. & FALTINSEN, O. M. 1970. Ship Motions and Sea Loads. *Transactions of the Society of Naval Architects and Marine Engineers,* 78**,** 250-287.

TVETE, M. R. & BORGEN, H. 2012. *A Ship's Fore Body Form*. PCT/NO2010/000030.
UENO, M., NIMURA, T. & MIYAZAKI, H. On Steady Horizontal Force and Moment due to Short Waves Acting on Ships in Maneuvring Motion. Proceedings of the 8th international symposium on practical design of ships and other floating structure, 2001 Shanghai, China. 671-677.
WILSON, P. A. 1985. A Review of the Methods of Calculation of Added Resistance for Ships in a Seaway. *Journal of Wind Engineering and Industrial Aerodynamics,* 20**,** 187-199.

Appendix A Scatter Diagram

This is posted as an example. Input files to ShipX can be found in the attached zip-file.

APPENDIX FIGURE 1 – WEIGHTED SCATTER DIAGRAM FOR THE WHOLE ROUTE FROM RAS TANURA TO LOOP

Hs \ Tz	2	3	4	5	6	7	8	9	10	11	12	13	14	15	16	17		Cummulative sum
0.5	392089	1158575	2606822	3807976	3180799	1545938	475085	106601	20761	4258	1089	360	142	62	28	14		13300599
1	122828	459195	1392982	3157625	4166045	3161786	1473191	469398	115227	24499	5102	1194	351	130	57	27		27850236
1.5	52875	234320	819781	2343612	4075185	4150393	2568542	1056000	320749	79547	17654	3852	923	270	100	44		43574083
2	22271	113833	447147	1506650	3180309	4044938	3133058	1580128	571947	163411	40052	9080	2061	515	157	60		58389700
2.5	9234	52980	230730	882303	2143875	3242747	3033140	1823476	767665	248271	66949	16149	3719	879	233	76		70912126
3	3779	23772	113653	482151	1298977	2248268	2474601	1741409	839493	303134	89053	22838	5436	1276	318	92		80560376
3.5	1528	10353	53720	249708	726699	1394157	1767798	1437818	785734	313745	99512	26955	6634	1571	380	102		87436790
4	610	4405	24450	123990	383704	795799	1140978	1061619	653022	286502	97472	27707	7016	1676	400	102		92046242
4.5	241	1844	10746	59553	194858	429819	685485	722284	496967	238493	86696	25759	6682	1605	378	93		95007745
5	94	763	4572	27847	96626	225294	394551	465447	355535	185855	72053	22361	5939	1432	332	79		96866525
5.5	36	313	1888	12731	47278	116867	222979	290839	244235	138351	57130	18549	5061	1231	282	65		98024360
6	14	128	759	5705	22956	60663	125752	179236	163610	99750	43786	14905	4202	1038	237	53		98747154
6.5	5	52	299	2509	11087	31613	71234	109966	107941	70287	32688	11677	3417	866	200	44		99201039
7	2	21	115	1084	5327	16521	40518	67377	70525	48690	23887	8947	2725	712	168	37		99487695
7.5	1	8	44	460	2545	8639	23075	41208	45748	33292	17153	6721	2131	576	139	31		99669466
8	0	3	17	192	1208	4511	13121	25118	29483	22524	12141	4963	1636	458	114	26		99784981
8.5	0	1	6	79	569	2349	7436	15234	18872	15097	8488	3610	1235	358	91	21		99858427
9	0	0	2	32	266	1218	4194	9183	11988	10025	5867	2591	918	275	72	17		99905075
9.5	0	0	1	13	123	628	2353	5496	7553	6594	4010	1836	673	208	56	14		99934633
10	0	0	0	5	56	322	1311	3264	4715	4293	2710	1284	486	154	43	11		99953287
10.5	0	0	0	2	26	163	725	1922	2915	2765	1810	886	346	113	32	8		99965000
11	0	0	0	1	11	82	398	1121	1783	1761	1194	604	243	82	24	6		99972310
11.5	0	0	0	0	5	41	217	647	1079	1108	778	406	168	58	17	5		99976839
12	0	0	0	0	2	20	117	370	645	689	500	269	114	41	12	3		99979621
12.5	0	0	0	0	1	10	62	209	381	422	317	176	77	28	9	2		99981315
13	0	0	0	0	0	5	33	117	222	256	198	113	51	19	6	2		99982337
13.5	0	0	0	0	0	2	17	64	128	153	122	72	33	13	4	1		99982946
14	0	0	0	0	0	1	9	35	73	90	74	45	21	8	3	1		99983306
14.5	0	0	0	0	0	0	3	11	23	30	25	16	8	3	1	0		99983426
Sum	605607	2060566	5707734	12664228	19538537	21482794	17659983	11215597	5639019	2303892	788510	233925	62448	15657	3893	1036		99983426

Appendix B Calculated Resistance Coefficients

APPENDIX FIGURE 2 - KVLCC2A

V [kn]	Fn	Rn	Cf	ΔCf - MARINTEK	(1+k)*(Cf+ΔCf)	C_DB	Cw (wave cut)	Cw (IP)	Cr mod	Ct mod
10.98428	0.1	1.55E+09	1.45E-03	1.06E-04	2.09E-03	8.52E-06	0.00E+00	0.00E+00	9.96E-04	3.10E-03
13.18113	0.12	1.86E+09	1.42E-03	1.37E-04	2.09E-03	8.62E-06	5.21E-06	9.09E-04	1.00E-03	3.10E-03
15.37799	0.14	2.17E+09	1.39E-03	1.62E-04	2.09E-03	8.70E-06	1.45E-05	8.14E-04	1.01E-03	3.11E-03
15.59767	0.142	2.20E+09	1.39E-03	1.64E-04	2.09E-03	8.70E-06	1.65E-05	8.08E-04	1.01E-03	3.11E-03
16.47642	0.15	2.32E+09	1.38E-03	1.73E-04	2.09E-03	8.73E-06	2.16E-05	7.97E-04	1.02E-03	3.11E-03
17.57484	0.16	2.48E+09	1.37E-03	1.83E-04	2.09E-03	8.77E-06	3.39E-05	7.88E-04	1.03E-03	3.13E-03
19.7717	0.18	2.79E+09	1.35E-03	2.01E-04	2.09E-03	8.83E-06	1.93E-04	9.54E-04	1.19E-03	3.28E-03

APPENDIX FIGURE 3 - KVLCC2B

V [kn]	Fn	Rn	Cf	ΔCf - MARINTEK	(1+k)*(Cf+ΔCf)	C_DB	Cw (wave cut)	Cw (PI)	Cr mod	Ct mod
10.9842781	0.1	1.55E+09	1.45E-03	1.06E-04	2.09E-03	8.31E-06	1.29E-06	5.73E-06	9.96E-04	3.10E-03
13.1811337	0.12	1.86E+09	1.42E-03	1.37E-04	2.09E-03	8.40E-06	1.56E-05	7.30E-05	1.01E-03	3.11E-03
15.3779893	0.14	2.17E+09	1.39E-03	1.62E-04	2.09E-03	8.48E-06	3.47E-05	1.23E-04	1.03E-03	3.13E-03
15.5976749	0.142	2.20E+09	1.39E-03	1.64E-04	2.09E-03	8.49E-06	4.03E-05	1.23E-04	1.03E-03	3.14E-03
16.4764171	0.15	2.32E+09	1.38E-03	1.73E-04	2.09E-03	8.52E-06	5.03E-05	1.40E-04	1.04E-03	3.14E-03
17.5748449	0.16	2.48E+09	1.37E-03	1.83E-04	2.09E-03	8.55E-06	9.37E-05	1.83E-04	1.09E-03	3.19E-03
19.7717005	0.18	2.79E+09	1.35E-03	2.01E-04	2.09E-03	8.61E-06	3.30E-04	4.50E-04	1.32E-03	3.42E-03

APPENDIX FIGURE 4 - KVLCC2C

V [kn]	Fn	Rn	Cf	ΔCf - MARINTEK	(1+k)*(Cf+ΔCf)	C_DB	Cw (wave cut)	Cw (PI)	Cr mod	Ct mod
11.118	0.1	1.61E+09	1.44E-03	1.07E-04	2.06E-03	8.54E-06	9.97E-07	1.76E-03	9.96E-04	3.07E-03
13.342	0.12	1.93E+09	1.41E-03	1.38E-04	2.06E-03	8.64E-06	5.72E-06	1.26E-03	1.00E-03	3.07E-03
15.566	0.14	2.25E+09	1.39E-03	1.63E-04	2.06E-03	8.72E-06	1.34E-05	9.58E-04	1.01E-03	3.08E-03
15.788	0.142	2.28E+09	1.39E-03	1.65E-04	2.06E-03	8.72E-06	1.65E-05	9.30E-04	1.01E-03	3.08E-03
16.678	0.15	2.41E+09	1.38E-03	1.74E-04	2.06E-03	8.75E-06	2.64E-05	8.49E-04	1.02E-03	3.09E-03
17.79	0.16	2.57E+09	1.37E-03	1.84E-04	2.06E-03	8.78E-06	4.73E-05	7.65E-04	1.04E-03	3.11E-03
20.013	0.18	2.89E+09	1.35E-03	2.02E-04	2.06E-03	8.84E-06	1.45E-04	6.73E-04	1.14E-03	3.21E-03

APPENDIX FIGURE 5 - KVLCC2D

V [kn]	Fn	Rn	Cf	ΔCf - MARINTEK	(1+k)*(Cf+ΔCf)	C_DB	Cw (wave cut)	Cw (PI)	Cr mod	Ct mod
10.9843	0.1	1.55E+09	1.45E-03	1.06E-04	2.09E-03	8.52E-06	2.41E-06	1.90E-04	9.96E-04	3.10E-03
13.1811	0.12	1.86E+09	1.42E-03	1.37E-04	2.09E-03	8.61E-06	9.55E-06	2.51E-04	1.00E-03	3.11E-03
15.378	0.14	2.17E+09	1.39E-03	1.62E-04	2.09E-03	8.69E-06	1.75E-05	2.86E-04	1.01E-03	3.11E-03
15.5977	0.142	2.20E+09	1.39E-03	1.64E-04	2.09E-03	8.70E-06	1.88E-05	2.95E-04	1.01E-03	3.11E-03
16.4764	0.15	2.32E+09	1.38E-03	1.73E-04	2.09E-03	8.73E-06	2.46E-05	3.24E-04	1.02E-03	3.12E-03
17.5748	0.16	2.48E+09	1.37E-03	1.83E-04	2.09E-03	8.76E-06	5.41E-05	3.74E-04	1.05E-03	3.15E-03
19.7717	0.18	2.79E+09	1.35E-03	2.01E-04	2.09E-03	8.82E-06	2.41E-04	6.77E-04	1.23E-03	3.33E-03

APPENDIX FIGURE 6 - KVLCC2E

V [kn]	Fn	Rn	Cf	ΔCf - MARINTEK	(1+k)*(Cf+ΔCf)	C_DB	Cw (wave cut)	Cw (PI)	Cr mod	Ct mod
11.251	0.1	1.66E+09	1.44E-03	1.09E-04	2.03E-03	8.42E-06	9.91E-07	1.57E-03	9.96E-04	3.03E-03
13.501	0.12	2.00E+09	1.41E-03	1.39E-04	2.03E-03	8.51E-06	5.15E-06	1.12E-03	1.00E-03	3.04E-03
15.751	0.14	2.33E+09	1.38E-03	1.64E-04	2.03E-03	8.59E-06	1.83E-05	8.56E-04	1.01E-03	3.05E-03
15.976	0.142	2.36E+09	1.38E-03	1.66E-04	2.03E-03	8.60E-06	2.39E-05	8.38E-04	1.02E-03	3.05E-03
16.877	0.15	2.50E+09	1.37E-03	1.75E-04	2.03E-03	8.63E-06	4.87E-05	7.87E-04	1.04E-03	3.08E-03
18.002	0.16	2.66E+09	1.36E-03	1.85E-04	2.03E-03	8.66E-06	1.00E-04	7.49E-04	1.09E-03	3.13E-03
20.252	0.18	3.00E+09	1.34E-03	2.02E-04	2.03E-03	8.72E-06	2.42E-04	7.26E-04	1.24E-03	3.27E-03

Appendix C RAO added resistance

APPENDIX FIGURE 7 - KVLCC2A: RAO ADDED RESISTANCE

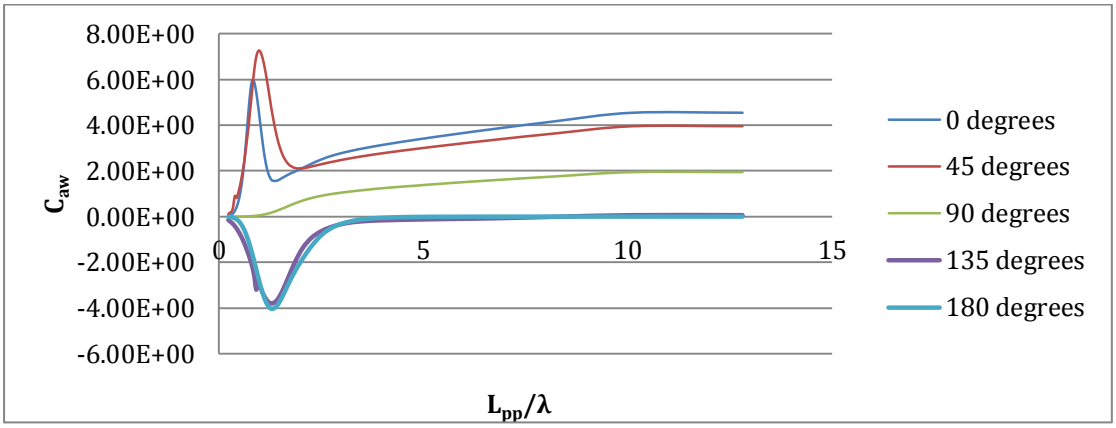

APPENDIX FIGURE 8 - KVLCC2B: RAO ADDED RESISTANCE

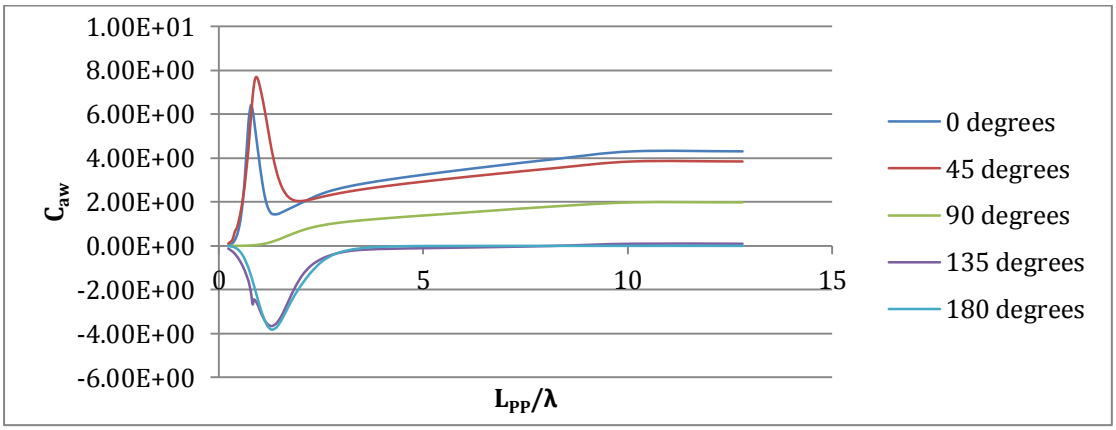

APPENDIX FIGURE 9 - KVLCC2C: RAO ADDED RESISTANCE

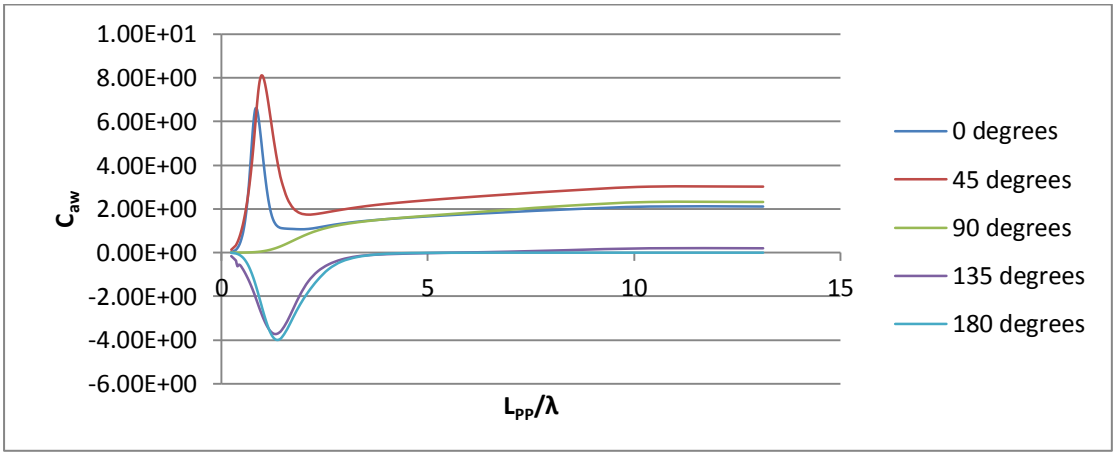

APPENDIX FIGURE 10 - KVLCC2D: RAO ADDED RESISTANCE

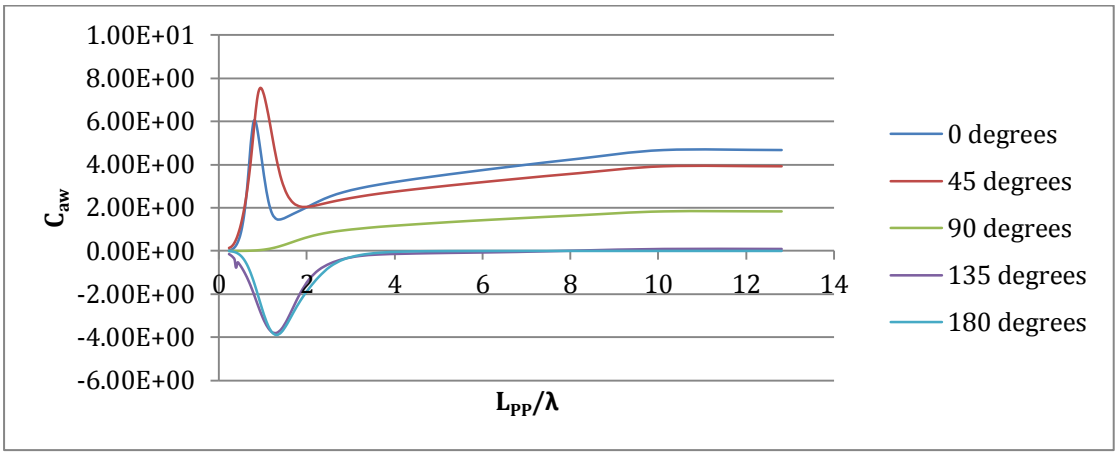

APPENDIX FIGURE 11 - KVLCC2E: RAO ADDED RESISTANCE

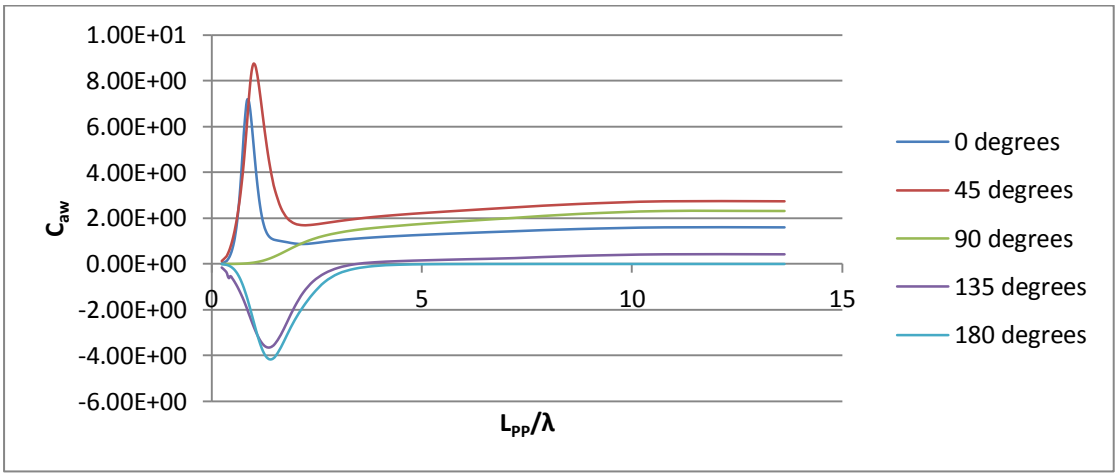

Appendix D Attached Files in Zip-folder

Scatter diagram input files for ShipX:

AG-LOOP.sea – Arabian Gulf (Ras Tanura) to LOOP (USA)

AG-Chiba.sea - Arabian Gulf (Ras Tanura) to Chiba (Japan)

Mongstad-NY.sea – Mongstad (Norway) to New York (USA)

Tubarão-Quindao.sea – Tubarão (Brazil) to Quindao (China)

.igs-files, 3D models used in analyses:

KVLCC2_original.igs – Original KVLCC2 design

KVLCC2B.igs

KVLCC2C.igs

KVLCC2D.igs

KVLCC2E.igs